AD-A136 538 REPETITIEELY PULSED ELECTRIC LASER ACOUSTIC STUDIES 1/2
VOLUME 1. (U) MASSACHUSETTS INST OF TECH CAMBRIDGE DEPT
OF AERONAUTICS ANDAA.. K U INGARD ET AL. SEP 83
UNCLASSIFIED AFWAL-TR-83-2058-VOL-1 F33615-80-C-2040 F/G 20/5 NL

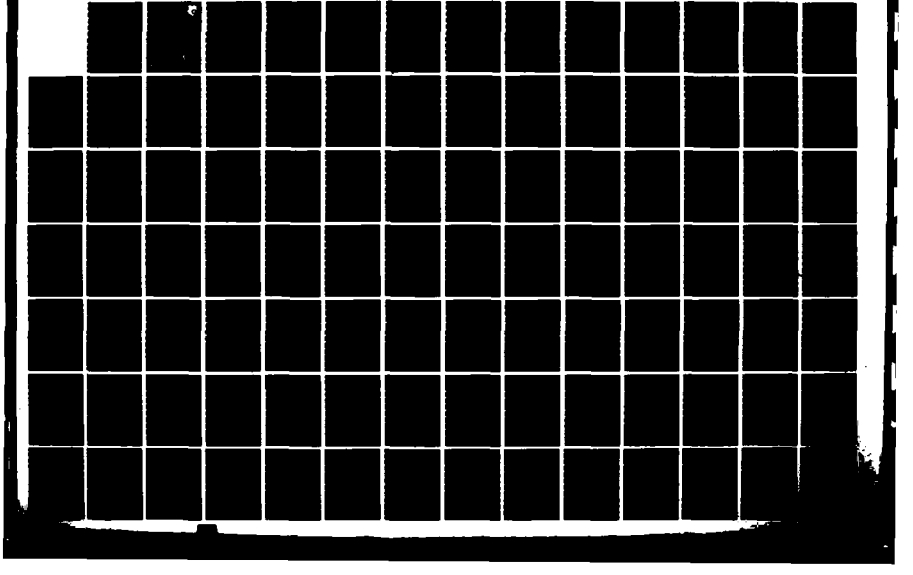

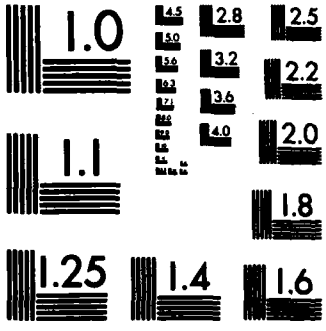


MICROCOPY RESOLUTION TEST CHART
NATIONAL BUREAU OF STANDARDS-1963-A

(12)




AFWAL-TR-83-2058, Vol I

# REPETITIVELY PULSED ELECTRIC LASER ACOUSTIC STUDIES

Volume I

K. U. INGARD, CHARLES F. MCMILLAN

DEPARTMENT OF AERONAUTICS AND ASTRONAUTICS
MASSACHUSETTS INSTITUTE OF TECHNOLOGY
CAMBRIDGE, MASSACHUSETTS 02139

SEPTEMBER 1983

FINAL REPORT FOR PERIOD JUNE 1980 - JUNE 1983



AERO PROPULSION LABORATORY
AIR FORCE WRIGHT AERONAUTICAL LABORATORIES
AIR FORCE SYSTEMS COMMAND
WRIGHT-PATTERSON AIR FORCE BASE, OHIO 45433

*NOTICE*

*When Government drawings, specifications, or other data are used for any purpose other than in connection with a definitely related Government procurement operation, the United States Government thereby incurs no responsibility nor any obligation whatsoever; and the fact that the government may have formulated, furnished, or in any way supplied the said drawings, specifications, or other data, is not to be regarded by implication or otherwise as in any manner licensing the holder or any other person or corporation, or conveying any rights or permission to manufacture use, or sell any patented invention that may in any way be related thereto.*

*This report has been reviewed by the Office of Public Affairs (ASD/PA) and is releasable to the National Technical Information Service (NTIS). At NTIS, it will be available to the general public, including foreign nations.*

*This technical report has been reviewed and is approved for publication.*

ALAN GARSCADDEN
Plasma Physics Group
Energy Conversion Branch

PAUL R. BERTHEAUD, Chief
Energy Conversion Branch
Aerospace Power Division

*FOR THE COMMANDER*

JAMES D. REAMS
Chief, Aerospace Power Division
Aero Propulsion Laboratory

*"If your address has changed, if you wish to be removed from our mailing list, or if the addressee is no longer employed by your organization please notify* AFWAL/POOC, *W-PAFB, OH 45433 to help us maintain a current mailing list".*

*Copies of this report should not be returned unless return is required by security considerations, contractual obligations, or notice on a specific document.*

UNCLASSIFIED

SECURITY CLASSIFICATION OF THIS PAGE (When Data Entered)

| REPORT DOCUMENTATION PAGE | | READ INSTRUCTIONS BEFORE COMPLETING FORM |
|---|---|---|
| 1. REPORT NUMBER<br>AFWAL-TR-83-2058 Volume I | 2. GOVT ACCESSION NO.<br>AD-A136538 | 3. RECIPIENT'S CATALOG NUMBER |
| 4. TITLE (and Subtitle)<br>REPETITIVELY PULSED ELECTRIC LASER ACOUSTIC STUDIES<br>Volume I | | 5. TYPE OF REPORT & PERIOD COVERED<br>Final Report for Period JUN 80 - JUN 83<br>6. PERFORMING ORG. REPORT NUMBER |
| 7. AUTHOR(s)<br>K.U. Ingard and Charles F. McMillan | | 8. CONTRACT OR GRANT NUMBER(s)<br>F33615-80-C-2040 |
| 9. PERFORMING ORGANIZATION NAME AND ADDRESS<br>Department of Aeronautics and Astronautics<br>Massachusetts Institute of Technology<br>Cambridge MA 02139 | | 10. PROGRAM ELEMENT, PROJECT, TASK AREA & WORK UNIT NUMBERS<br>61102F<br>2301S230 |
| 11. CONTROLLING OFFICE NAME AND ADDRESS<br>Aero Propulsion Laboratory (AFWAL/POOC-3)<br>Air Force Wright Aeronautical Laboratories (AFSC)<br>Wright-Patterson Air Force Base, Ohio 45433 | | 12. REPORT DATE<br>September 1983<br>13. NUMBER OF PAGES<br>200 |
| 14. MONITORING AGENCY NAME & ADDRESS(if different from Controlling Office) | | 15. SECURITY CLASS. (of this report)<br>Unclassified<br>15a. DECLASSIFICATION/DOWNGRADING SCHEDULE |

16. DISTRIBUTION STATEMENT (of this Report)

Approved for public release; distribution unlimited.

17. DISTRIBUTION STATEMENT (of the abstract entered in Block 20, if different from Report)

18. SUPPLEMENTARY NOTES

AFWAL-TR-83-2058, Volume II contains computer software; distribution is limited to DOD components only. Non-DOD requests must include the statement of terms and conditions contained in Atch 21 to AFR 300-6.

19. KEY WORDS (Continue on reverse side if necessary and identify by block number)

Closed Loop, Acoustical Disturbances, Shock Wave Propagation, Parallel-Baffle, Reflection Coefficients

20. ABSTRACT (Continue on reverse side if necessary and identify by block number)

This report summarizes a study of the acoustical characteristics of a closed loop duct system for pulsed lasers with emphasis on acoustic suppression technology.

Several topics are considered involving shock wave propagation reflection and attenuation in a shock tube, in which pulse waves are generated, simulating those in a pulsed laser system.

A detailed analysis of the design of parallel-baffle attenuators for

cont

DD FORM 1 JAN 73 1473 EDITION OF 1 NOV 65 IS OBSOLETE

UNCLASSIFIED

SECURITY CLASSIFICATION OF THIS PAGE (When Data Entered)

cont →

suppression of acoustic waves is given, allowing for the contributions of the reflectiom transmitted and reverberant contributions to the sound pressure field in the optical cavity. ←

The work carried out in the project involved theoretical and experimental studies of the following topics:

1. Development of a shock wave generator simulating the wave pulses produced in a pulsed laser.
2. Planning and assembling a data acquisition and processing system.
3. Experimental and theoretical studies of the propagation of shock wave pulses in a duct with hard walls and the reflection from discontinuities. This includes a procedure for numerical integration of the equations of motion (with associated computer program) as well as an approximate analysis leading to closed form expressions for attenuation and reflection of these waves.
4. Theoretical study of the attenuation and reflections characteristics of parallel-baffle attenuators with nonlocally reacting flexible porous baffles. The results are presented in a series of formulas and graphs and results for optimum design are given. In this context the theory for wave propagation in a porous flexible material is reviewed and extended. Furthermore, the pressure drop for the mean flow in is calculated with the results presented in graphical form.
5. Theoretical and experimental studies of the reflection of wave pulses from a perforated plate. This includes the determination of the optimum design for minimum flow resistance.
6. Acoustical system analysis of the closed loop, in which the relative significance of the reflected, transmitted, and reverberant sound fields in the laser cavity are compared.
7. Experimental studies of the interaction of a shock wave pulse with a porous flexible material. Compression of the material by the wave is demonstrated and measured as a function of the peak pressure of the incident pulse. The related pressure reflection coefficient is measured also.
8. Development of a FFT routine for determination of the frequency spectrum of the shock wave pulses.
9. Measurements of the frequency dependence of the insertion loss of parallel baffle attenuators and other elements.

# PREFACE

This report, presented in two volumes, describes acoustical studies related to repetitively pulsed electric lasers. The work was carried out in the Department of Aeronautics and Astronautics, Massachusetts Institute of Technology, Cambridge, Mass. under Contract F33615-8°C-2040.

The work was performed during the period June 1980-June 1983 under the direction of K.U. Ingard, Principal Investigator, and Charles F. McMillan. James Abbott assisted in the experimental work during the summer of 1982.

The valuable help extended by Dr. Alan Garscadden during the course of the program is gratefully acknowledged.



## TABLE OF CONTENTS

## SUMMARY

The acoustical problems associated with a closed loop pulsed gas laser ("circulator") involves the generation, transmission, and reflection of the shock wave pulses produced by the periodic ionization of the gas in the optical cavity and the noise produced by the compressor in the loop.

This report focuses on the problems of propagation and reflection of these waves, with special attention to the attenuation and reflection and optimum design of parallel-baffle attenuators and perforated plates. On the basis of these studies an acoustical system analysis is carried out, including a discussion of muffler design.

Thus, the work carried out in this project has involved both theoretical and experimental studies and can be structured as follows:

1. **Development of a shock wave generator simulating the wave pulses produced in a pulsed laser.**
2. **Planning and assembling a data acquisition and processing system.**
3. **Experimental and theoretical studies of the propagation of shock wave pulses in a duct with hard walls and the reflection from discontinuities.** This includes a procedure for numerical integration of the equations of motion (with associated computer program) as well as an approximate analysis leading to closed form expressions for attenuation and reflection of these waves.
4. **Theoretical study of the attenuation and reflection characteristics of parallel-baffle attenuators with nonlocally reacting flexible porous baffles.** The results are presented in a series of formulas and graphs and results for optimum design are given. In this context the theory for wave propagation in a porous flexible material is reviewed and extended. Furthermore, the pressure drop for the mean flow in is calculated with the results

presented in graphical form.

5. **Theoretical and experimental studies of the reflection of wave pulses from a perforated plate.** This includes the determination of the optimum design for minimum reflection.

6. **Acoustical system analysis of the closed loop,** in which the relative significance of the reflected, transmitted, and reverberant sound fields in the laser cavity are compared.

7. **Experimental studies of the interaction of a shock wave pulse with a porous flexible material.** Compression of the material be the wave is demonstrated and measured as a function of the peak pressure of the incident pulse. The related pressure reflection coefficient is measured also.

8. **Development of a FFT routine for determination of the frequency spectrum of the shock wave pulses.**

9. **Measurements of the frequency dependence of the insertion loss of a parallel baffle attenuators and other elements.**

# I. ACOUSTIC SYSTEM ANALYSIS

## 1. Introduction

In this section we shall analyze the overall acoustical characteristics of the closed loop laser duct system. Such a duct system is shown schematically in Fig. 1.

The purpose of the analysis is to determine the relative importance of the different contributions to the acoustic "contamination" of the optical cavity of the laser. This will aid in design of the attenuator in the loop, both in regard to the choice of material and dimensions. We shall use a linear acoustic model, assuming the sound to be generated by a pulsed sound source.

The acoustic contamination in the optical cavity can be considered to consist of three parts:

a). Sound pulses reflected from the entrance to the acoustic attenuator (or any other discontinuity in the duct loop).

b). Transmitted sound pulses returning to the cavity after one round trip in the loop.

c). Reverberant sound, built up through multiple reflections and transmissions in the loop in steady state operation of the pulsed source. Included in the reverberant field, which can be regarded as a "background" noise, is the contribution from the blower or compressor, which moves the gas through the loop.

Generally, when the attenuation of the attenuator is large, the reflection is large also, and the appropriate design involves a trade off between attenuation and reflection, so as to minimize to the pressure level in the laser cavity.

## 2. The attenuator.

In order to carry out a system analysis, we must be able to calculate the reflected, transmitted, and reverberant contributions to the sound pressure field in the optical cavity

in terms of the physical parameters of the attenuator and the duct system.

We make such an analysis tractable by using the results of our studies of the characteristics of parallel-baffle attenuators, summarized in VI and Appendix A. By considering nonlocally reacting (rather than the usually assumed locally reacting) baffles, we are able to express in closed form the attenuation and the reflection coefficient of the attenuator. In doing so, we have assumed the attenuator to be acoustically compact (baffle thickness and baffle separation small compared to a wavelength). As it turns out, this assumption can be made valid over the entire frequency range of interest

The interesting and important characteristic of such an attenuator is, that at a given frequency, the attenuation per unit length depends only on <u>one</u> gemometrical parameter, namely the fraction open area of the attenuator. This means, that for a given porous material the attenuation does not depend separately on the thickness and separation of the baffles, only on their ratio.

In other words, thick baffles, and a corresponding large separation of the baffles (for a given open area fraction) are not required for high attenuation at low frequencies. This is a distinct advantage at high frequencies, because with thin baffles and a corresponding small separation between them, the problem of acoustic "beaming" and a corresponding reduction in the attenuation at high frequencies can be avoided without a penalty at low frequencies.

It is possible also, as shown in Appendix B, to derive simple expressions for the optimum flow resistance of the porous material in the baffles and the corresponding maximum attenuation. The maximum attenuation thus obtained is compared with the optimum attenuation curves for locally reacting baffles for different baffle thicknesses. Here the reduction in attenuation due to

beaming for an attenuator is clearly seen to occur at frequencies above a certain characteristic value, at which the wavelength is of the order of the width of the air gap between baffles.

## 3. Comparison of pressure levels.

We assume the sound source to be pulsed with an acoustic energy E emitted per pulse. With a pulse duration $\tau$, the average acoustic intensity is $E/\tau$, and the corresponding mean square value of the sound pressure in the cavity $\langle p^2 \rangle = (1/\rho c)(E/\tau A)$, where A is the duct area in the cavity (perpendicular to the axis of the duct).

The pressure reflection coefficient $R_p$ at the entrance to the attenuator is calculated in Section VI as a function of the various physical parameters of the system. Examples of the computed frequency dependence of the reflection coefficient are also given.

The acoustic power reflected from the attenuator will be $R^2 P$, where P is the incident power, and the mean square pressure level in dB will be

$$L_A = 10 \cdot \log(R_p^2) \tag{3.1}$$

with respect to the reference level

$$L_{ref} = 10 \cdot \log[(1/\rho c)(W/\tau A)] \tag{3.2}$$

of the incident wave.

The attenuation characteristics of the attenuator are calculated in detail in Section VI,3, where examples of the computed frequency dependence are given. The attenuation constant is the imaginary part of the propagation constant, $k_i$, and the corresponding sound pressure level of the transmitted wave is

$$L_B = 10 \cdot \log[\exp(-k_i L)] \simeq -8.7\ k_i L \ \text{dB} \tag{3.3}$$

with respect to the reference level in Eq. 3.2. Both $L_A$ and $L_B$ are independent of the cross sectional area of the attenuator.

In our calculation of the level of the reverberant field, we assume, that the acoustic energy absorption in the duct occurs in the attenuator only. The mean square pressure $<p^2>$ in the region between the attenuator and the optical cavity will be approximately uniform. The power entering the attenuator is then $I(1-R_p^2)A$, where $I=G(<\rho^2>/\rho c)$ and A the duct area at the entrance to the attenuator.

The factor G is 1 for a plane sound wave along the duct and 1/4 in a diffuse sound field. The actual value for G depends on the duct diameter and the wavelength range of interest. With a duct diameter D, there will be no propagating higher modes in the duct at frequencies below the cut-off frequency c/1.7D. Below this frequency only the plane wave can propagate and G=1. For example, with D=12", the cut-off frequency typically will be 600-700 Hz. Actually, for the purposes of the present discussion, the value of G is not critical.

The acoustic power absorbed by the attenuator will be $FIA_1(1-R_p^2)[1-\exp(-2k_iL)]$. In steady state, this must equal the average power W/T emitted by the source, where W is the acoustic energy per pulse and T the time interval between pulses. Using the same reference level, $L_{ref}$, as before, we then obtain for the level of the reverberant field

$$L_C=10\cdot\log[C'/(1-R_p)(1-\exp(-1k_iL))] \qquad (3.4)$$

$$C'=(\tau/T)(A/A_1)$$

In Figs.3-6 , we have plotted the reflected, transmitted, and reverberant sound pressure levels as a function of the open area fraction of the attenuator for some different values of the flow resistance of the baffle material and the frequency. The total length of the attenuator in this example is L=3 m, but the result

for L=1 and 2 m are quite similar, as will discussed later. The attenuator may be split into two sections, on either side of the laser cavity.

The parameter $\eta=(\tau/T)(A/A_1G)$ has been chosen to be .01. Typically, $A/A_1=.5$, and with $G\simeq.5$, this parameter is approximately equal to the duty cycle $\tau/T$ of the source. Actually, the level of the reverberant field turns out to be close to $10\log(\eta)$, which in the present example is -20 dB relative to the reference level of the incident wave.

As a specific example, consider Fig. 4 , for which the flow resistance is R=.05 and L=3 m. At a frequency of 100 Hz, the reflected sound pressure is larger than the transmitted for open area fractions less than .35, and the opposite holds true for values larger than .35. The corresponding value for the open area fraction for 500 Hz is .45. At this latter value, and with =.01, assumed here, the reverberant level dominates. On the other hand, an equally realistic value for $\eta$ would have been .001, in which case the reverberant level will be approximately -30 dB, below either of the two other levels.

## 4. Optimum design.

Another presentation of the results, less detailed but more useful from the standpoint of design, is used in Figs. 7-11. In these, we have considered only the reflected and transmitted sound and have plotted the larger of the levels of these as a function of the flow resistance R, with the frequency F and open area fraction S as parameters.

We note, that for each set of values of F and S, there exist an optimum value of the flow resistance of the baffle material, for which the sound pressure level is a minimum. For example, with L=3 m, S=.5 and F=500 Hz, the optimum resistance is R=.06 ro-ce units/cm, and for L=2 and 1 m with the same values for S and F, the optimum values for R are .09 and .18, respectively. The

corresponding minimum values for the sound pressure level for L=1, 2, and 3 m are -13, -20, and -22 dB, respectively. For another value of the open area fraction, S=.25, with F=500 Hz, the optimum values of R are seen to be .08, .043, and .03 for L=1, 2, and 3 m, with the corresponding minimum sound pressure levels -17, -19, and -20.5 dB, respectively.

From similar computations for other values of S, we can determine, for each value of F, the set of values of S and R, which yields the lowest minimum value of the sound pressure level. With reference to Figs. 3-6, this corresponds to the parameter values, for which the levels of the reflected and transmitted sounds are equal.

In Fig. 13 , we have shown this optimum relationship between the open area fraction S and the flow resistance R, and in Fig. 14 the corresponding lowest value of the sound pressure level is plotted as a function of R.

These results may serve as useful guides in the optimum design of a parallel-baffle attenuator. The choice of parameter values depends, of course, on the frequency spectrum of the incident wave, and if a wide frequency range is involved, it may be advantageous to have two or more attenuator sections in series, each section being optimized for a particular frequency.

We note, that at a frequency of about 500 Hz, the optimum flow resistance is of the order of .1 ρc-units/cm, where ρ is the density and c the sound speed in the laser gas. Most flow resistance data refer to measurements in air at atmospheric pressure, corresponding to the density $\rho_0$ and the sound speed $c_0$. Thus, in terms of the characteristic impedance of air, the typical optimum value of the flow resistance is $R \simeq .1(\rho c/\rho_0 c_0)\ \rho_0 c_0$ units/cm. For a laser operating at a pressure of 100 mm Hg, the ratio $\rho c/\rho_0 c_0$ will be approximately .1, and the corresponding optimum flow resistance $R \simeq .01\ \rho_0 c_0$ units/cm.

The flow resistance of materials commonly used in noise con-

trol engineering is larger than this optimum value. Furthermore, these materials usually are flexible, and, as discussed elsewhere in this report, a rigid porous materis is preverable in the present application.

Examples of rigid porous materials with the proper flow resistance are porous ceramics and porous metals, such as porous aluminum, typically with 20-40 pores per inch.

5. Proposed attenuator configuration.

As discussed in Section IV of this report, the measured reflected amplitude of a shock wave from an open end of a tube is comparatively large. This applies also to the reflection at a sudden change in the cross section of the duct. The reflection can be reduced, if the change in cross section is gradual, as it is in the duct loop in Fig. 1 In order to be effective, however, this gradual change has to quite small, corresponding to a longer transition piece than that shown in Fig. 1.

With reference to our measurements of the reflection from orifice plates (or perforated plates) in Section IV, we note, however, that the reflected wave from the open end of a tube, (and, correspondingly, from a change in duct cross section), can be reduced considerably by covering the open end with a perforated plate, with a properly chosen open area fraction. The optimum open area fraction depends on the peak pressure of the incident pulse, as described in Section IV. Typically, the open area fraction is about 60 % for an incident peak pressure of about .75 atm., and it increases with increasing peak pressure.

This suggests, that the pressure reflection from the transition piece in the duct loop in Fig. 1 can be reduced by the insertion of a perforated plate or "wedge" (or cone), as indicated schematically in Fig. 15. This changes to transition piece into a "lossy" diffusor. The angle of the perforated wedge or cone can be varied to yield optimum acoustical performance

for a given permitted static pressure drop across the perforated plate. The pressure drop decreases with decreasing wedge angle, of course.

This diffusor should be combined with a parallel-baffle attenuator, as indicated, to reduce the transmitted pulse. We did not have an opportunity to study the optimum design of it, but the results presented in Section IV should provide guide lines in the design. Attenuators of this kind should be placed on both sides of the discharge cavity, as indicated.

The static pressure drop over the perforated plate due to the mean flow in the duct is of the order of $\Delta P=(1/S^2)\gamma PM^2/2$, where M is the average Mach number of the flow on the upstream side of the plate, P the static pressure, S the open area fraction of the plate, and $\gamma$ the specific heat ratio. With S=.6 and M=.03 the pressure drop will be less than 1" of water at atmospheric pressure.

Another observation, which may or may not be relevant, is the possibility of designing the parallel baffle attenuator in such a way, that it will function also as a heat exchanger. The baffles could be made of porous metal, and, as shown in Section VI, the attenuation depends only on the open area fraction and not on the thickness of baffles. This fact possibly could be exploited, leading to an attenuator-heat exchanger, which consists of thin, closely spaced porous plates.

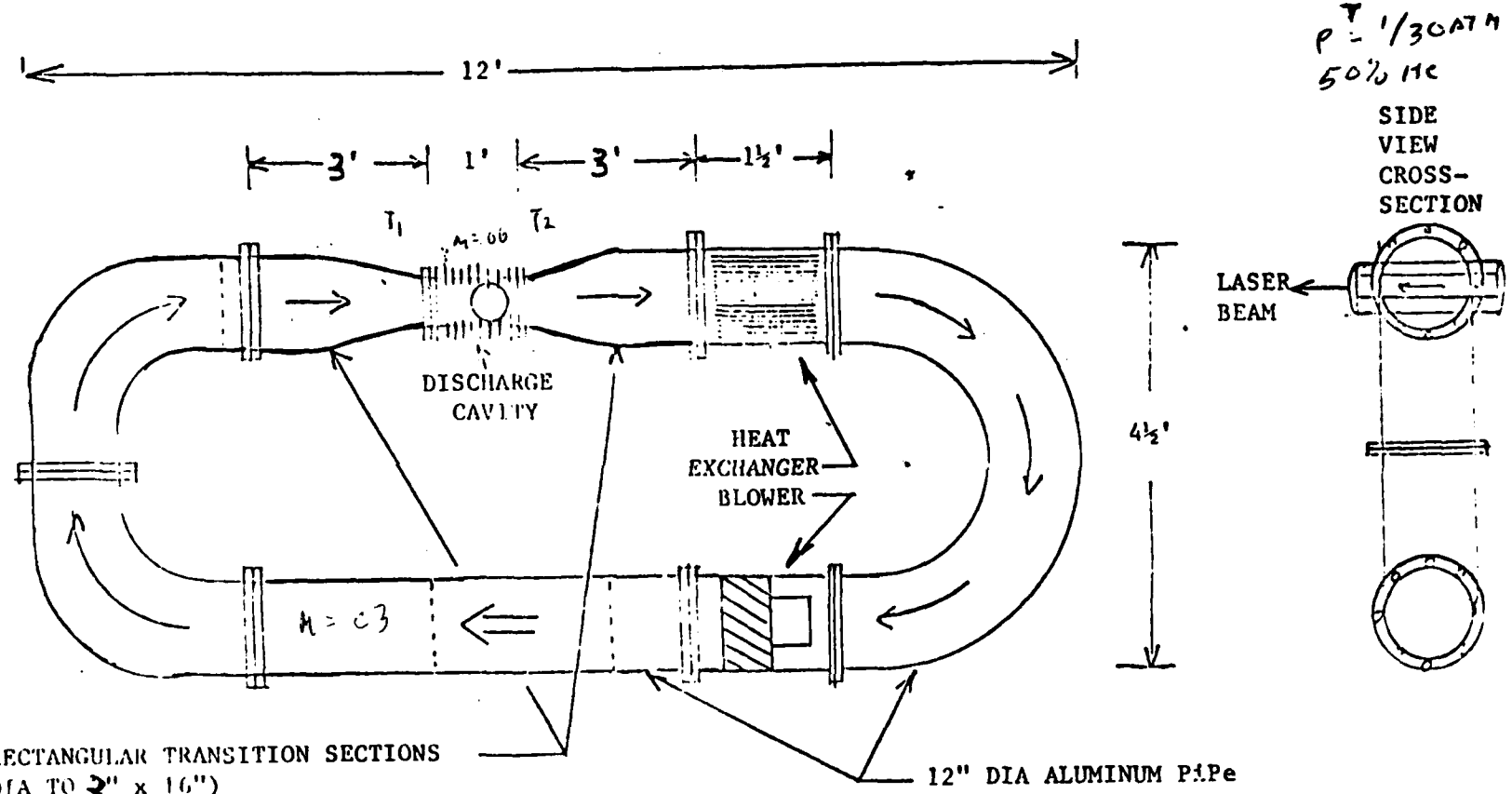


*Fig. II.1.*
*TYPICAL DUCT CONFIGURATION (not necessarily typical dimensions) FOR PULSED LASER.*

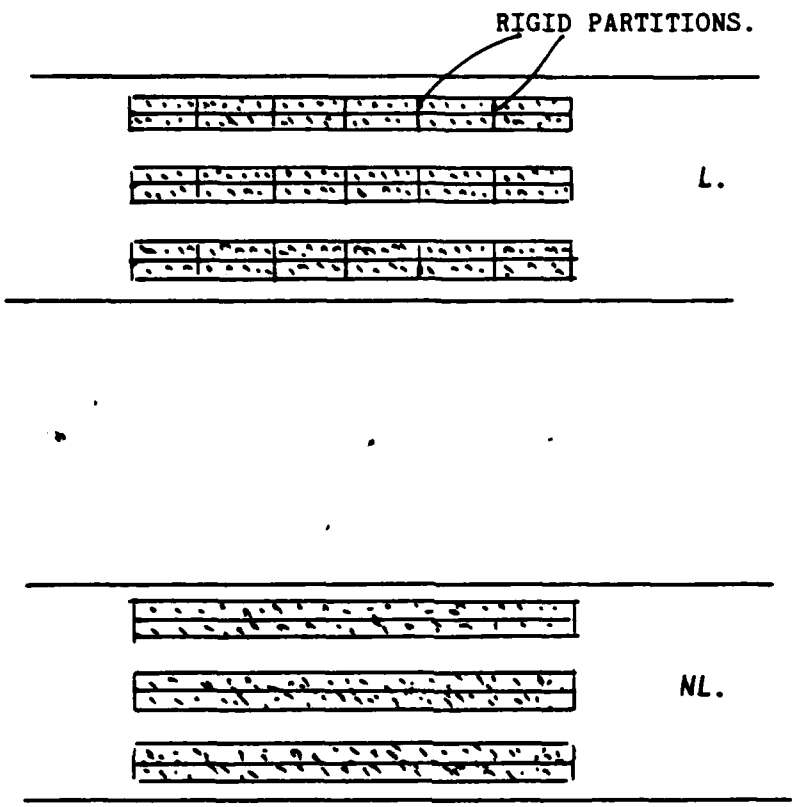


Fig. II.2.
LOCALLY (L) AND NONLOCALLY (NL) REACTING PARALLEL BAFFLE ATTENUATORS IN A DUCT.

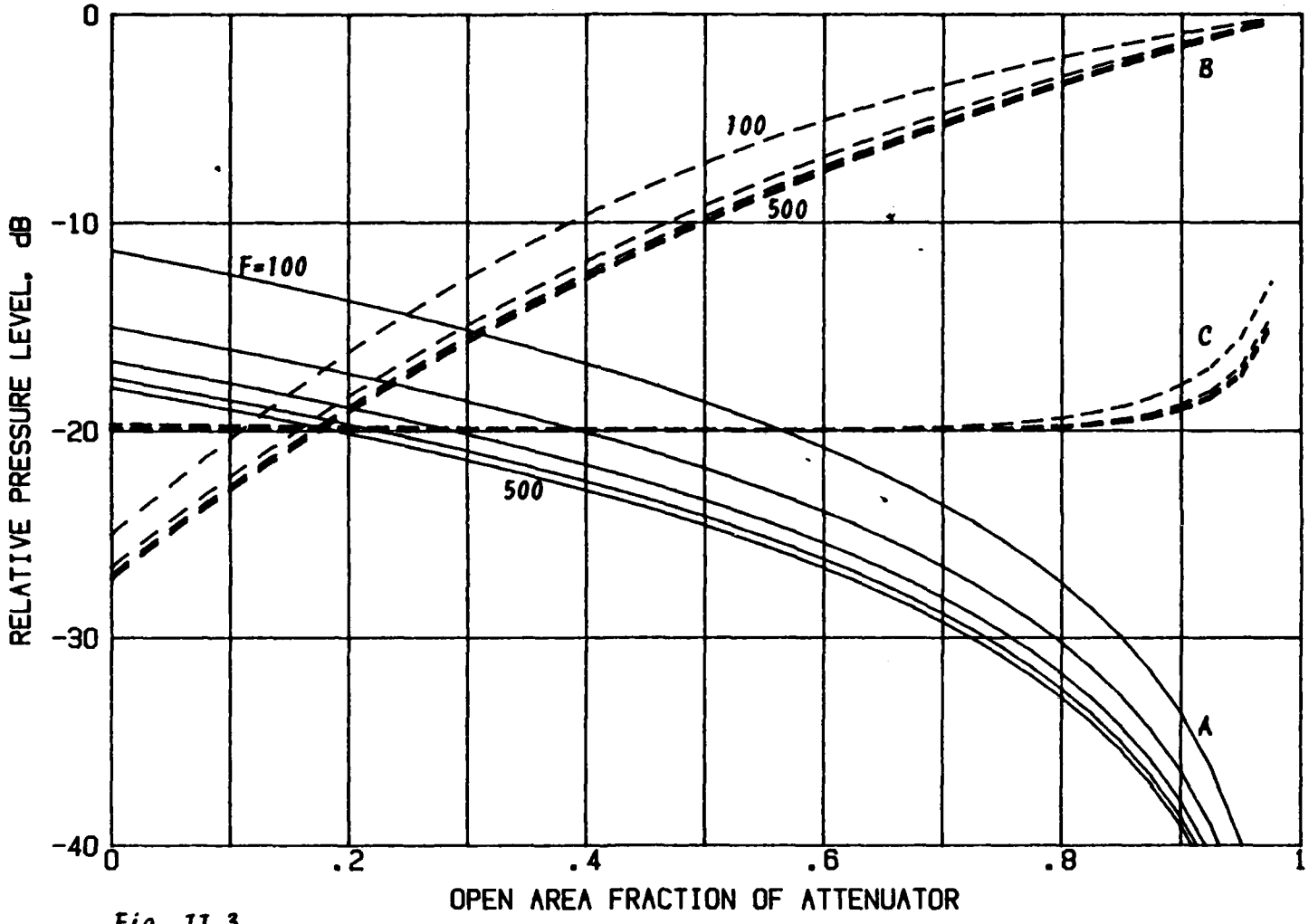


*Fig. II.3.*
*REFLECTED (A), TRANSMITTED (B), AND REVERBERANT (C) PRESSURE LEVELS IN A CLOSED LOOP DUCT CONTAINING A PARALLEL-BAFFLE ATTENUATOR.*

*DATA. Porous baffles: Rigid and nonlocally reacting. Flow resistance, R=.025 ro-ce units/cm. Porosity, H=.95. Structure factor, G=1.5*
*Length of attenuator, L=3 m.*
*Duty cycle of pulsed sound source, t/T=.01. Frequency, F=100, 200, 300, 400, 500 Hz*

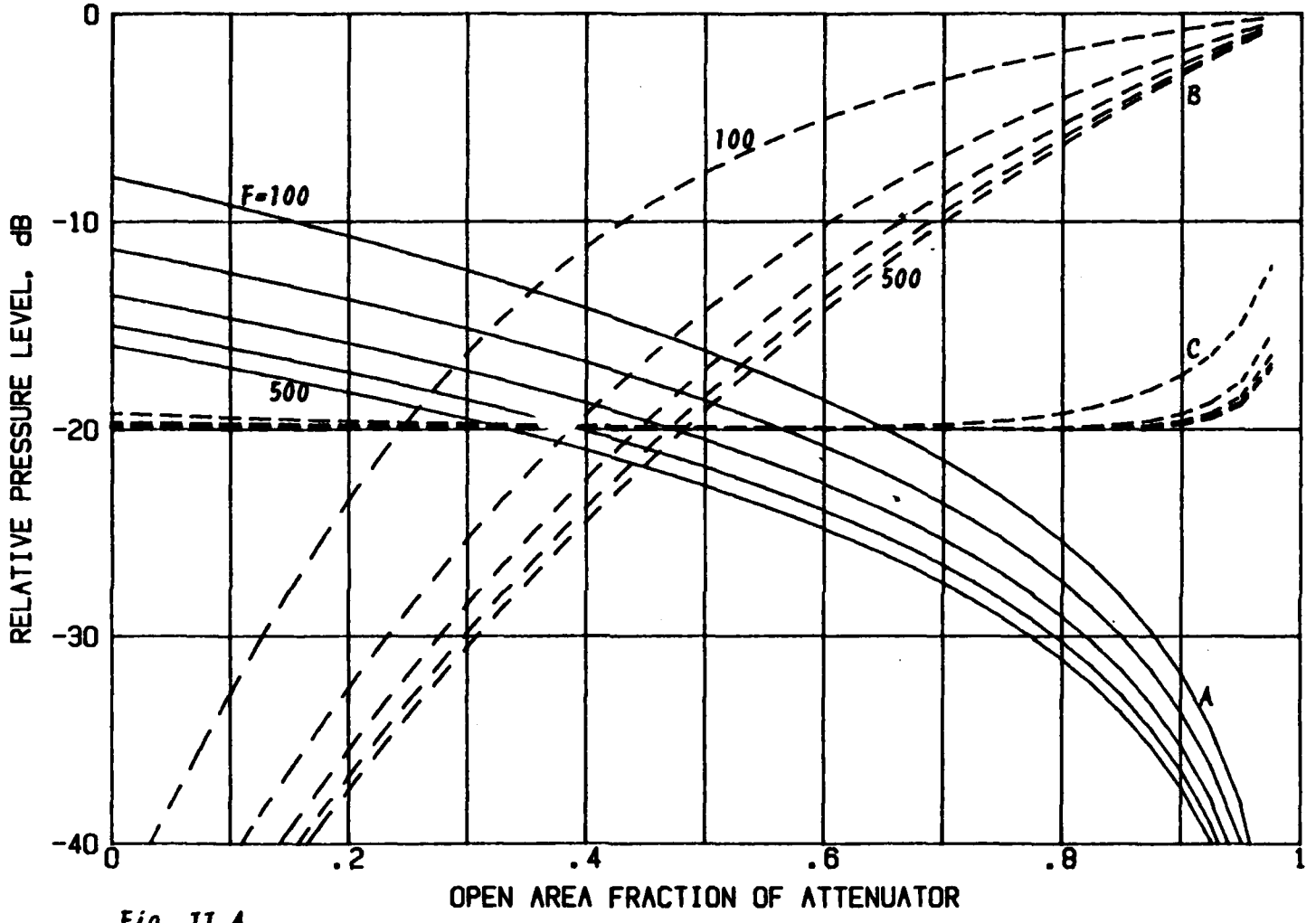


*Fig. II.4.*
*REFLECTED (A), TRANSMITTED (B), AND REVERBERANT (C) PRESSURE LEVELS IN A CLOSED LOOP DUCT CONTAINING A PARALLEL-BAFFLE ATTENUATOR.*

*DATA. Porous baffles: Rigid and nonlocally reacting. Flow resistance, R=.05 ro-ce units/cm. Porosity, H=.95. Structure factor, G=1.5*
*Length of attenuator, L=3 m.*
*Duty cycle of pulsed sound source, t/T=.01. Frequency, F=100, 200, 300, 400, 500 Hz*

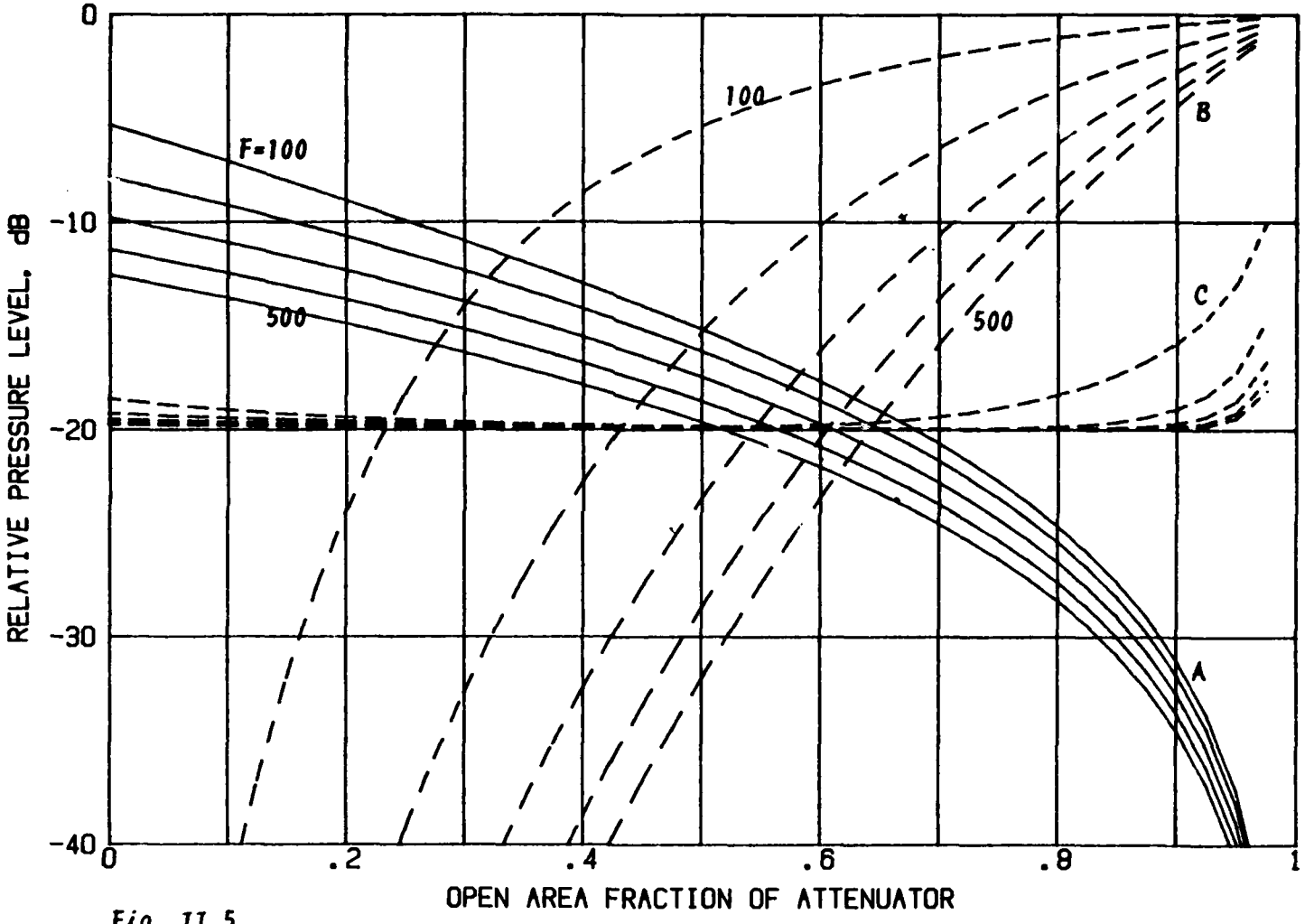


*Fig. II.5.*
*REFLECTED (A), TRANSMITTED (B), AND REVERBERANT (C) PRESSURE LEVELS IN A CLOSED LOOP DUCT CONTAINING A PARALLEL-BAFFLE ATTENUATOR.*

*DATA. Porous baffles: Rigid and nonlocally reacting. Flow resistance, R=.1 ro-ce units/cm. Porosity, H=.95. Structure factor, G=1.5*
*Length of attenuator, L=3 m.*
*Duty cycle of pulsed sound source, t/T=.01. Frequency, F=100, 200, 300, 400, 500 Hz*

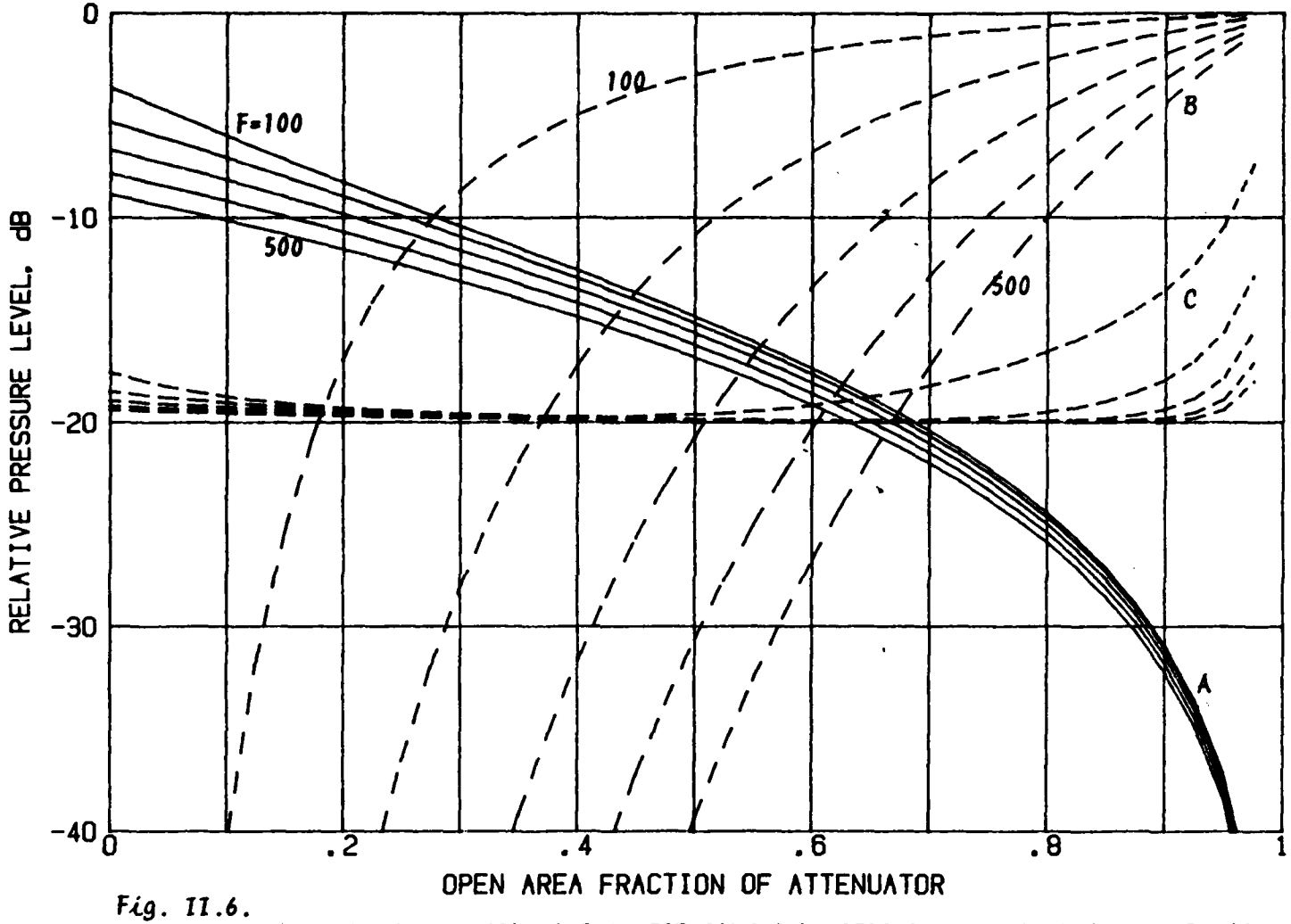


*Fig. II.6.*
REFLECTED (A), TRANSMITTED (B), AND REVERBERANT (C) PRESSURE LEVELS IN A CLOSED LOOP DUCT CONTAINING A PARALLEL-BAFFLE ATTENUATOR.

*DATA. Porous baffles: Rigid and nonlocally reacting. Flow resistance, R=.2 ro-ce units/cm. Porosity, H=.95. Structure factor, G=1.5*
*Length of attenuator, L=3 m.*
*Duty cycle of pulsed sound source, t/T=.01. Frequency, F=100, 200, 300, 400, 500 Hz*

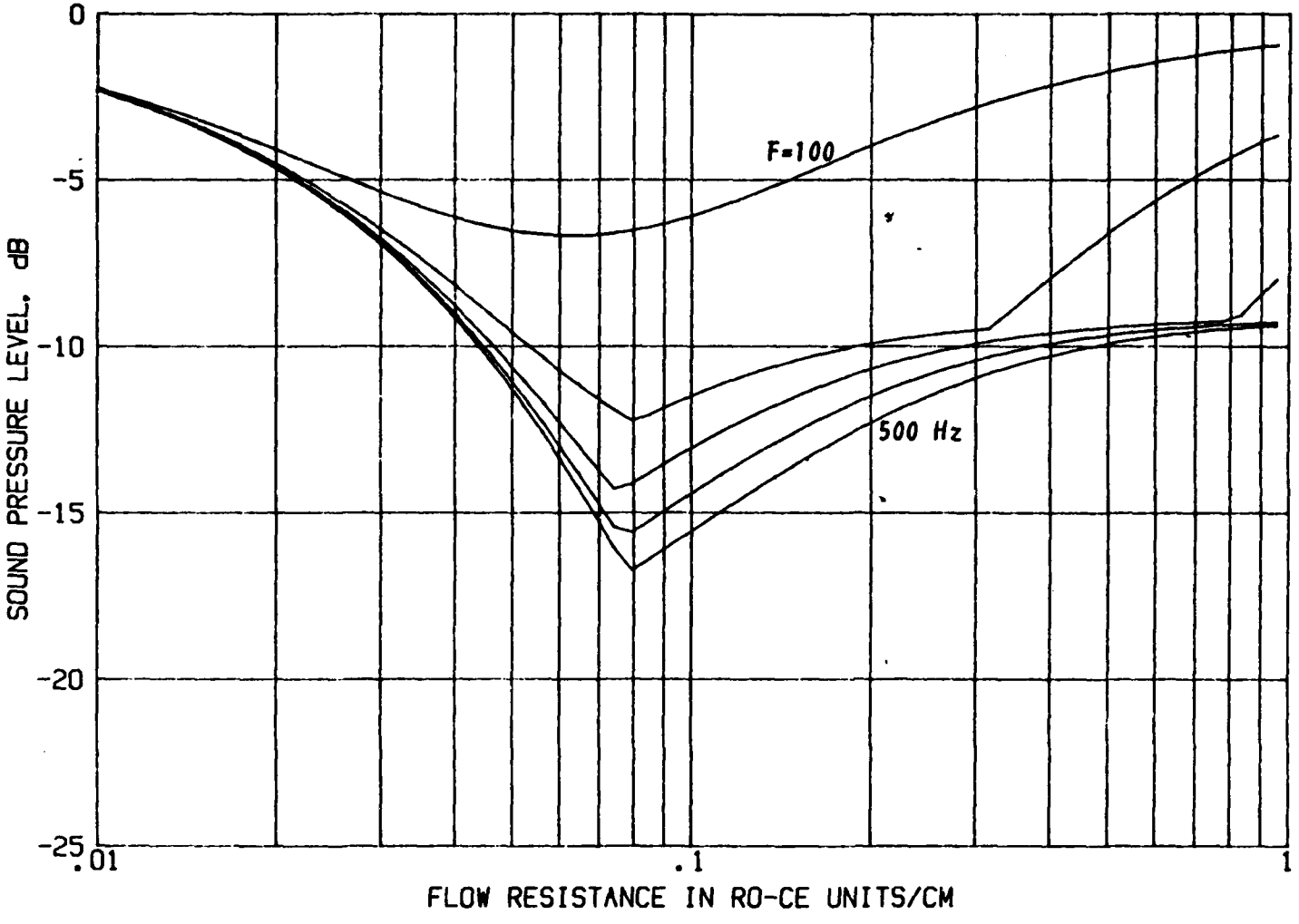


*Fig. II.7.*
PARALLEL-BAFFLE ATTENUATOR. LEVEL OF THE REFLECTED OR TRANSMITTED SOUND (WHICHEVER IS THE LARGER) RELATIVE TO THE LEVEL OF THE INCIDENT WAVE.

DATA. *Porous baffles: Rigid and nonlocally reacting. Porosity,* H=.95. *Structure factor,* G=1.5.
*Open area fraction,* S=.25. *Length,* L=1 m. *Frequency,* F=100, 200, 300, 400, 500 Hz.

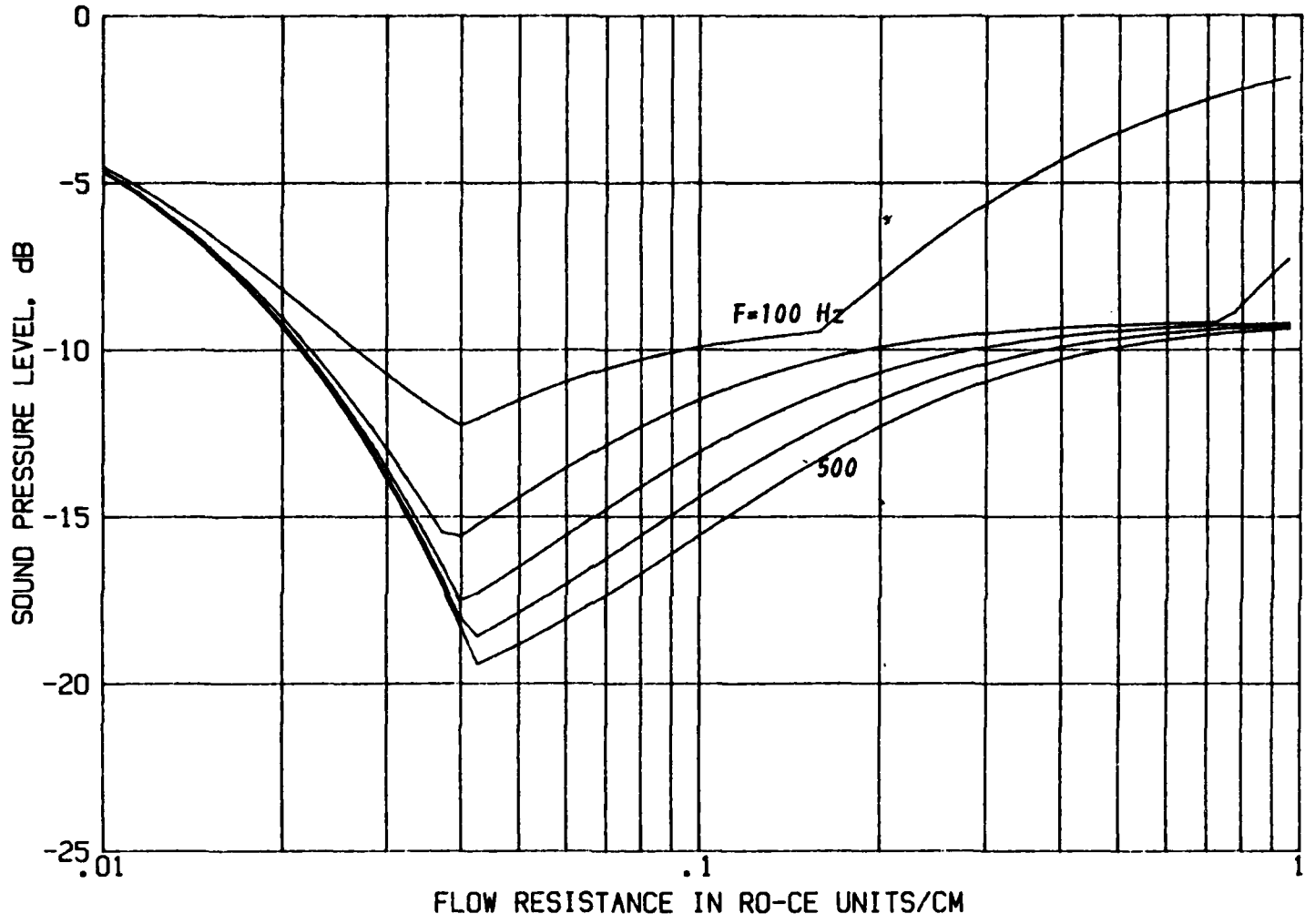


*Fig. II.8.*
PARALLEL-BAFFLE ATTENUATOR. LEVEL OF THE REFLECTED OR TRANSMITTED SOUND (WHICHEVER IS THE LARGER) RELATIVE TO THE LEVEL OF THE INCIDENT WAVE.

*DATA. Porous baffles: Rigid and nonlocally reacting. Porosity, H=.95. Structure factor, G=1.5.*
*Open area fraction, S=.25. Length, L=2 m. Frequency, F=100, 200, 300, 400, 500 Hz.*

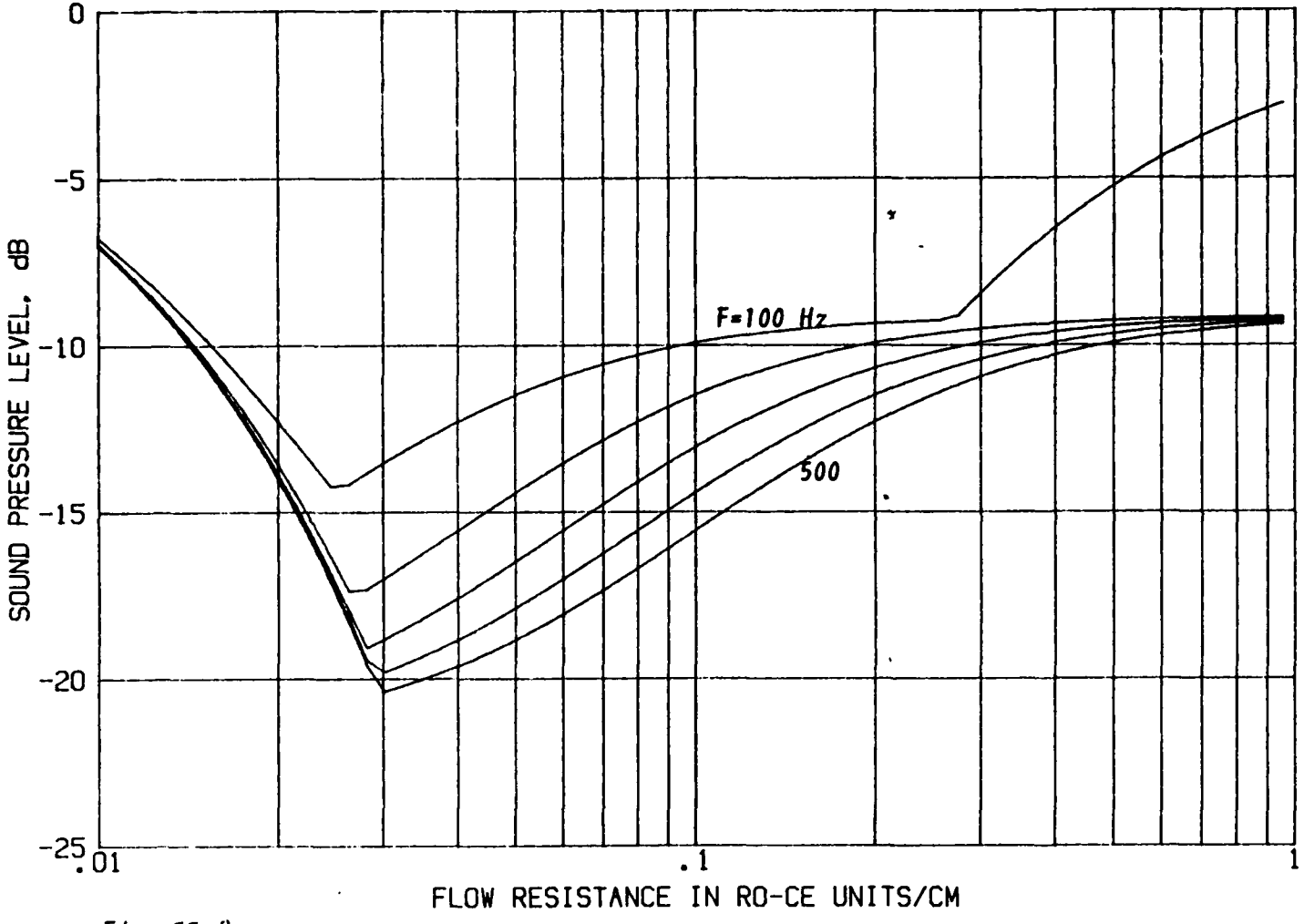


*Fig. II.9 .*
PARALLEL-BAFFLE ATTENUATOR. LEVEL OF THE REFLECTED OR TRANSMITTED SOUND (WHICHEVER IS THE LARGER) RELATIVE TO THE LEVEL OF THE INCIDENT WAVE.

*DATA. Porous baffles: Rigid and nonlocally reacting. Porosity, H=.95. Structure factor, G=1.5.*
*Open area fraction, S=.25. Length, L=3 m. Frequency, F=100, 200, 300, 400, 500 Hz.*

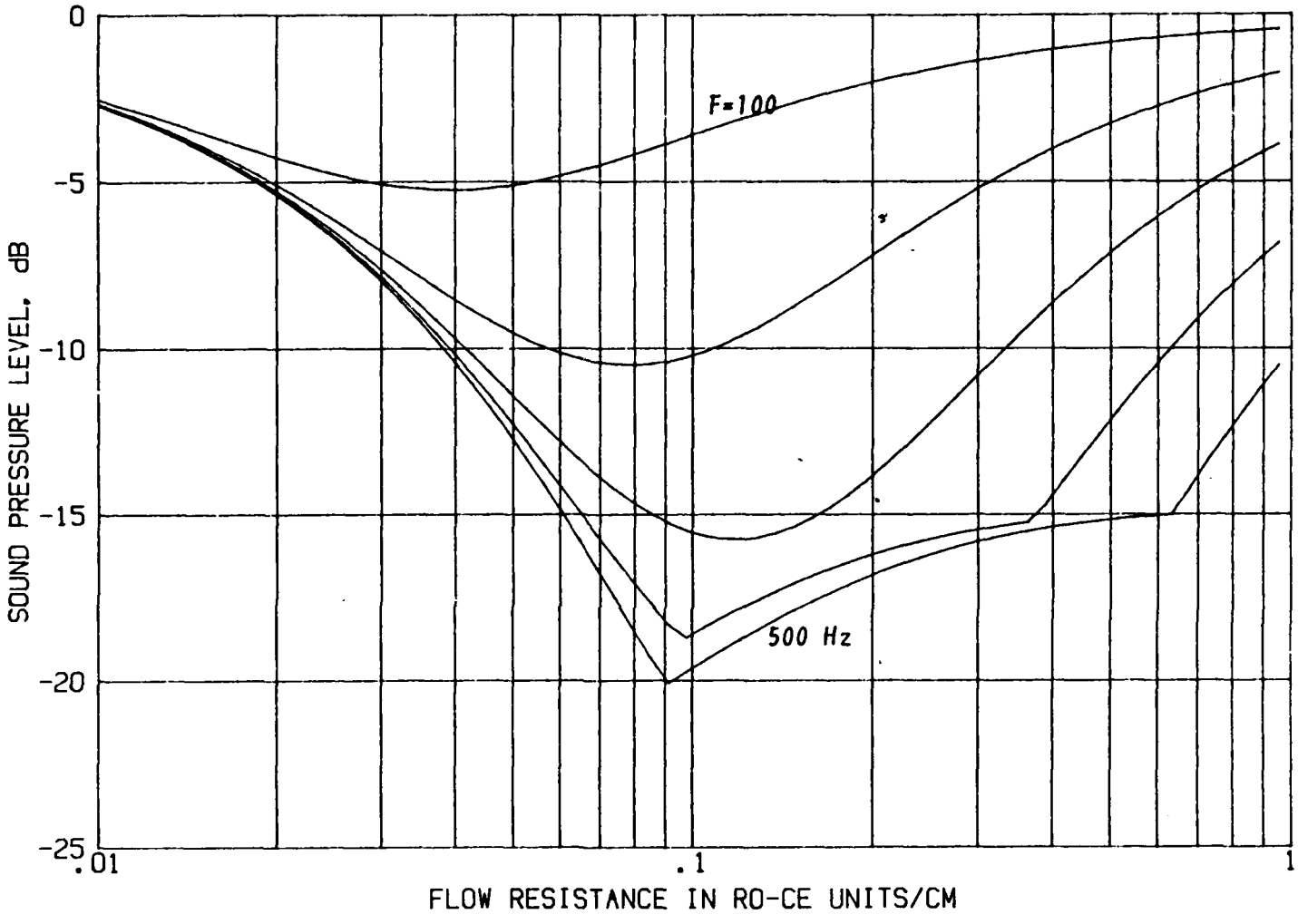


*Fig. II.10.*
PARALLEL-BAFFLE ATTENUATOR. LEVEL OF THE REFLECTED OR TRANSMITTED SOUND (WHICHEVER IS THE LARGER) RELATIVE TO THE LEVEL OF THE INCIDENT WAVE.

DATA. Porous baffles: Rigid and nonlocally reacting. Porosity, H=.95. Structure factor, G=1.5.
Open area fraction, S=.50. Length, L=2 m. Frequency, F=100, 200, 300, 400, 500 Hz.

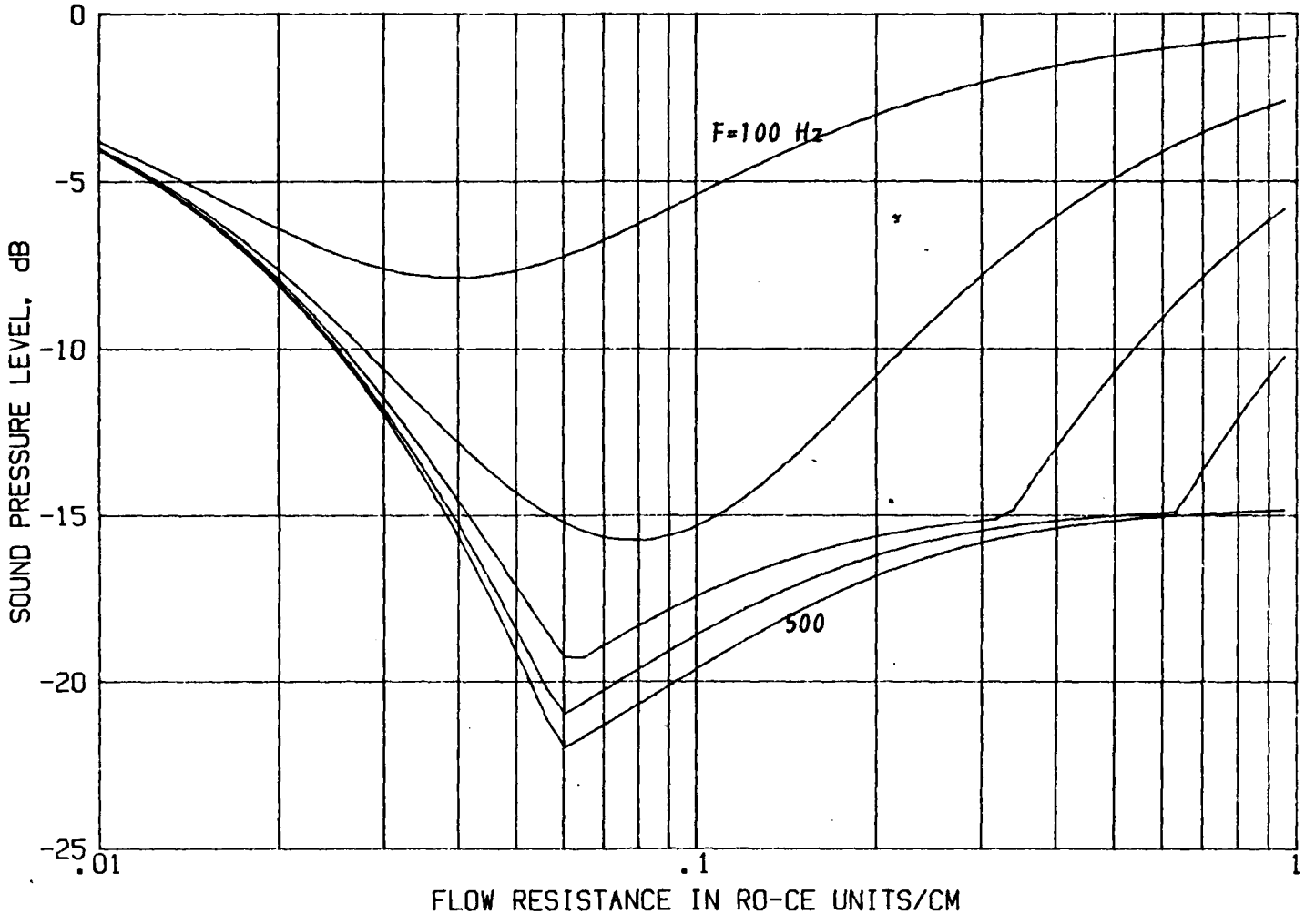


*Fig. II.11.*
*PARALLEL-BAFFLE ATTENUATOR. LEVEL OF THE REFLECTED OR TRANSMITTED SOUND (WHICHEVER IS THE LARGER) RELATIVE TO THE LEVEL OF THE INCIDENT WAVE.*

*DATA. Porous baffles: Rigid and nonlocally reacting. Porosity, H=.95. Structure factor, G=1.5.*
*Open area fraction, S=.50. Length, L=3 m. Frequency, F=100, 200, 300, 400, 500 Hz.*

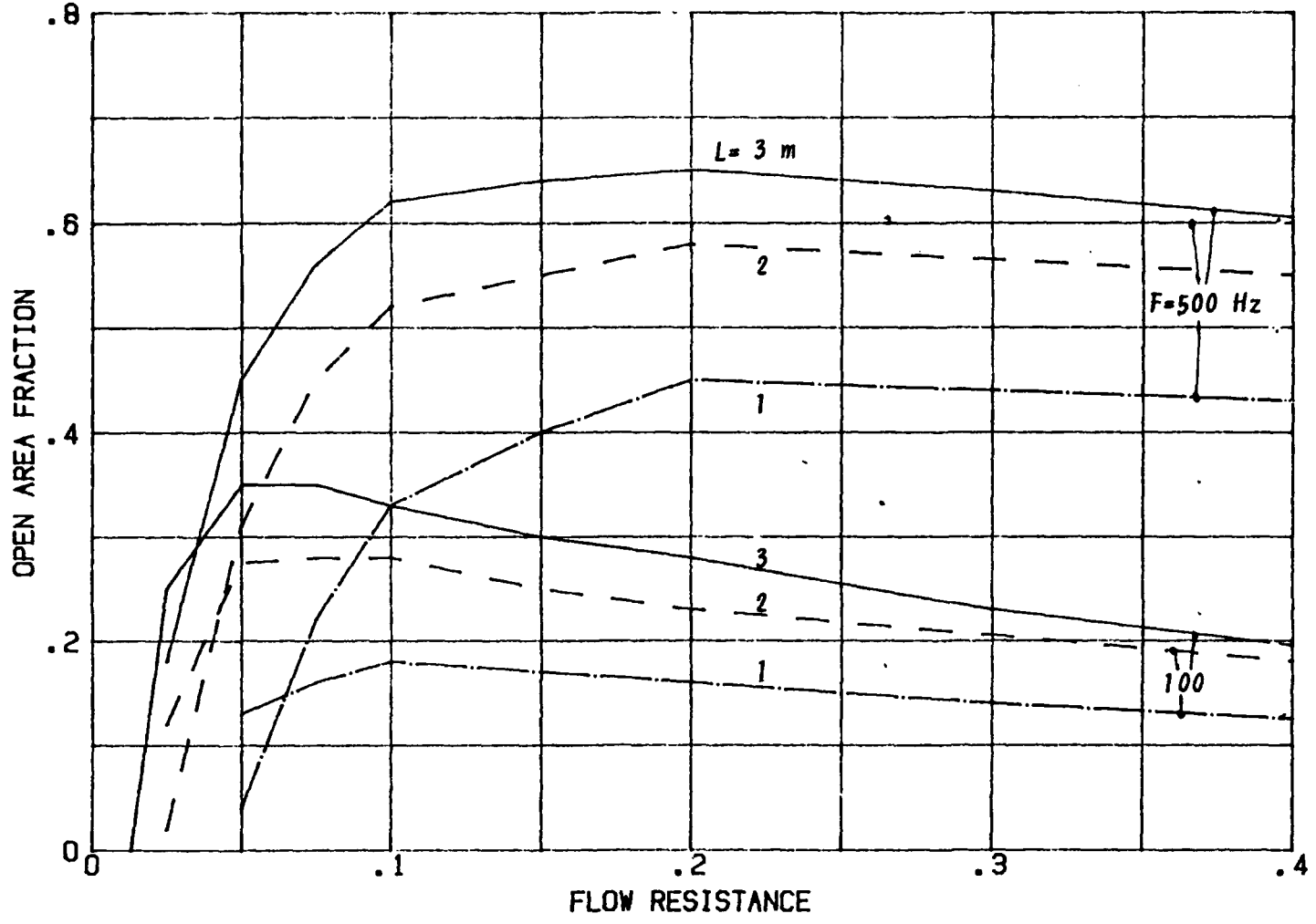


*Fig. II.12.*
PARALLEL-BAFFLE ATTENUATOR. OPTIMUM COMBINATION OF FLOW RESISTANCE AND OPEN AREA FRACTION TO YIELD THE MINIMUM SOUND PRESSURE LEVEL IN FIG.

*DATA. Porous baffles. Rigid and nonlocally reacting. Porosity H=.95. Structure factor, G=1.5. Flow resistance R in ro-ce units/cm.*
*Attenuator length, L=1, 2, 3 m. Frequency, F=100, 500 Hz.*

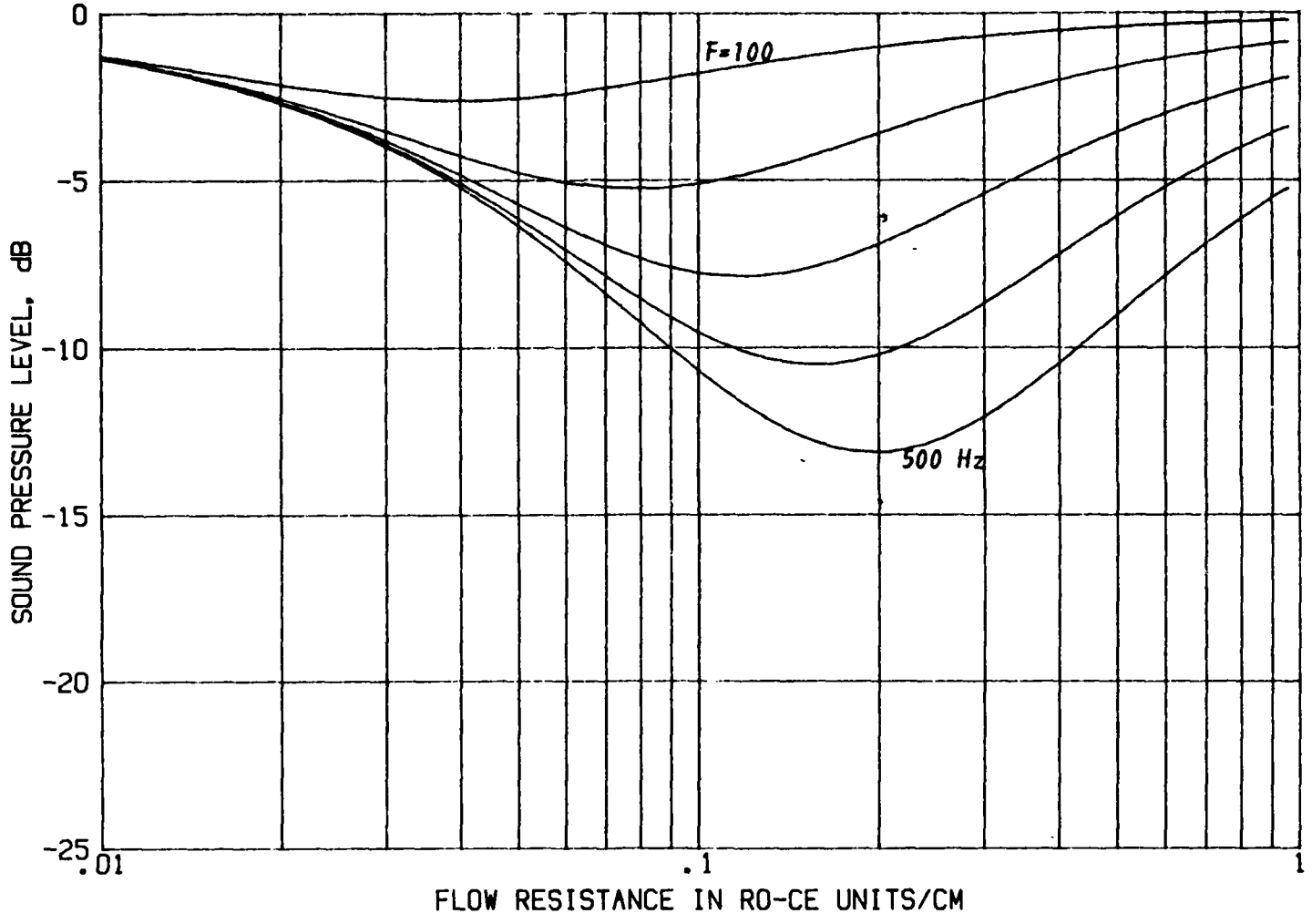


*Fig. II.13.*
*PARALLEL-BAFFLE ATTENUATOR. LEVEL OF THE REFLECTED OR TRANSMITTED SOUND (WHICHEVER IS THE LARGER) RELATIVE TO THE LEVEL OF THE INCIDENT WAVE.*

*DATA. Porous baffles: Rigid and nonlocally reacting. Porosity, H=.95. Structure factor, G=1.5.*
*Open area fraction, S=.50. Length, L=1 m. Frequency, F=100, 200, 300, 400, 500 Hz.*

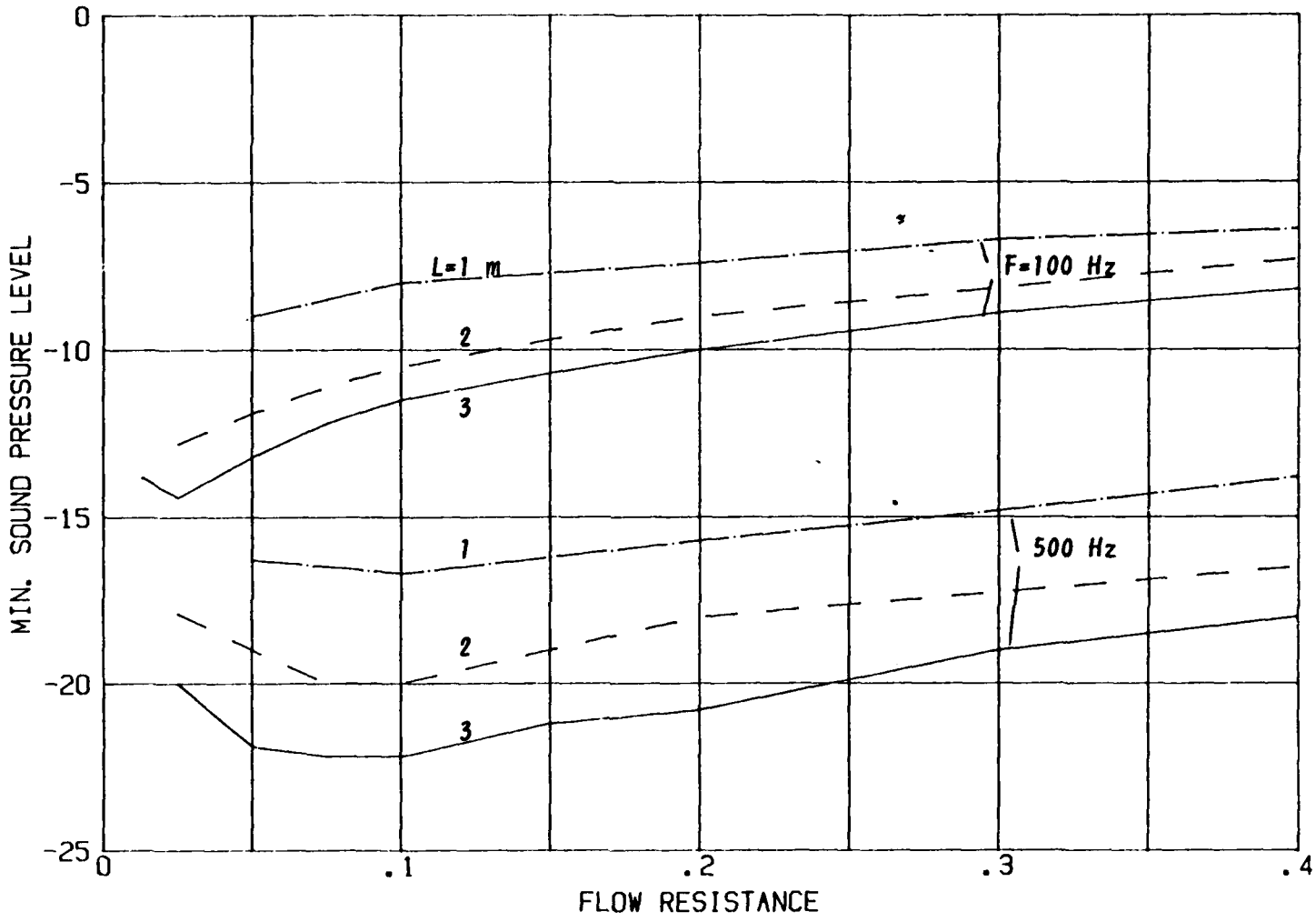


*Fig. II.14.*
PARALLEL-BAFFLE ATTENUATOR. MINIMUM SOUND PRESSURE LEVEL, WHICH OCCURS WHEN LEVELS OF REFLECTED AND TRANSMITTED SOUND PRESSURES ARE EQUAL.

*DATA. Porous baffles: Rigid and nonlocally reacting. Porosity, H=.95. Structure factor, G=1.5. Flow resistance R in ro-ce units/cm.*
*Length of attenuator, L=1, 2, 3 m. Frequency, F=100, 500 Hz.*
*Open area fraction, see Fig.12.*

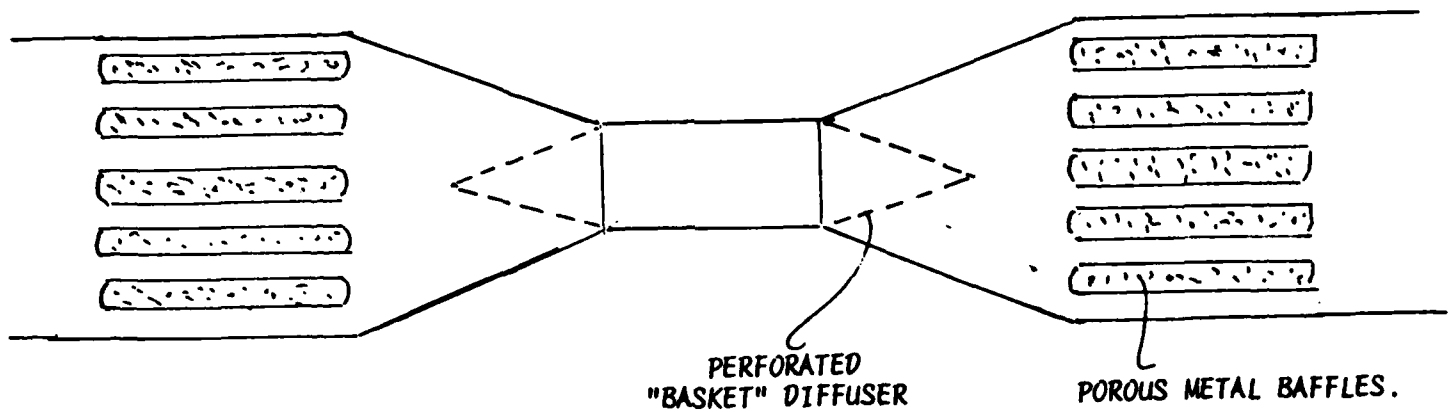


Fig. II.15.
PROPOSED ATTENUATOR CONFIGURATION. The perforated basket diffuser reduces the reflection from the area change in the duct.

## II. EXPERIMENTAL APPARATUS

Shock tube.

An essential initial experimental problem concerned the generation of a shock wave in a tube similar in character to the pulse generated in a pulsed laser. Our first attempt involved the use of spark generator. Two electrodes were inserted into a lucite tube section perpendicular to the tube axis and the spark gap was adjustable. The electrodes were connected to a bank of capacitors with low internal resistance (they had formally been used in studies of exploding wires). The capacitors were charged by means of a high voltage power supply (15 kV) and discharged by means of a switch through the spark gap. Although considerable efforts were made to get this shock wave generator to perform properly, we had serious problems with triggering, repeatability, and electrical noise affecting our data acquisition system. Therefore, this approach was eventually abandoned.

Instead we turned to the use of a shock tube with a short driver section. In an ordinary shock tube, the driver section is long enough, so that the shock wave will simulate a step function. This type of wave was not desired in our case, however, but rather a pulse with an approximately triangular shape. We found, that a desired pulse shape could be obtained by using a 4" long driver section. Drivers of lengths 1" and 2" were also used, but most of the experiments reported here were carried out with the 4" driver section.

A schematic of the experimental apparatus is shown in Fig. 1. The shock tube, 2 m long, was made of steel with a 3 mm thick wall, and supplied with appropriate flanges and ports for attaching the driver section, transducer(s), test sections, and tube extensions. Two extensions, one 91.8 cm and the other 213.4 cm long were available. One of them had holes over parts of its length, so that a transducer could be placed at different locations

Data acquisition system.

The transducer, a PCB 113A21 piezoelectric, was flush mounted with the interior wall in the shock tube. It is designed for the study of shock waves with a resonance frequency of 500 kHz, with an excellent transient response (no ringing). The diameter of the transducer was 5.5 mm, which determined the "resolution" of the system. The output of the transducer is proportional to the average pressure over the surface of the transducer, and with a shock speed of approximtely 480 m/sec, the travel time over the transducer is 12 microseconds, which sets an upper limit of 86 kHz on the meaningful sampling rate of the signal from the transducer.

To determine the pressure from the voltage output, we used the pressure-voltage calibration supplied by the manufacturer. Ten months after we began using the transducer, it was returned to the manufacturer for recalibration. Over this period, the calibration remained within 1 % of the original calibration. The uncertainty in the transducer calibration, approximately 1 %, was the dominant source of error in the data acquisition system.

The heart of our data acquisition system was a Digital Equipment Corporation MINC 11/23 laboratory computer. We used the Data Translation DT 2785/5714 DI 14 bit differential input A/D board for our analogue to digital conversion system. The manufacturer claims a 10 kHz sampling rate for the board. We found, however, that it was possible to drive the board at 19 kHz without introducing sampling errors. This sampling rate was well below the limit resulting from the resolution of the transducer described above. The clock signal for the A/D board was provided by the Data Translation DT 2769 real time clock. A graphic terminal was provided for immediate display of data.

The hardware was controlled through FORTRAN callable subroutines supplied by Data Translation software. This made possible

along the tube.

The working gas in the tube was air at atmospheric pressure. The driver section was terminated with a properly chosen membrane. We experimented with a variety of membrane materials, particularly mylar films of different thicknesses to obtain a peak pressure of the shock wave in the range from .3 to 2 atm. with corresponding over pressures in the driver section up to 5 atm. For example, mylar films with thicknesses .013 mm and 025 mm ruptured at driver pressures of 2.45 and 3.7 atm. and another plastic film of thickness .0065 mm ruptured at 1.5 atm.

The rupture pressure could be made quite repeatable from one membrane to the next with a proper experimental procedure. The pressure was monitored by means of a Heise pressure gauge. If the pressure was raised rapidly until the membrane ruptured, the value thus obtained would vary somewhat from one membrane to the next. To avoid this variation, the pressure was raised slowly to a value just below the rupture value and held there until the mylar weakened and broke at the preset pressure value. This procedure assured excellent repeatability in producing shocks of a specified peak pressure.

The needle valve attached to the driving section served as simple check valve, to minimize the amount of gas entering the shock tube after membrane rupture. The needle valve was adjusted to yield a very low flow rate, so that the mass flow entering the tube during data aquisition was only 1 % of the mass initially flowing into the driving sextion.

The shock tube could be terminated by various elements, such as a rigid plate, various orifice plates, or tube extensions containing porous baffles or lined duct elements. The rigid termination was a 1.5 cm thick steel plate, and the orifice plates were cut from 2.5 mm Al stock.

the initiation of clock pulses by firing one of the Schmidt triggers located on the clock board, have the A/D board take 2046 pieces of data at the 19 kHz clock rate, and display the data on the screen. The data could be expanded on the screen in order to examine detailed feature, and then stored on one of the floppy disks in the system for later retrievel.

In order to see the leading edge of the shock pulse, we used a signal other than the signal from the pressure transducer to fire the Schmidt trigger on the clock board. The trigger signal was produced by a piezoelectric crystal clamped to the flange of the driver section. When the membrane ruptured, the crystal was strained, producing the required trigger signal.

Sample data.

Fig. 2 shows an example of the recorded pressure pulse in the shock tube and the subsequent reflections from the ends of the tube. Actually, the pattern consists of the traces from two succesive firings of the tube with the same initial pressure in the driver but with different diaphragms, of course. The fact, that the two traces cannot be distuinguished from one another demonstrates the excellent repeatability, which is obtained, when the experimental procedure outlined above is followed.

The pressure is recorded at a distance of 1 m from the source. The first pulse arrives directly from the source. The positive portion of the pulse has a duration of about 2.5 milliseconds. The second pulse is the reflection from the open end of the tube. In linear acoustics the pressure reflection coefficient from an open end is approximately -1, and we note, that the reflection pulse is reversed in sign, as expected. The third pulse is the reflection from the rigid end of driver section. In linear acoustics the reflection coefficient from the rigid wall is +1, and, again as expected, there is no sign reversal between the second and the third pulses. This process

of alternate reflections from the open end and the rigid wall continues for many more reflections than are shown here.

In Fig. 3 are shown two pressure traces obtained with driving sections of different lengths, but with the same driving pressure, 3.7 atm. As expected, the duration of the pulse increases with increasing driver length, but otherwise the general behaviour of the pulses is much the same for both.

Pulses produced by different initial pressures in the driver section are shown in Fig. 4. The length of the driver is 4". It is interesting to see, that the large amplitude pulse arrives before the pulse with the lower amplitude, This demonstrates explicitly the pressure dependence of the wave speed.

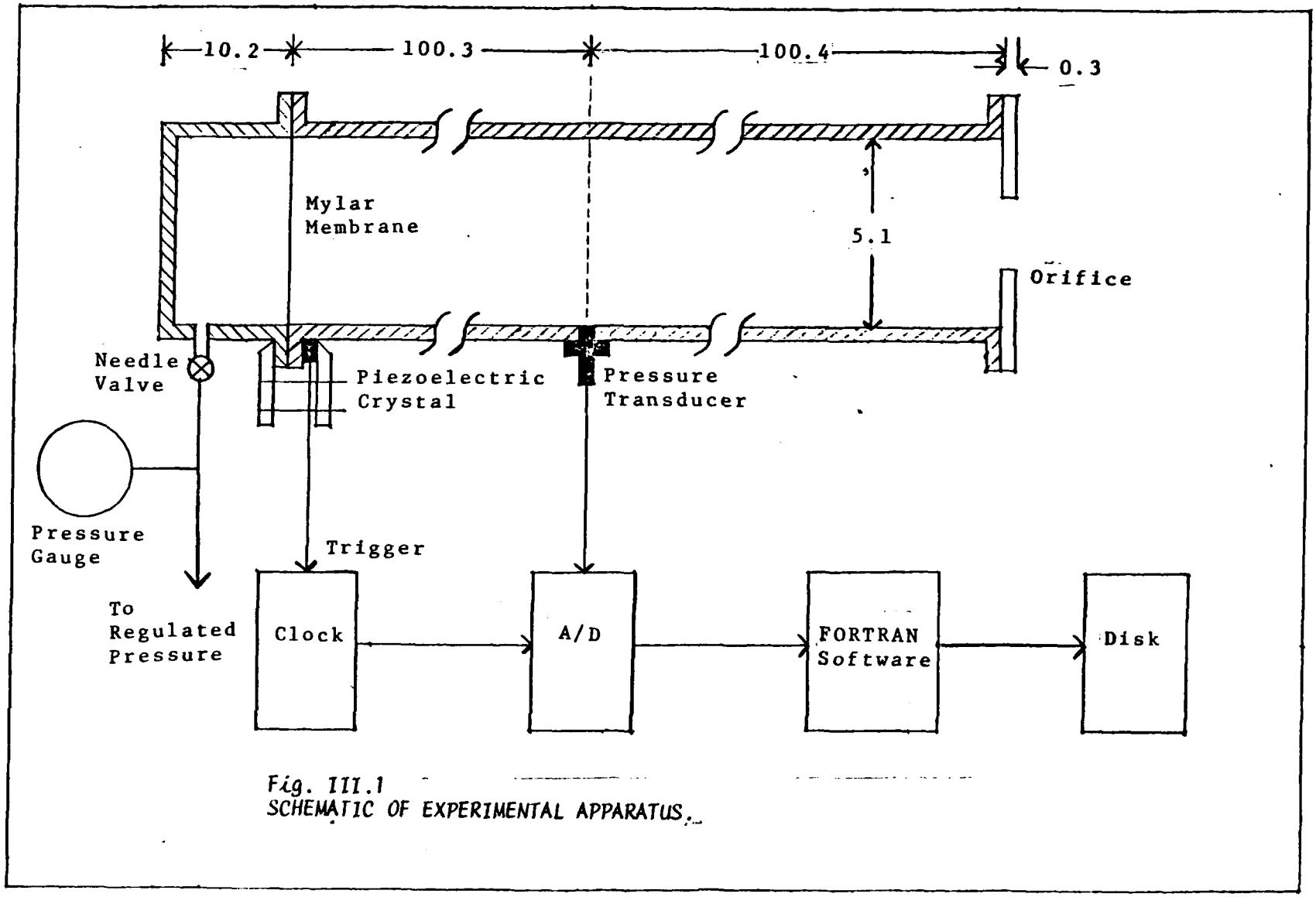


*Fig. III.1*
*SCHEMATIC OF EXPERIMENTAL APPARATUS.*

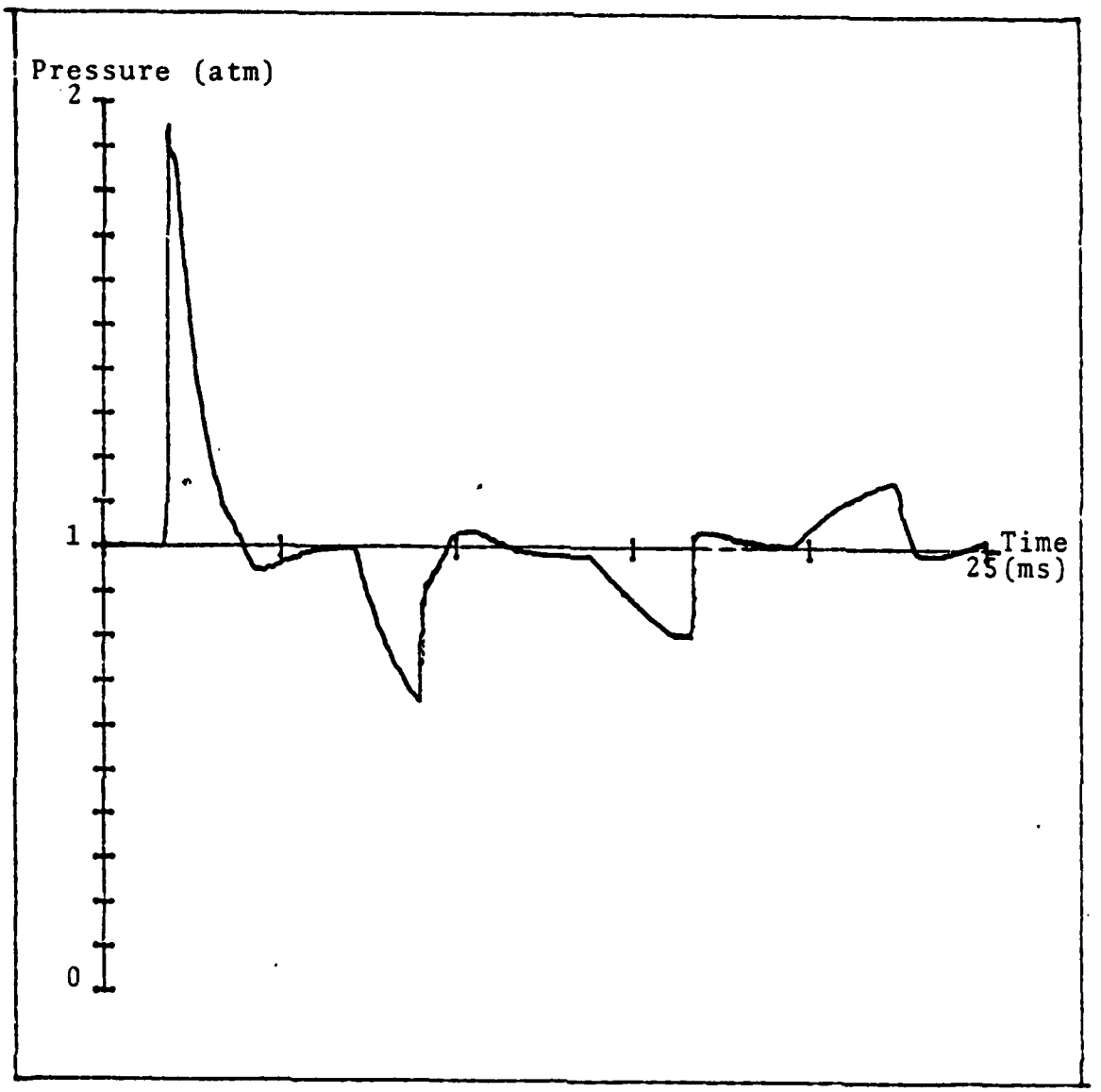


*Fig. III.2.*
*COMPARISON OT TWO EXPERIMENTASL PRESSURE RECORDS FROM TWO EXPERIMENTAL RUNS WITH THE SAME PRESSURES IN THE DRIVER SECTION OF THE SHOCK TUBE, DEMONSTRATING REPRODUCIBILITY.*

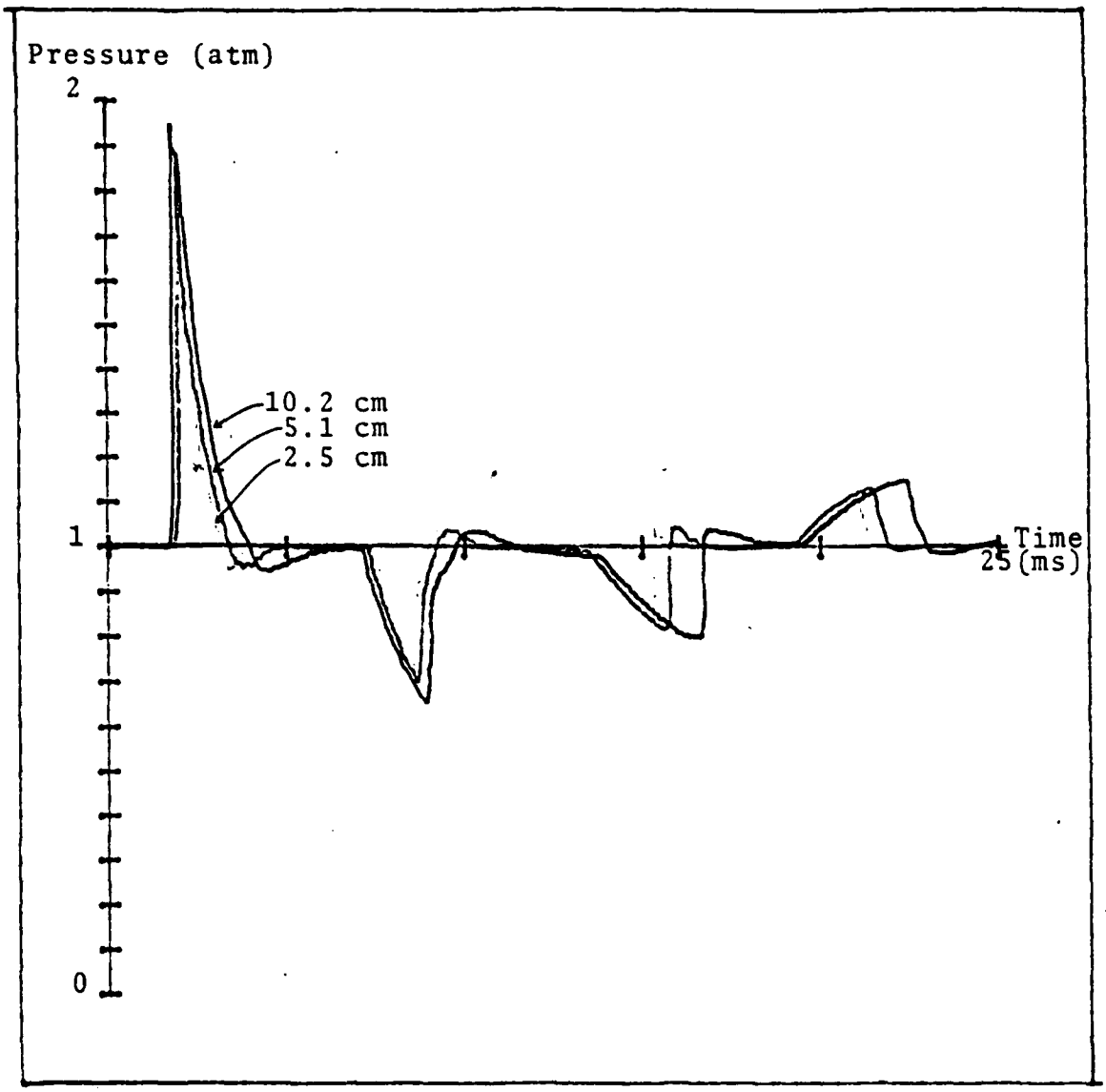


*Fig. III.3.*
*COMPARISON OF THE PRESSURE RECORDS OBTAINED IN EXPERIMENTAL RUNS WITH THREE DIFFERENT LENGTHS OF THE DRIVING SECTION.*

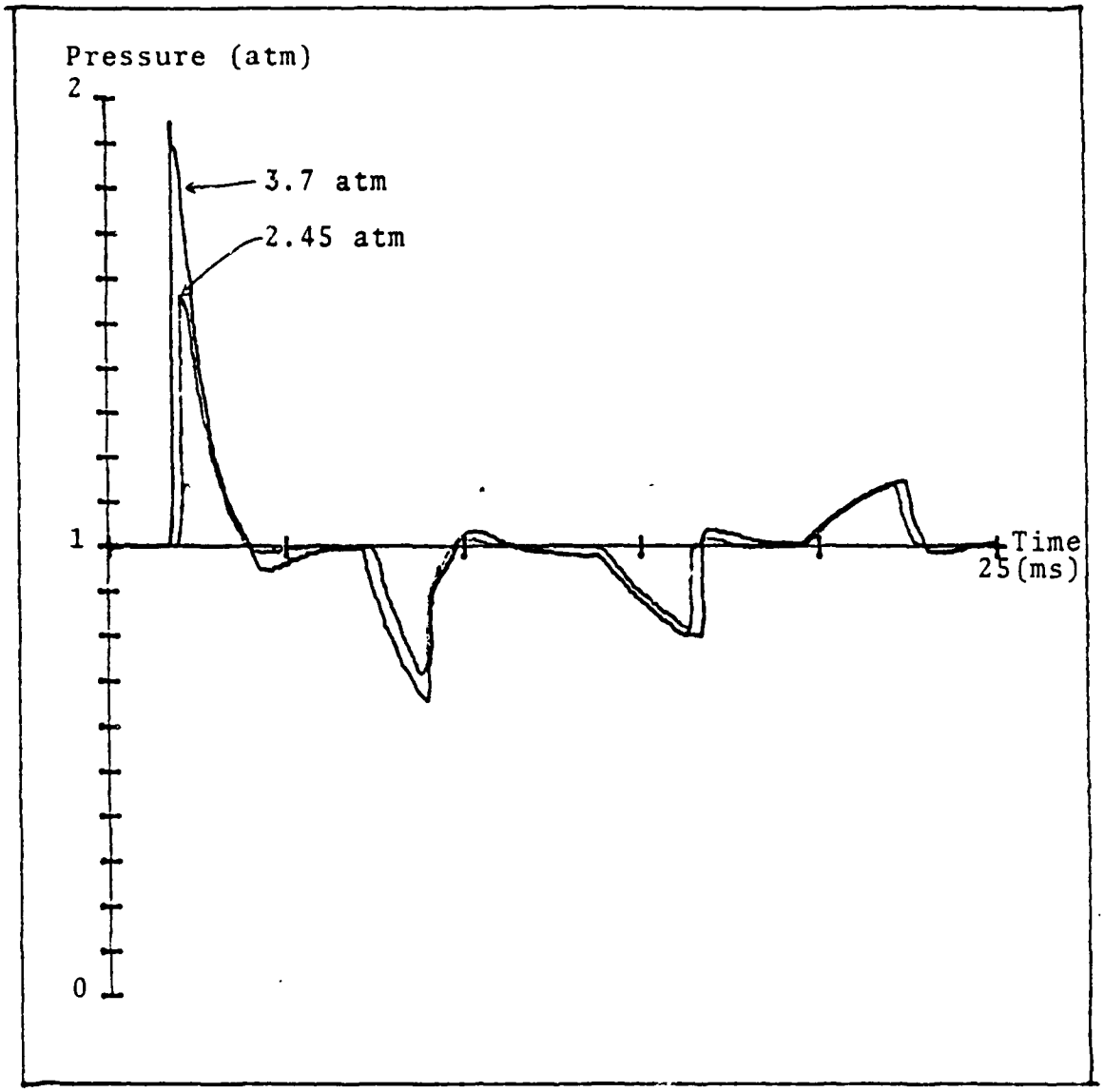


*Fig. III.4.*
*COMPARISON OF THE PRESSURE RECORDS OBTAINED IN EXPERIMENTAL RUNS WITH A DRIVER SECTION LENGTH OF 10.2 CM AT TWO DIFFERENT PRESSURES IN THE DRIVER SECTION.*

## III. STUDIES OF SHOCK WAVE PROPAGATION AND REFLECTION

Reflection from closed and open ends of a duct.

Starting from the initial static pressure in the driver section of the shock tube, we have used the computational procedure described in Appendix D to calculate the pressure pulse pattern at the location of the transducer, 1 m from the driver for both a rigid and open termination of the shock tube. The results are shown in Figs. 1 and 2. For comparison, we have included in Figs. 3 and 4 the results obtained from linear acoustic theory. We note, that the linear theory fails not only to predict the shape but also the location of the pulses.

Of particular interest is the result obtained for the open ended tube. In the linear theory the reflection coefficient is close to -1 at the open end, and the reflected pulse is in essence the mirror image of the incident pulse with respect to the x-axis. In other words, the sudden rise in pressure is associated with the leading edge of both the incident and reflected waves. This is not the case in reality, however, as can be seen from Fig. 2; the steepest part of the pulse belongs to the trailing edge of the pulse.

In order to explore the reason for this behaviour, we have studied in detail the process of reflection from the open end, with the results shown in Figs. 5-8. The x-dependences of both the pressure and the velocity in the wave have been computed at various times, before, during and after the reflection from the open end.

In the first figure, corresponding to the normalized time $t/(x/c_0)=.0924$, a region of almost uniform flow has formed behind the shock wave, and the rarefaction wave, travelling to the left, has already reflected from the hard end of the driver section and has begun to travel to the right. The speed of the shock wave is smaller than the local sound speed behind

the shock, so a disturbance within the shock will catch up with the shock front. Thus the rarefaction wave will overtake the shock, as indicated in the next two figures.

As the wave arrives at the open end of the tube, the flow accelerates and the flow velocity remains high even after the pressure in the tube has dropped below the outside pressure. This pressure drop propagates back as a rarefaction wave. Now the sound speed is larger behind the wave than in it, so that the portions of the trailing part of the pulse with the smallest rarefaction will have the highest speed. Consequently, the trailing part of the wave will be distorted to form a trailing shock, as shown in the last figure.

It should be remarked, that the result obtained here are applicable approximately also to the reflection from a sudden expansion in a tube.

Reflection from an orifice plate.

As was shown in the previous section, the peak pressures of the waves reflected from a rigid termination and from the open end of a duct were .63 and -.40 times the peak pressure of the incident wave, as measured at the location of the transducer, 1 m from the end of the tube. With a perforated plate placed at the end of the tube, the reflected peak pressure is expected to fall between this positive and negative values. For a large open area fraction S of the plate, the reflected wave should be negative and for a small value of S it should be positive. Thus, the magnitude of the reflected peak pressure should be a minimum for some value of the open area fraction. To explore this question, we carried out a set of measurements of the reflection from perforated plates, with S ranging from .22 to .79. The results are shown in Figs. 9-12.

As we go from the smallest (.22) to largest (.79) value of S, we note, as expected, that the positive portion of the

reflected pulse decreases. At S=.79 it has essentially disappeared, and the dominant reflected pressure is negative. For S=.6, the positive and negative contributions are about the same, and for this approximately this value of S, the magnitude of the reflected pressure pulse is a minimum, about 10 % of the incident pressure peak at the location of the plate. In other words, it is about 4 times smaller than the reflected pressure from the open end and 6 times smaller than from the rigid termination.

The optimum value of S for an orifice plate for minimum reflected pressure amplitude depends on the peak value of the incident wave. From the nonlinear acoustic theory of reflection, presented below, the reflection coefficient can be expressed in closed form in terms of the incident pressure, and the pressure dependence of the optimum value of the open area fraction readily can be determined.

It is interesting in this context to compare the measured reflections with the nonlinear acoustic theory. This is done in Fig. 13, where we have computed the reflection coefficient as a function of the open area fraction for some different values of the incident peak pressure, namely .2, .4, .6, and .8 times the ambient static pressure. The frequency dependence of the reflection coefficient is quite weak, and affects only the minimum value of the reflection coefficient. The curves shown refer to a frequency of 400 Hz, but the curves are essentially the same for frequencies in the range 100-500 Hz.

The reason for the weak frequency dependence of the reflection coefficient is that the nonlinear impedance of the orifice plate is dominated by the resistive part. In this particular case, with the plate terminating a tube with the wave radiating into free space, the reactive part of the impedance arises from the inertial mass in the orifice(s) of the plate and the near field flow at the end of the tube, as described in the theory,

presented below.

Accounting for the nonlinear attenuation in the tube of the incident wave pulse, which has an amplitude of .93 atm. at 1 m from the termination, we obtain a value of .73 atm. at the orifice plate. Correcting the reflected waves in a similar manner, we obtain from the experimental data in Figs. 9-12 the reflection coefficients .64, .35, .105, and .23 for the open area fractions S=.22, .42, .60, and .79.

The results are seen in Fig. 13 to be in good general agreement with the predicted S-dependence except for a slight systematic shift of the data in the S-direction. With a small correction for the contraction of the flow in the orifices of the plate, which in effect reduces S, this systematic shift can be eliminated.

Nonlinear acoustic theory of reflection of a shock wave from an orifice plate.

For values of the incident peak pressure of the pulse, such that $p/P<1$, the interaction of a harmonic wave with a plate with one or more orifices can be described quite well by treating the flow through the orifice(s) quasistatically. This leads to an acoustic characterization of the orifice plate in terms of an amplitude dependent acoustic impedance, in which the resistive part is proportional to the velocity amplitude in the orifice, thus accounting for the losses related to the flow separation in the orifice at large amplitudes. The reactive part of the impedance decreases somewhat with amplitude, but it is a good approximation to use the linear value of the reactance ( ).

With the open area fraction of the orifice plate denoted by S, the velocity amplitude in the orifice will be u/S, where u is the amplitude in the duct before the flow has contracted in the orifice. The resistive part $\theta'$ of the normalized impedance $\zeta'=\theta'+i\chi'$ of the orifice plate has been found to be proportional

to this velocity amplitude (17)

$$\theta' \simeq u/cSS' \qquad (1)$$

$$S' = S/(1-S^2)$$

where c is the ambient sound speed. The normalized reactance is

$$\chi' \simeq (1/S')(\omega/\ )0.6d = (1/S')\sqrt{S}(\omega/c)0.6D \qquad (2)$$

where d is the orifice diameter and D the tube diameter. In the last step, we have assumed, that the plate has only one orifice.

With the normalized impedance of the region on the downstream side of the orifice plate denoted by $\zeta''$, the total normalized impedance in front of the orifice plate is

$$\zeta = \zeta' + \zeta'' = \theta + i\chi \qquad (3)$$

If the orifice plate is located in a long uniform tube, we have $\zeta''=1$, the normalized characteristic wave impedance of a plane wave.

In the present case, the experimental data in Fig. 1 refer to an orifice plate at the end of a tube radiating into free space. For long wavelengths, the resistive and reactive parts of the impedance $\zeta''$ are proportional to $(kD)^2$ and $(kD)$, respectively, where $k=\omega/c$. These are less then unity at wavelengths larger than the circumference of the tube. In our case, with D=5 cm and typical wave length of the order of 1 m, this condition is fulfilled. Under these conditions, the reactive part dominates, and it is approximately equal to 0.3 D/c, corresponding to a mass "end correction" 0.3D of the tube.

The velocity amplitude in the orifice is not known a priori,

but it can be expressed in terms of the incident pressure amplitude p from the boundary condition $p_i/u=\rho c\zeta$, where $p_i$ is the sum of the incident and reflected pressures at the orifice plate. This condition can be expressed in terms of the incident pressure p

$$u=2p/[\rho c(\zeta+1)] \tag{4}$$

We shall use for the total impedance the approximation

$$\zeta=\zeta'+\zeta''\simeq u/\hat{c}SS'+i(\chi'+\chi'') \tag{5}$$

i.e. omitting the resistive part of $\zeta''$.

Using this expression in Eq. 4, we obtain an equation for u. Since the reactance is small compared to the resistance, we may omit the reactance in Eq. 4 so that $u=(2p/\rho c)/[1+(u/cSS')]$ with the solution

$$u/cSS'=\sqrt{1/4+2\beta}-1/2 \tag{6}$$

$\beta=p/\gamma PSS'$ ($\gamma$=specific heat ratio).

Having obtained the velocity amplitude, we can now express the impedance in terms of the incident pressure amplitude

$$\zeta\simeq\sqrt{1/4+2\beta}-1/2+i\chi \tag{7}$$

$\chi=(\omega D/c)[0.3+(\sqrt{S}/S')0.6]$

The reflection coefficient is then

$$C=(\zeta-1)/(\zeta+1) \tag{8}$$

with the magnitude $|C|=[(\theta-1)^2+\chi^2]^{\frac{1}{2}}/[(\theta+1)^2+\chi^2]^{\frac{1}{2}}$, which is

plotted in Fig. 1 as a function of S for a frequency of 200 Hz, typical of the spectrum of the incident wave.

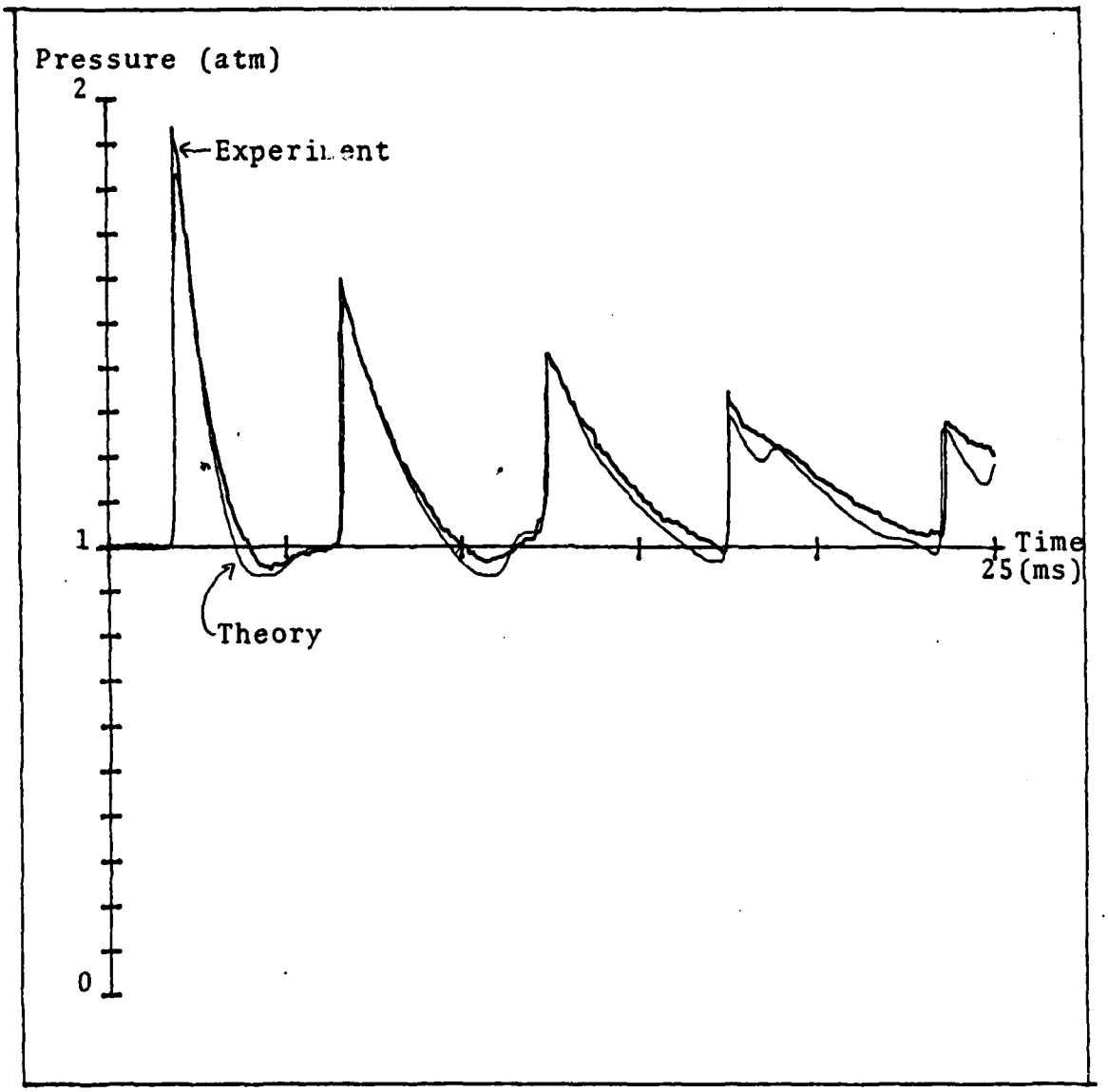


*Fig. IV.1.*
*COMPARISON OF NUMERICAL SOLUTION WITH MEASURED PRESSURE WAVES IN THE REFLECTION FROM A RIGID TERMINATION OF THE SHOCK TUBE. Pressure in driver section: 3.7 atm.*

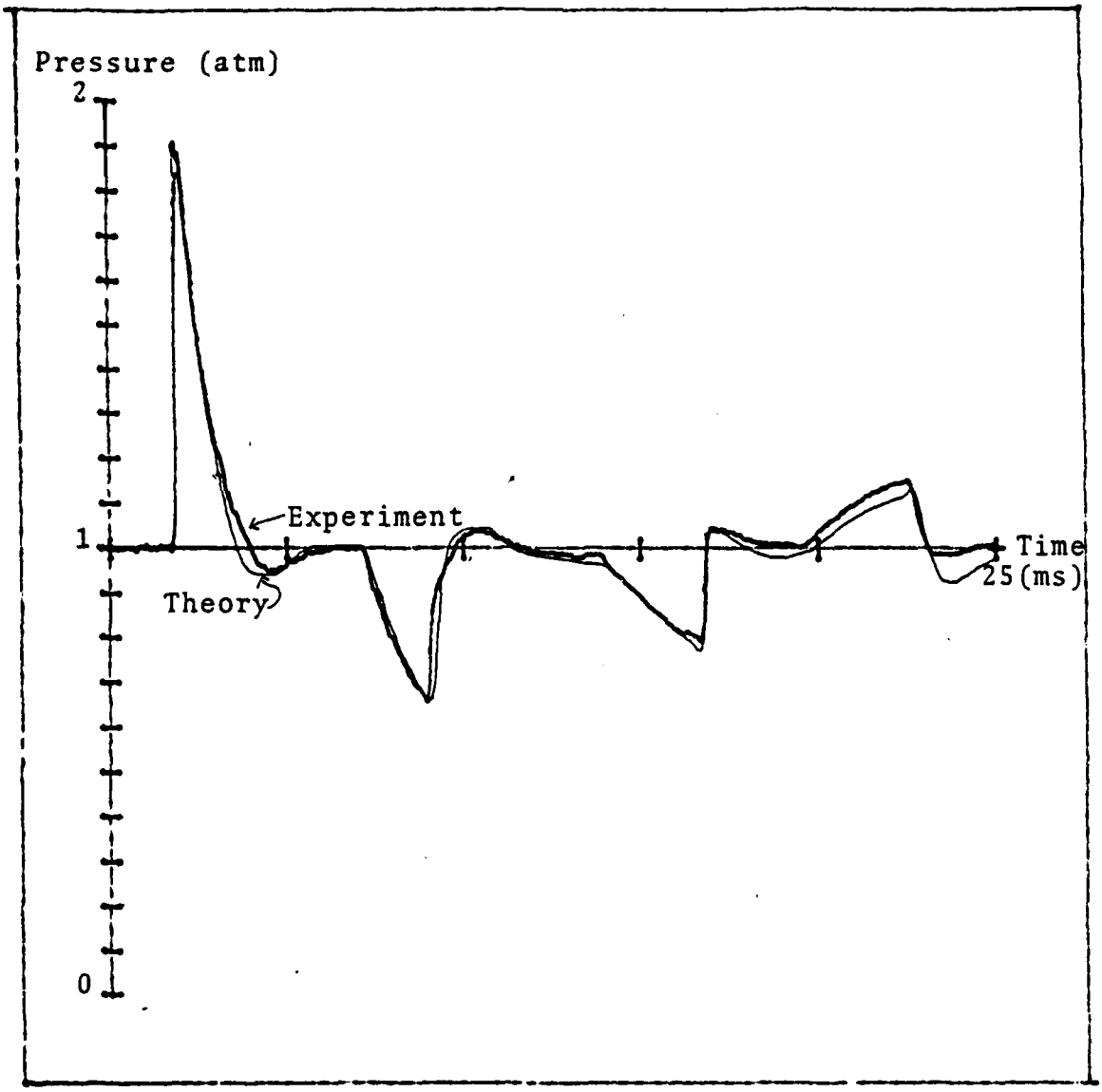


*Fig. IV.2.*
*COMPARISON OF NUMERICAL SOLUTION WITH MEASURED PRESSURE WAVES IN THE REFLECTION FROM THE OPEN END OF THE SHOCK TUBE.*
*Pressure in driver section: 3.7 atm.*

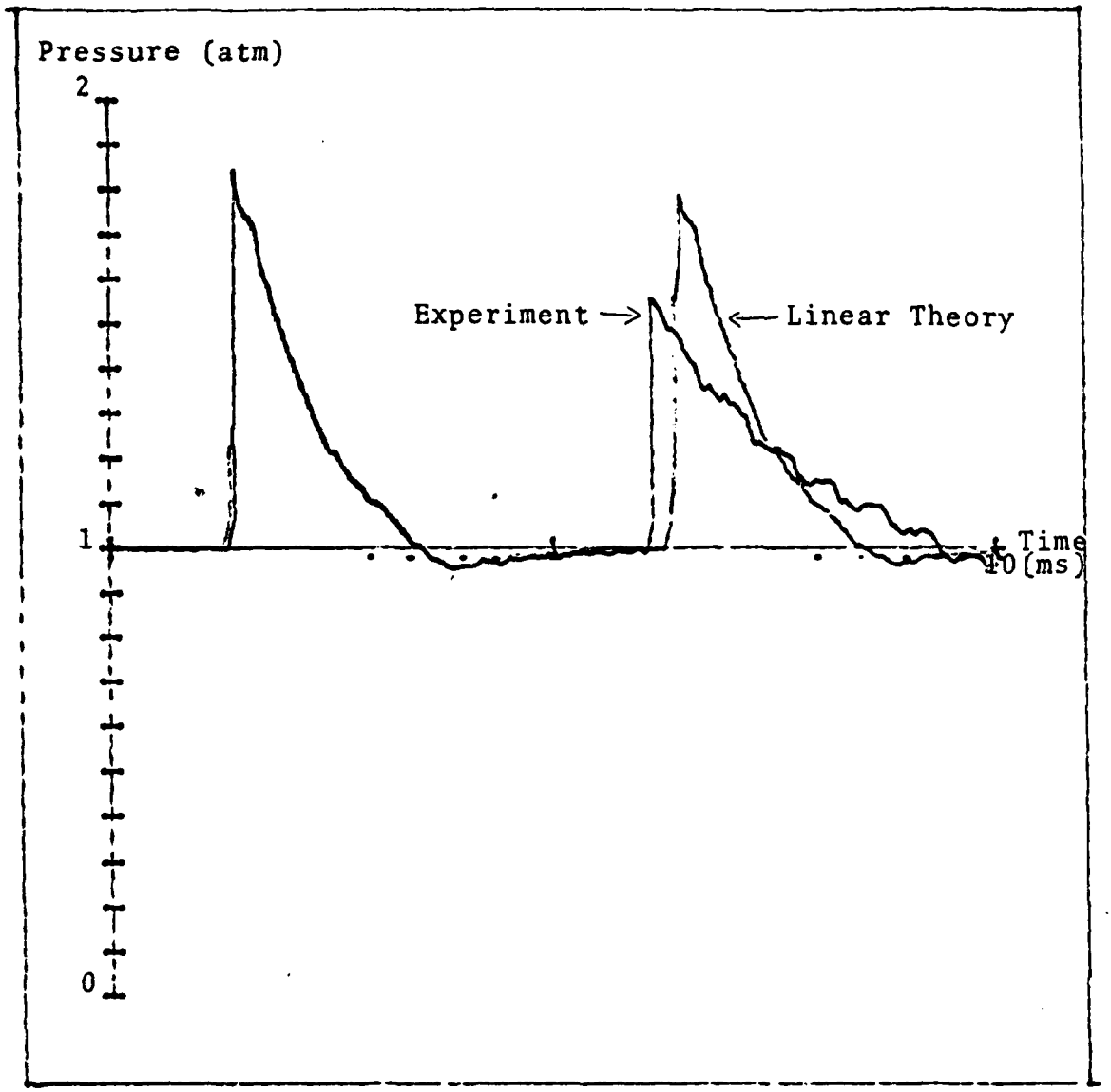


*Fig. IV.3.*
*COMPARISON OF LINEAR THEORY WITH MEASURED PRESSURE PATTERNS IN THE REFLECTION FROM A RIGID TERMINATION OF THE SHOCK TUBE.*
*Pressure in driver section: 3.7 atm.*

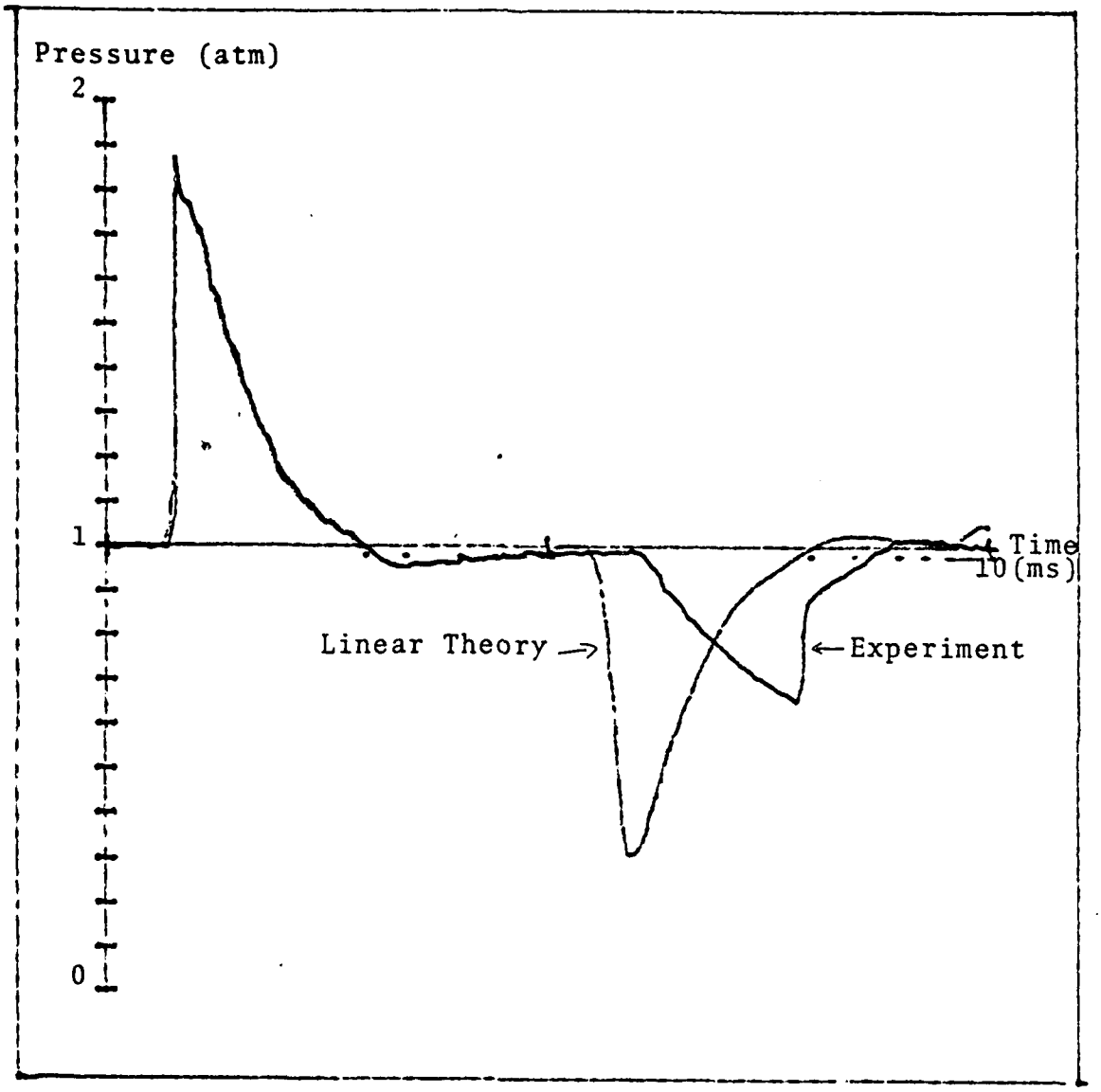


*Fig. IV.4.*
*COMPARISON OF LINEAR THEORY WITH MEASURED PRESSURE PATTERN IN REFLECTION FROM THE OPEN END OF THE SHOCK TUBE.*
*Pressure in driver section: 3.7 atm.*

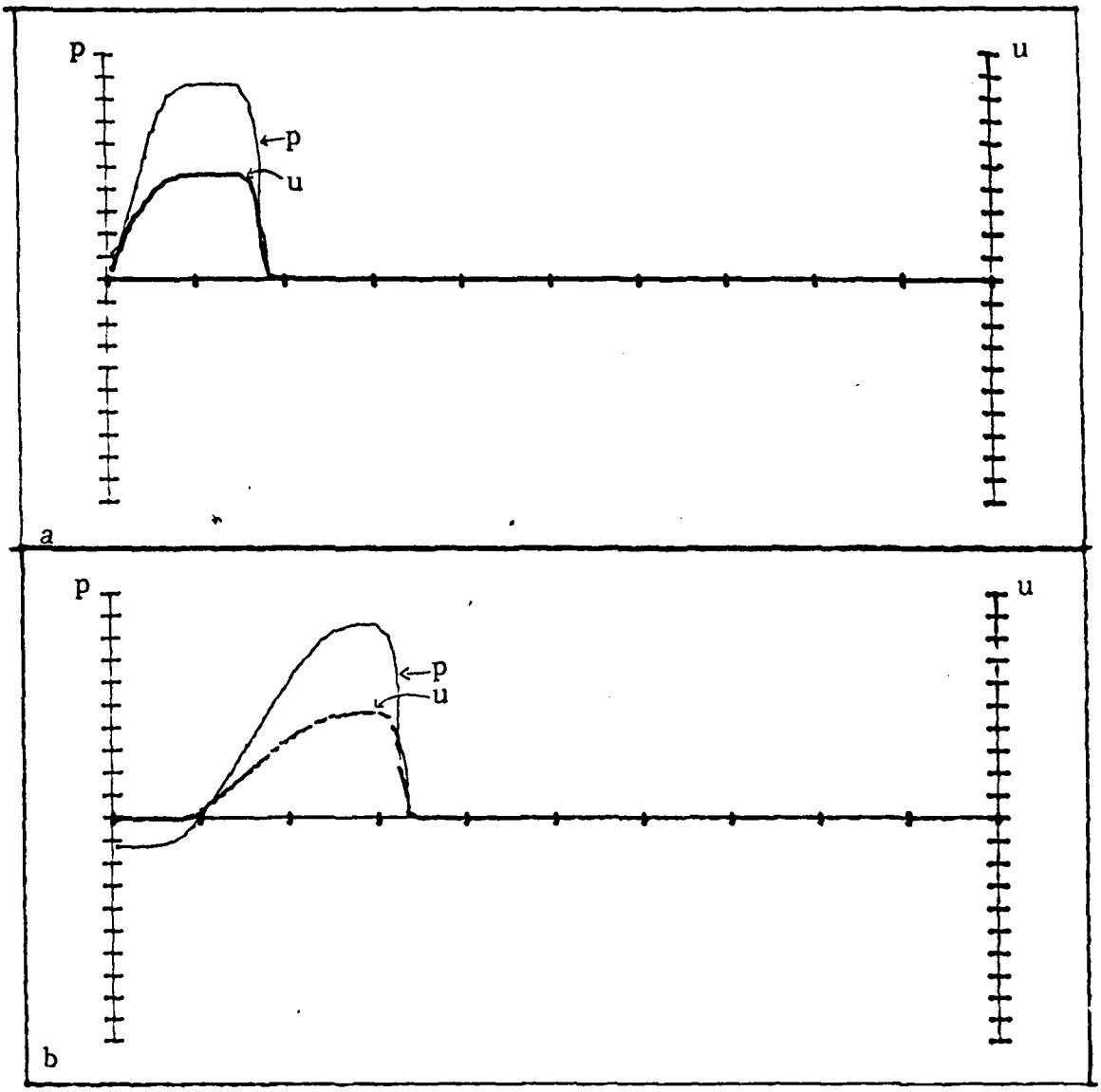


*Fig. IV.5.*
NUMERICAL SOLUTION FOR THE X-DEPENDENCE OF THE PRESSURE AND FLOW VELOCITY IN A SHOCK WAVE AT DIFFERENT TIMES.
*Normalized times, $t/(x/c_0)$*
*Upper figure: .0924. Lower figure: .2077.*

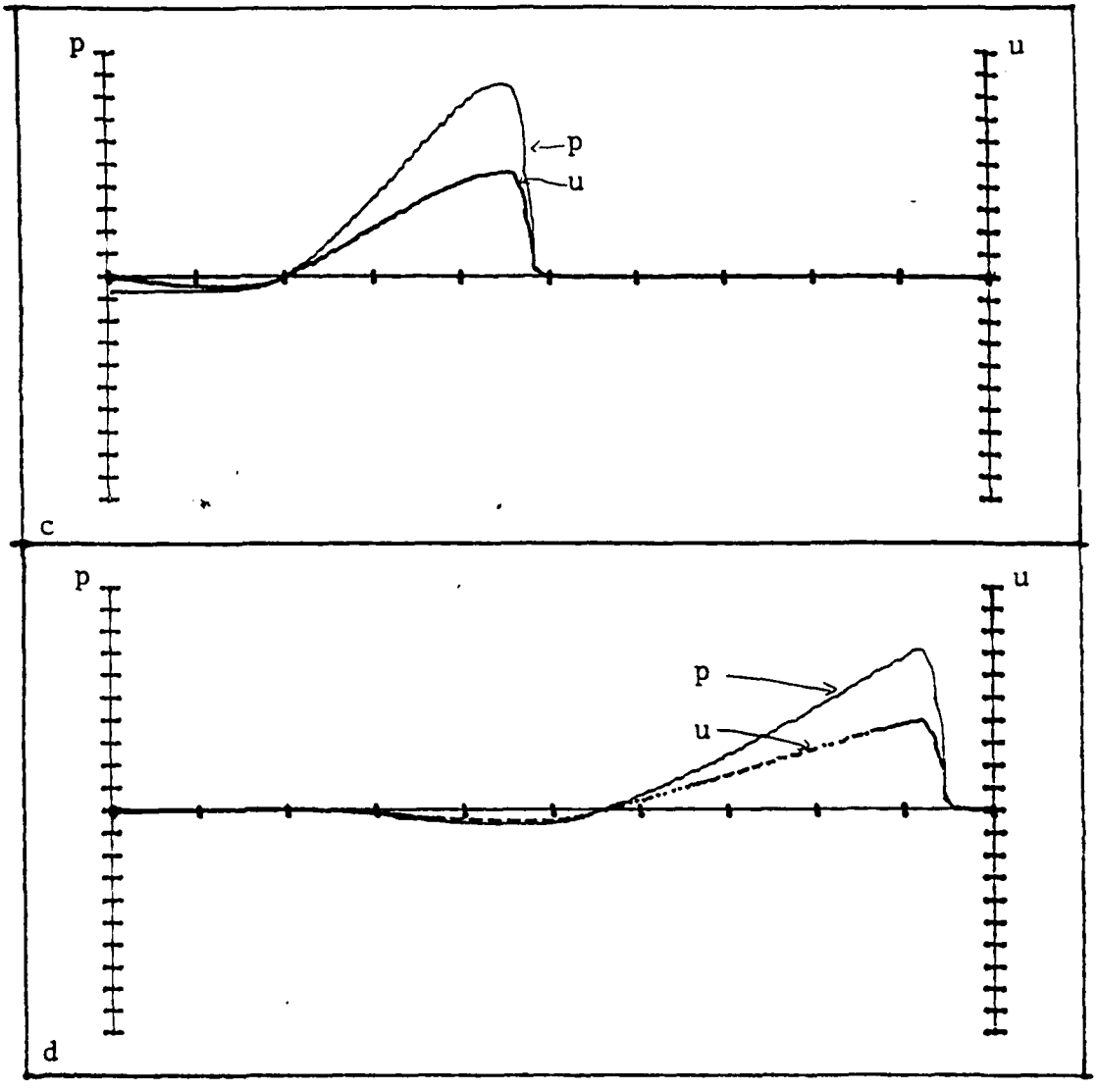


*Fig. IV.6.*
*NUMERICAL SOLUTION FOR THE X-DEPENDENCE OF THE PRESSURE AND FLOW VELOCITY IN A SHOCK WAVE AT DIFFERENT TIMES.*
*Normalized times, t/(x/co)*
*Upper figure: .3202*
*Lower figure: .6774*

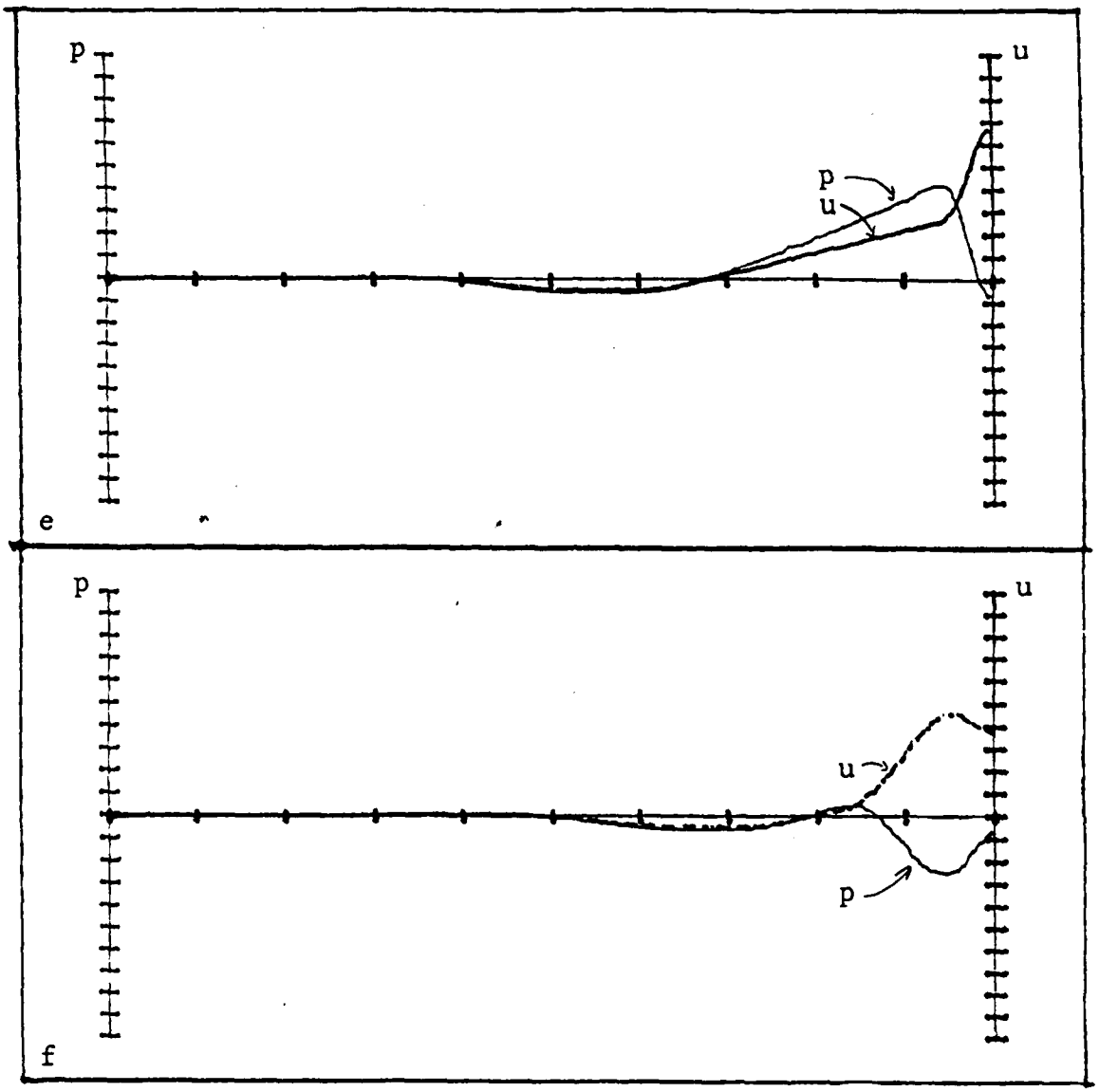


*Fig. IV.7..*
*NUMERICAL SOLUTION FOR THE X-DEPENDENCE OF THE PRESSURE AND FLOW VELOCITY IN A SHOCK WAVE AT DIFFERENT TIMES.*
*Normalized times, t/(x/co)*
*Upper figure: .7943*
*Lower figure: .9112*

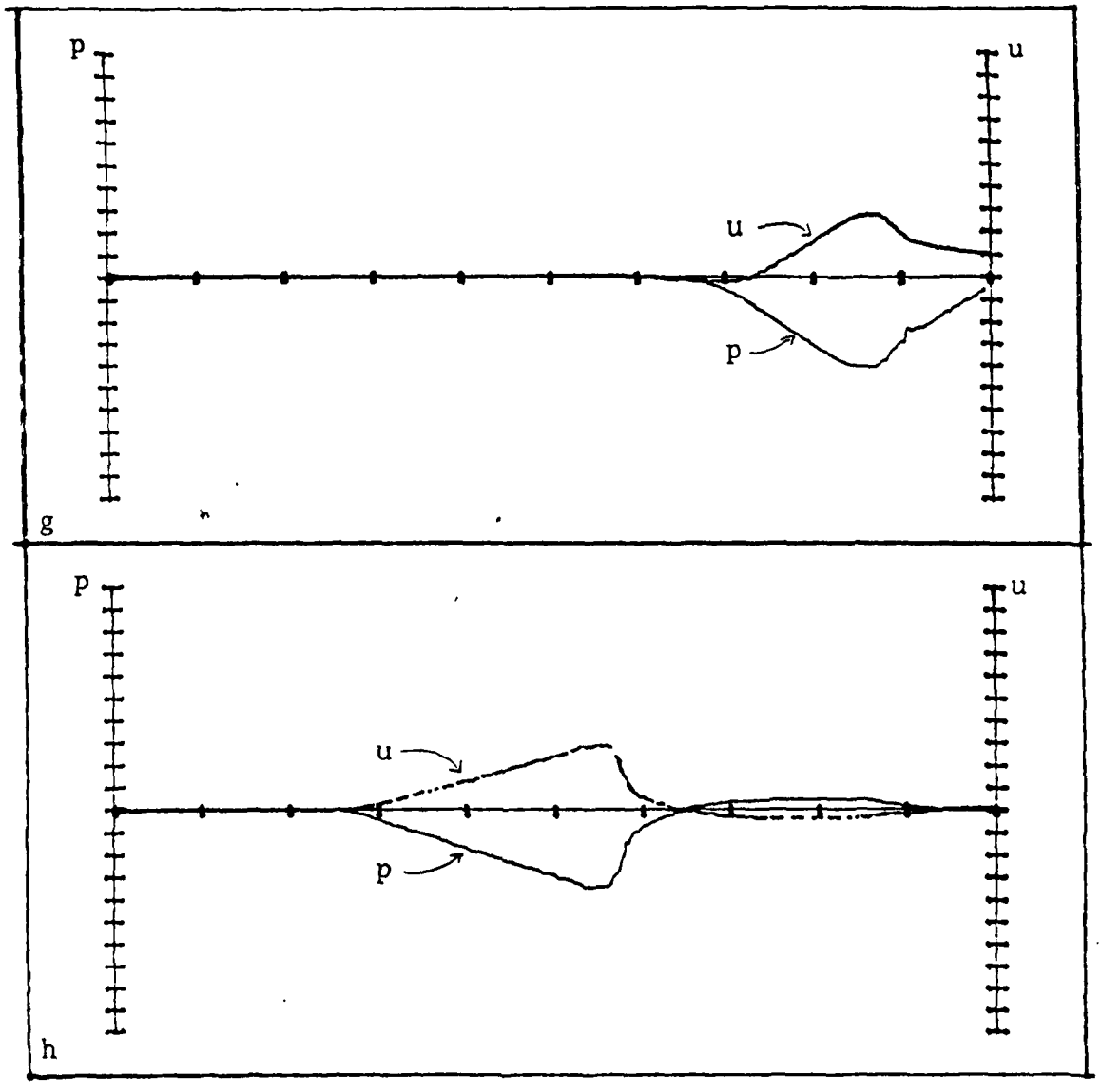


Fig. IV.8..
NUMERICAL SOLUTION FOR THE X-DEPENDENCE OF THE PRESSURE AND FLOW VELOCITY IN A SHOCK WAVE AT DIFFERENT TIMES.
Normalized times, $t/(x/c_0)$
Upper figure: 1.049
Lower figure: 1.406

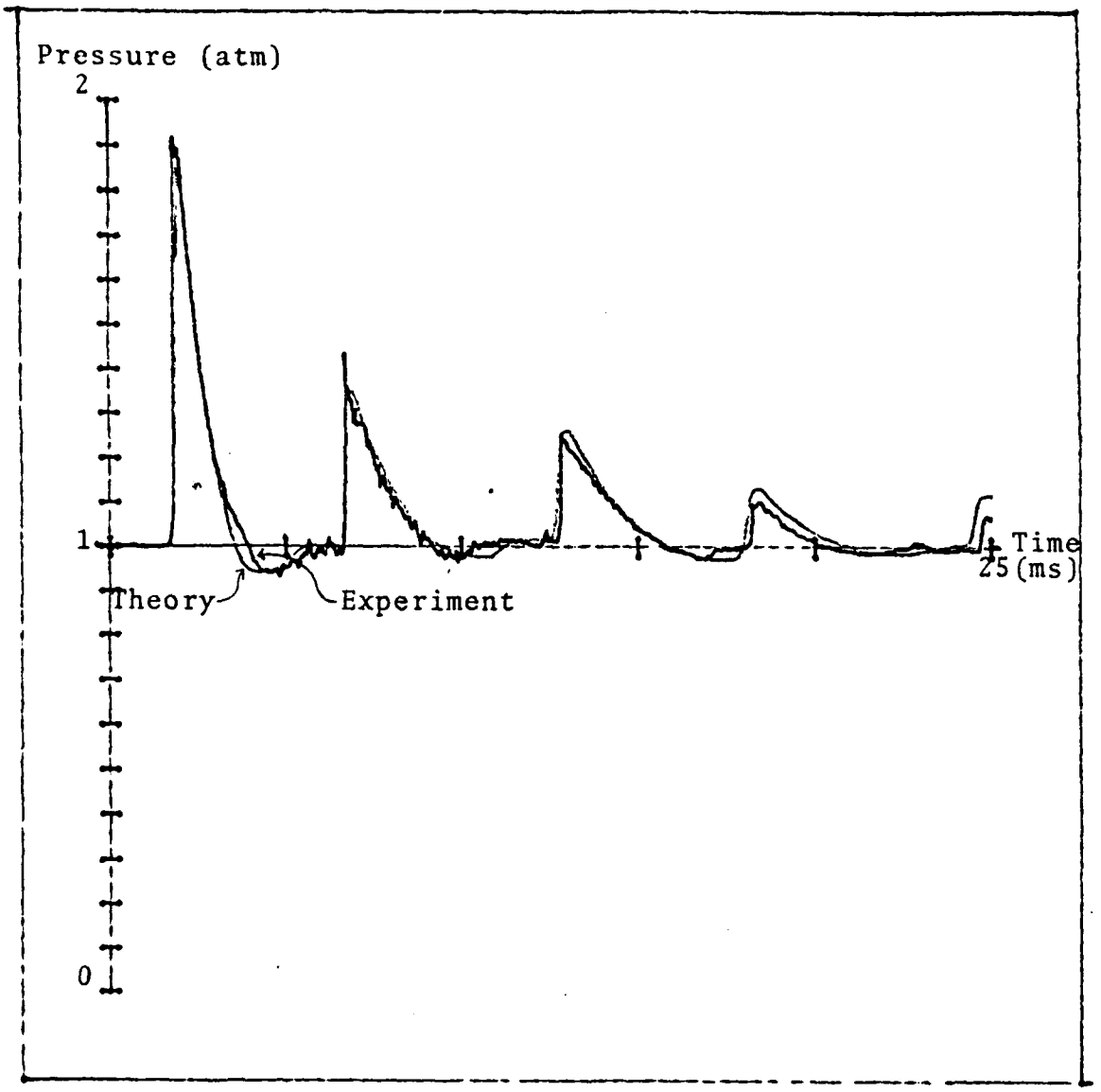


*Fig. IV.9.*
*COMPARISON OF MEASURED PRESSURE WAVES AND NUMERICAL SOLUTION IN A SHOCK TUBE WITH AN ORIFICE PLATE TERMINATION.*
*Open area fraction of the orifice plate: .22.*
*Pressure in driver section: 3.7 atm.*

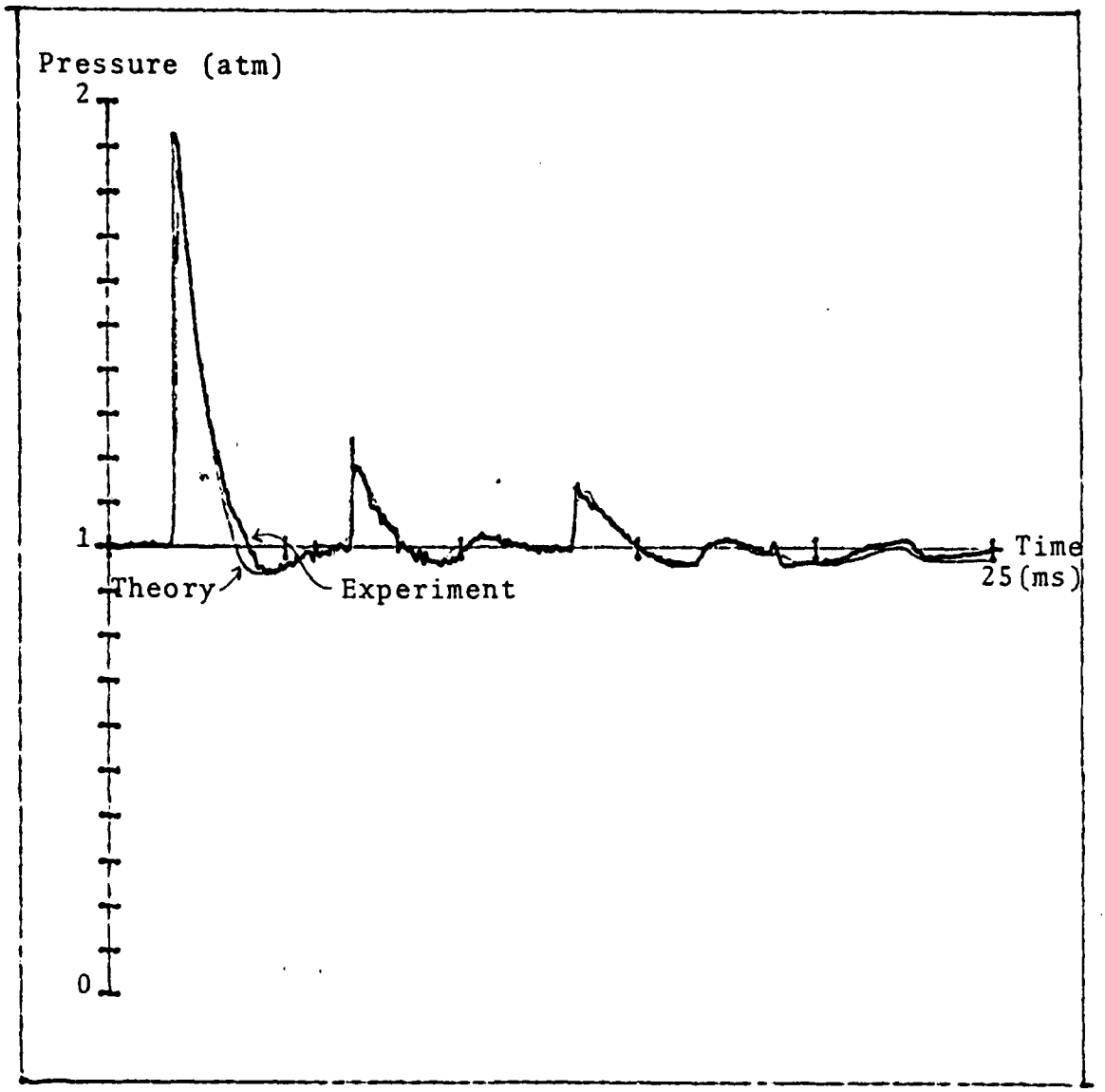


*Fig. IV.10..*
*COMPARISON OF MEASURED PRESSURE WAVES AND NUMERICAL SOLUTION IN A SHOCK TUBE WITH AN ORIFICE PLATE TERMINATION.*

*Open area fraction of the orifice plate: .42.*
*Pressure in driver section: 3.7 atm.*

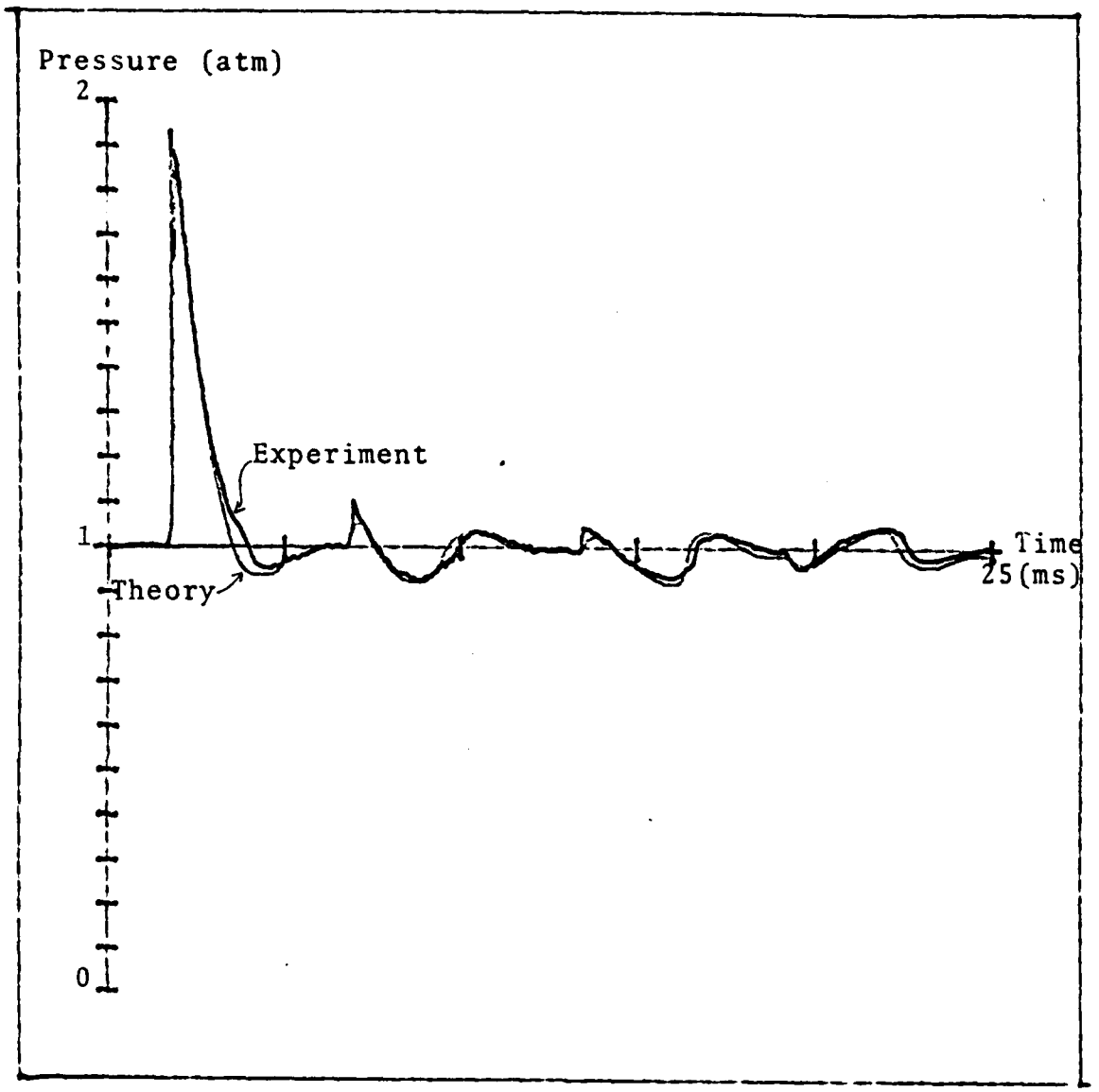


*Fig. IV.11.*
COMPARISON OF MEASURED PRESSURE WAVES AND NUMERICAL SOLUTION IN A SHOCK TUBE WITH AN ORIFICE PLATE TERMINATION.

*Open area fraction of the orifice plate: .60.*
*Pressure in driver section: 3.7 atm.*

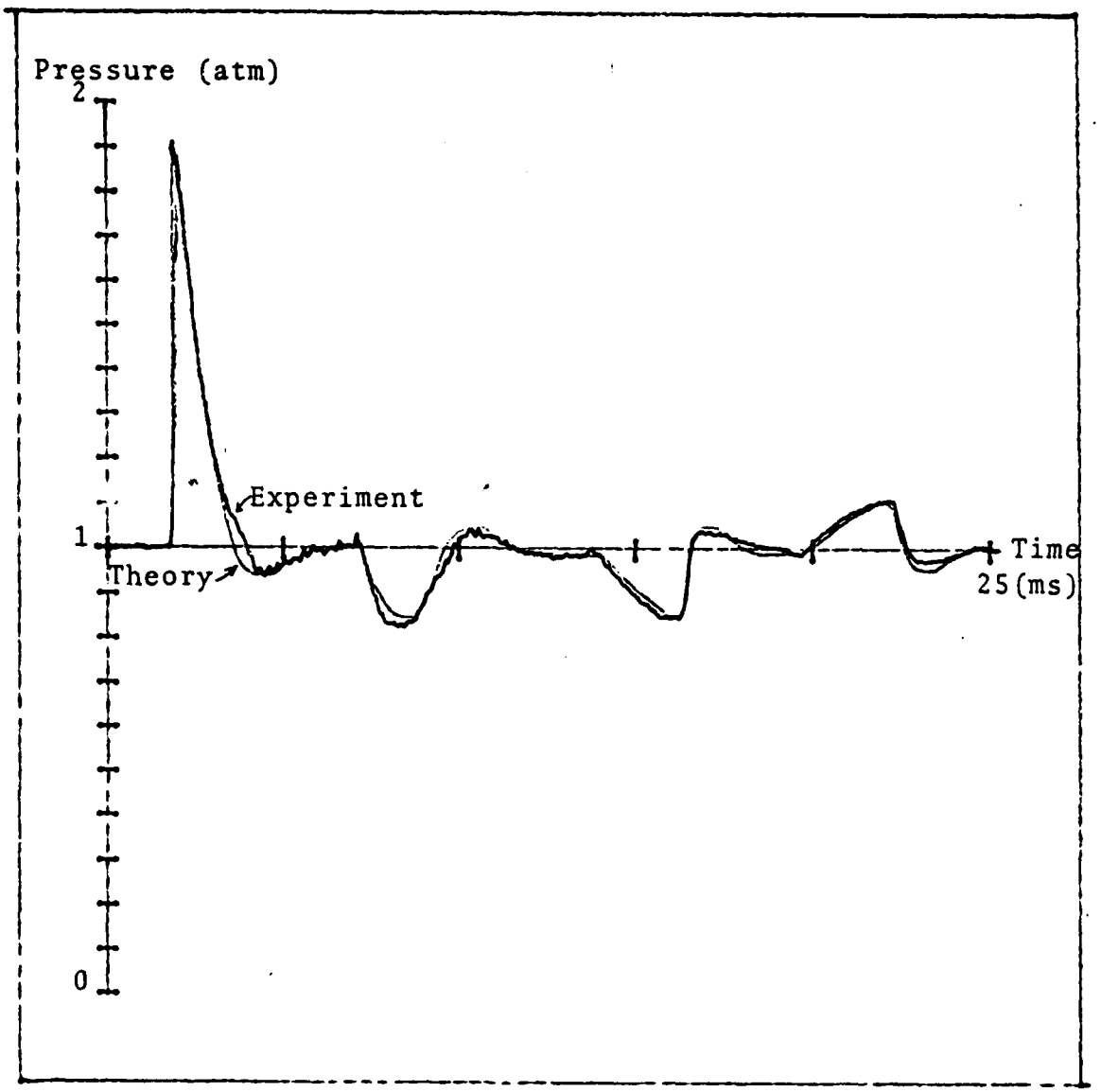


*Fig. IV.12.*
*COMPARISON OF MEASURED PRESSURE WAVES AND NUMERICAL SOLUTION IN A SHOCK TUBE WITH AN ORIFICE PLATE TERMINATION.*

*Open area fraction of the orifice plate: .79.*
*Pressure in driver section: 3.7 atm.*

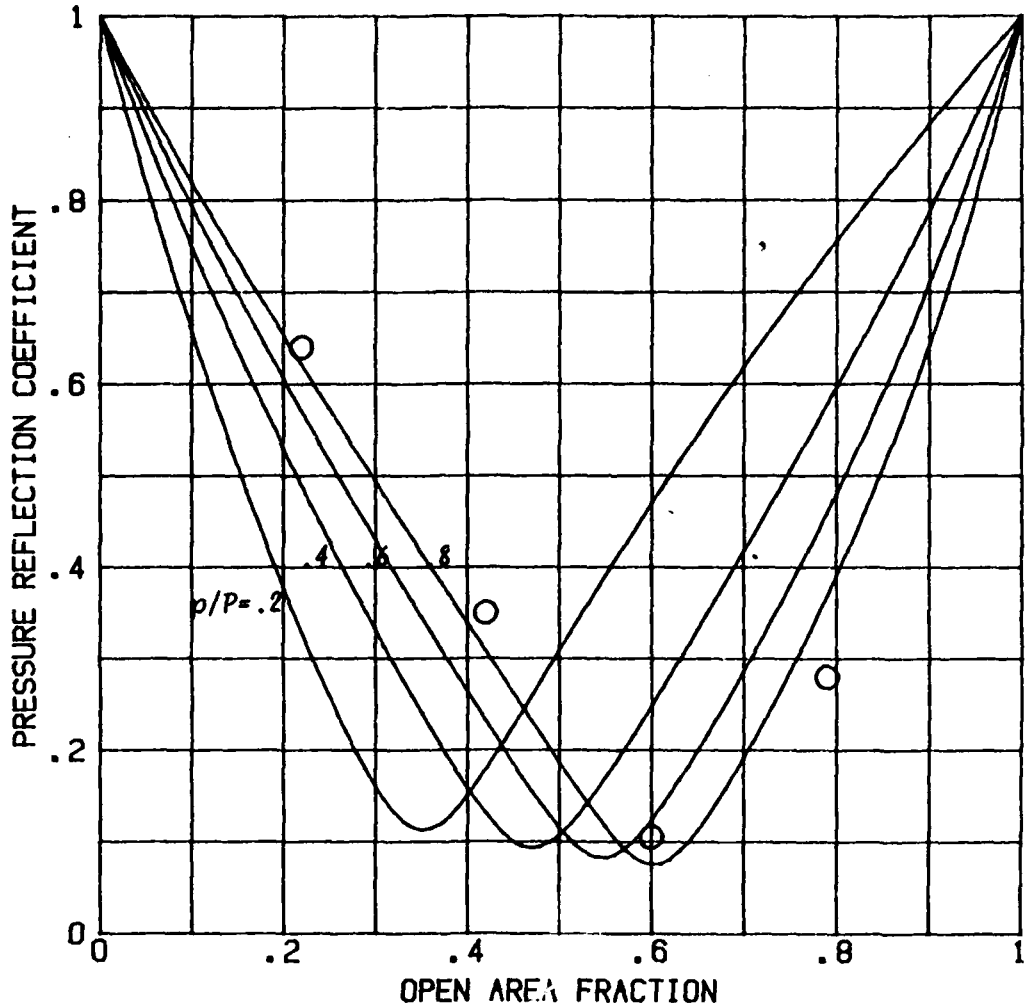


PRESSURE REFLECTION COEFFICIENT OF AN ORIFICE PLATE AT THE END OF A TUBE FOR AN INCIDENT SHOCK WAVE PULSE AS A FUNCTION OF THE OPEN AREA FRACTION.

DATA. Relative peak pressure of incident wave at the surface of the plate, p/P=.2, .4, .6, .8. Tube diamter, D=5 cm.
Circles: Experimental data at p/P=.73.
Curves computed from Eq. 8.

## IV. NONLINEAR ACOUSTIC ANALYSIS OF SHOCK WAVE ATTENUATION

The results on shock wave propagation and reflection in Section IV were obtained from the program in Appendix B through numerical integration of the fluid equation, and excellent agreement with experiments were well demonstrated. Nevertheless, it instructive and useful to carry out a simple acoustic analysis of the problem, which leads to a closed form expression for the attenuation of the peak amplitude of a large amplitude acoustic pulse wave.

The attenuation is casued by the entropy production in the bulk of the gas and at the walls of the tube. The resulting heat produced per unit length in the tube from the sudden compression of the gas as the shock wave travels through it is given by

$$E_1 = A\rho T\Delta S = A[(\gamma+1)/12\gamma^2]p^3/P^2 \qquad (1)$$

A=duct area
p=peak pressure of the pulse
P=ambient static pressure
T=absolute temperature
$\rho$=density
$\Delta S$=entropy increase across the shock
$\gamma$=specific heat ratio

There will be entropy produced also in the remainder of the pulse, where the pressure varies continuously with position, and the corresponding rate of heat production per unit volume is

$$\rho T dS/dt = \mu'(du/dx)^2 + (K/T)(dT/dx)^2 \qquad (2)$$

$\mu' = 4\mu/3 + \eta$
K=heat conduction coefficient
$\mu$=coefficient of shear viscosity
$\eta$=coefficient of bulk viscosity.

The perturbation in the temperature is $T(\gamma-1)u/c$, and if we introduce the characteristic length $L_2$ in the expressions for the gradients, we obtain from Eq. 2 the following expression for the heat production per unit length of the duct

$$H_2 = Ak^2 u^2 \mu'(1+\delta_2) \tag{3}$$

$$k = 1/L_2$$

$$\delta_2 = (\gamma-1)K/C_p\mu'$$

In the case of harmonic time dependence, we have $k=2\pi/\lambda$, where $\lambda$ is the wavelength, and to obtain the time average, an additional factor 1/2 should be used in Eq. 3. In that case the acoustic power transmitted in the duct is $Ap^2/2\rho c$, and Eq. 3 then leads to an exponential power decay, $\exp(-\beta_2 x)$, where

$$\beta_2 = k^2(\mu'/\rho c)(1+\delta_2) \tag{4}$$

a familiar result in acoustics.

In calculating the heat production at the boundaries of the duct, we can use Eq. 2 if we replace $\mu'$ by $\mu$ and let x be the coordinate normal to the boundary. The characteristic lengths, which determine the gradients are now the thicknesses of the viscous and thermal acoustic boundary layers. For harmonic time dependenc these thicknesses are

$$d_v = \sqrt{2\mu/\omega\rho} \tag{5}$$

$$d_t = \sqrt{2K/\rho\omega C_p} \tag{6}$$

With the perimeter of the duct denoted by D', the volume per unit length of the duct of a boundary layer will be dD', and the time average power lost per unit length of the duct is then

$$H_3 = D'(p^2/4\rho c)q \qquad (p=\rho cu) \tag{7}$$

$$q=(1+\delta_3)\sqrt{2\mu\omega/\rho c^2}$$

$$\delta_3 = (\gamma-1)/\sqrt{P_r}$$

$$P_r = \mu C_p/K \qquad \text{(Prandtl number)}$$

The corresponding exponential power decay will be $\exp(-\beta_3 x)$, where

$$\beta_3 = (D'/2A)q \tag{8}$$

with q given in Eq. 7.

Next we express the total energy of the pulse by integrating the energy density over the length of the pulse to obtain the expression $\alpha ALp^2/\rho c^2$, where p is the peak pressure and L the length of the pulse. The numerical factor $\alpha$ depends on the shape of the pusle. For rectangular, sinusoidal, and triangular pulses, the values of $\alpha$ are 1, 1/2, and 1/3, respectively. For pulses with pronounced narrow peaks, the values of $\alpha$ can be considerably smaller.

Returning to the Eq. 1, we note, that it expresses the energy lost per unit length in the duct due to the entropy production in the shock front. The visco-thermal boundary losses in Eq. 8, on the other hand, refers to the power loss, and we have to integrate over the duration T of the pulse to obtain the energy loss. In this integration we again obtain a numerical factor expressing the shape of the pulse, and we shall assume here that this factor is $\alpha$, i.e. the same factor as we used in the expression for the total energy of the pulse. Thus, in order to get the energy loss per unit length we have to multiply $H_3$ in Eq. 7 by $\alpha T = \alpha L/v$.

Having now determined the energy of the pulse and the losses per unit length, we can calculate the rate of decay of the pulse

*energy from the energy* balance equation

$$dW/dx=-E_1-E_3 \tag{9}$$

$W=x\alpha Lp^2$

$x$=compressiblity of gas, $1/\rho c^2$

$E_1$: (see Eq. 1)

$E_3=\alpha(L/v)H_3$

The average value $\hat{L}$ is $(L_0+L)/2$, where $L_0$ is the reference value at $x=x_0$ and L the value at the point of observation x. In other words, $\hat{L}$ depends (weakly) on x, and the same holds true for the factor $\alpha L/v$ in the expression for $E_3$. In the first approximation, we shall neglect this x-dependence and use the values $\hat{L}\simeq(v_0+c_0)T/2$, where $v_0$ is the value of v at $x=x_0$, $c_0$ the ambient sound speed, and $T_0$ the duration of the pulse at $x=x_0$.

Under these conditions Eq. (13) can be written in the form

$$dp/dx=-B_1 p-B_2 p^2 \tag{10}$$

$B_1=(D'/4A)(c/\hat{v})q$ (q: see Eq. 7)

$B_2=(1/2\alpha\hat{L}P)(1+\gamma)/12\gamma$

and the solution can be expressed as

$$p(x)/p(x_0)=E(x')/[1+F(x')/x_{\frac{1}{2}}] \tag{11}$$

$E(x')=\exp(-B_1 x')$

$F(x')=[1-E(x')]/B_1$

$x_{\frac{1}{2}}=\hat{L}[P/p(x_0)]\alpha 24\gamma/(1+\gamma)$

$x'=x-x_0$

The quantity $x_{\frac{1}{2}}$ is inversely proportional to the pressure ratio $p(x_0)/P$, so that for a weak pressure pulse, the denominator

simply reduces to 1. The pressure then decays exponentially as $\exp(-B_1 x')$. This is also the asymptotic form of the attenuation as x' goes to infinity, indendent of the value of $p(x_0)/P$.

In the other limit, for small values of x' and with $p(x_0)/P$ not negligible, we approximate F(x') by x' and obtain

$$p(x)/p(x_0) \cong 1/[1+(x-x_0)/x_{\frac{1}{2}}] \qquad (12)$$

From this relation we note, that the pressure amplitude is reduced by a factor of 2 (i.e. by 6 dB) after a travel distance $x_{\frac{1}{2}}$, the "half pressure distance".

As we shall see shortly, the appropriate value for $\alpha$ in our case is .26 (recall that for a triangular wave $\alpha=1/3$), so that the half pressure distance will be $3.6[P/p(x_0)]L$. With L typically .82 m in our experiments and with $p(x_0)/P \cong 1$, the half pressure distance will be 3 m.

Pulse length. In determining the viscothermal losses at the duct walls, we used the result for harmonic time dependence with the frequency chosen to be that, which yields the dominant contribution to the loss contribution in the frequency spectrum of the pulse. To go into further details and express the visco-thermal losses for an arbitrary time dependence does not seem to be justified in this context.

In selecting a frequency or the corresponding characteristic period to be used in the evaluation of the visco-thermal losses, we account for the fact, that the pulse length and its duration increases with the distance of wave travel. The leading (shocked) portion of the wave travels with the speed v(x), which depends on the pressure amplitude

$$v(x)=c_0 [1+(p(x)/P)(1+\gamma)/2\gamma]^{\frac{1}{2}} \qquad (13)$$

and the trailing part of the pulse travels with the ambient sound speed $c_0$.

The length of the pulse x is then

$$L(x)=L(x_0)+\int(v-c_0)dx/v\simeq L(x_0)+x(\hat{v}-c_0)/\hat{v} \qquad (14)$$

$$\hat{v}=(v_0+v)/2$$

If we use the x-dependence of the pressure in Eq. 11, we can determine the corresponding x-dependence of the propagation speed v(x) and evaluate the integral. For the present purpose, however, we approximate the integral as shown in Eq. 14.

The duration of the wave pulse at location x is

$$T(x)=L(x)/v(x)\simeq L_0/c_0+(x/\hat{v})(\hat{v}/c_0-1) \qquad (15)$$

where $L_c$ and $v_0$ ae the values of length and wave speed at $x=x_0$.

In the expression for the viscothermal losses, we used the duration T and the corresponding characteristic frequency $\omega=2\pi/T$, obtain at the half pressure point $x=x_{\frac{1}{2}}$

$$T_{\frac{1}{2}}\simeq L_0/c_0+(x_{\frac{1}{2}}/\hat{v})(\hat{v}/c_0-1)\simeq(v_0/c_0)T_0[1+(x_{\frac{1}{2}}/L_0)(v_0/c_0-1)] \qquad (16)$$

with $x_{\frac{1}{2}}/L_0\simeq(P/p_0)\alpha 24\gamma/(1+\gamma)\simeq(P/p_0)8\gamma/(1+\gamma)$ and $\alpha\simeq 1/3$, and where $p_0=p(x_0)$ is the peak pressure at $x=x_0$.

Comparison with experiments. In Fig. 1 is shown an example of the recorded pressure pattern resulting from multiple reflections of a pulse wave in our shock tube, when it was terminated by a rigid wall. The distance from the membrane in the driver section of the tube to the termination was 2 m, and the length of the driver sesction was .1 m. The pressure transducer was located at a distance from the membrane of $x_0=1$ m, where the peak pressure of the original pulse in this example was

$p_0 = p(x_0) = .94P$, where P is the ambient static pressure.

Sixteen reflections are shown in the figure, corresponding to a total travel distance of 32 m, and several more can readily be observed. The average pressure in the tube increases slowly toward the asymptotic value $(L_d/L)P_d$ above ambient where, $L_d$ is the length of the driver section, L the length of the shock tube (including the driver section), and $P_d$ the initial pressure above the ambient in the driver section. In our case $P_d$ was 3.67 atm., so that the asymptotic pressure should be .17 atm above ambient, which is in good agreement with the observed value. ($L=2.1$ m, $L_d=.1$ m).

The travel distance of a pulse versus time obtained from this record is shown in Fig. 2. The slope of the curve is the wave speed. According to Eq. 13, the wave speed at $x=1$, where $p(1)=.94P$, should be 1.34 times larger than the ambient sound speed in air (with $\gamma=1.4$). Within the experimental accuracy, the data in Fig. 2 are consistent with this prediction.

Of more interest is the x-dependence of the peak pressure of the pulse, as shown in Fig. 3, where $p(x)/p(x_0)$ is plotted as a function of x. The solid curve in the figure is the decay curve obtained from Eq. 11, in which we have chosen the "pulse shape factor" to be .28, i.e. close to the theoretical value for a triangular pulse.

The agreement between the measured and predicted results is quite satisfactory. We note that the "half pressure distance" $x_{\frac{1}{2}}$, corresponding to a 6 dB reduction in the peak pressure is $xx = 3$ m, as predicted.

In Fig. 4 are shown the computed curves for other values of the initial peak pressure. Unfortunately, experimental data for these were not obtained. The initial reduction in pressure per unit length is considerable, being about 4.7 db/m for the pulse with a peak pressure $p(1)=2$ atm. It is important to account for this decay in the acoustic analysis of the overall system.

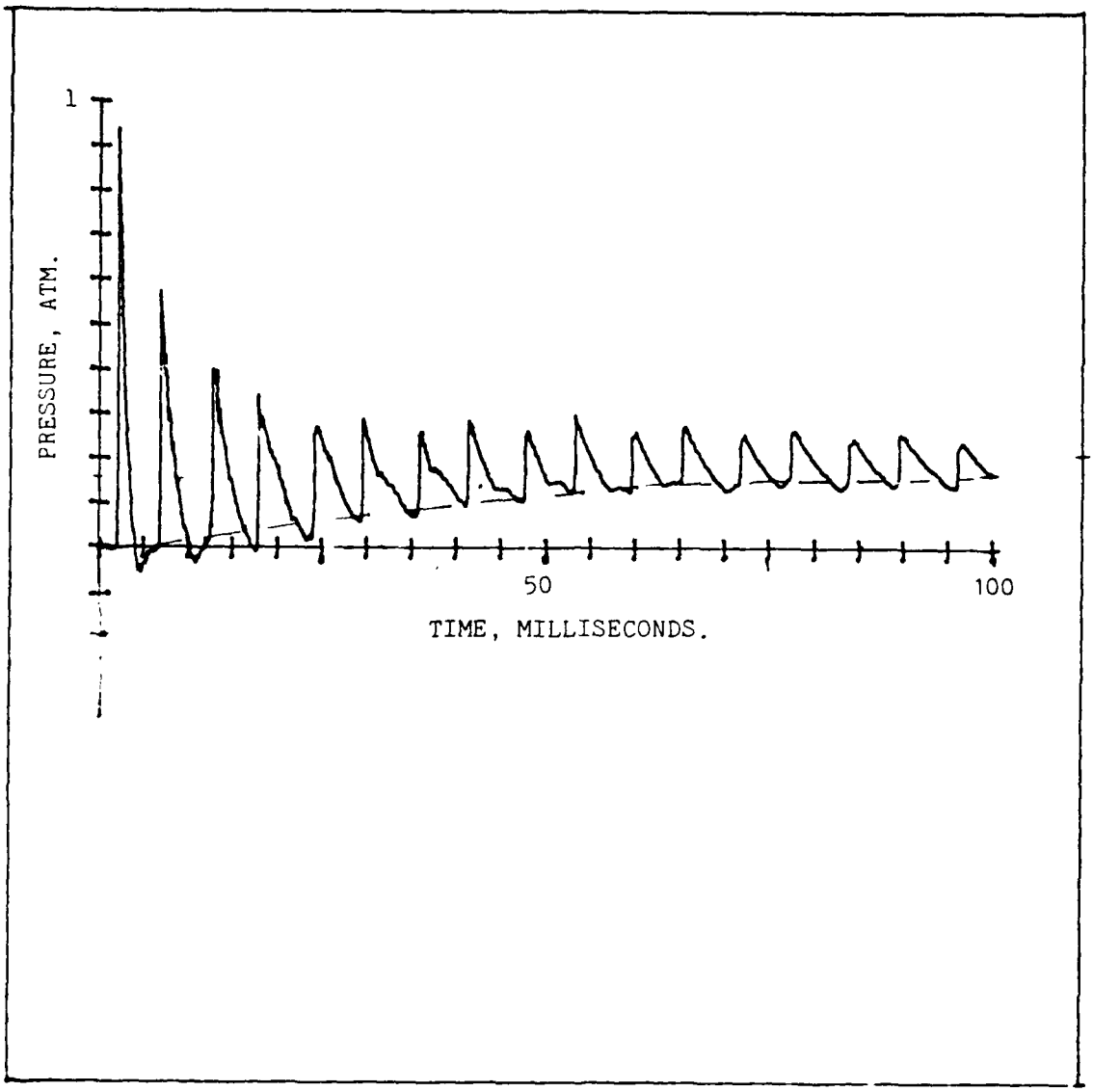


Fig. V.1.
MULTIPLE REFLECTIONS OF A PULSE WAVE IN A SHOCK TUBE CLOSED AT BOTH ENDS

DATA: Pressure peak at x =1 m. p(1)=.94 atm.
Tube length: 2m. Driver length: .1 m.
Driver pressure: 3.67 atm (above ambient).
Gas: Air at atm. pressure.

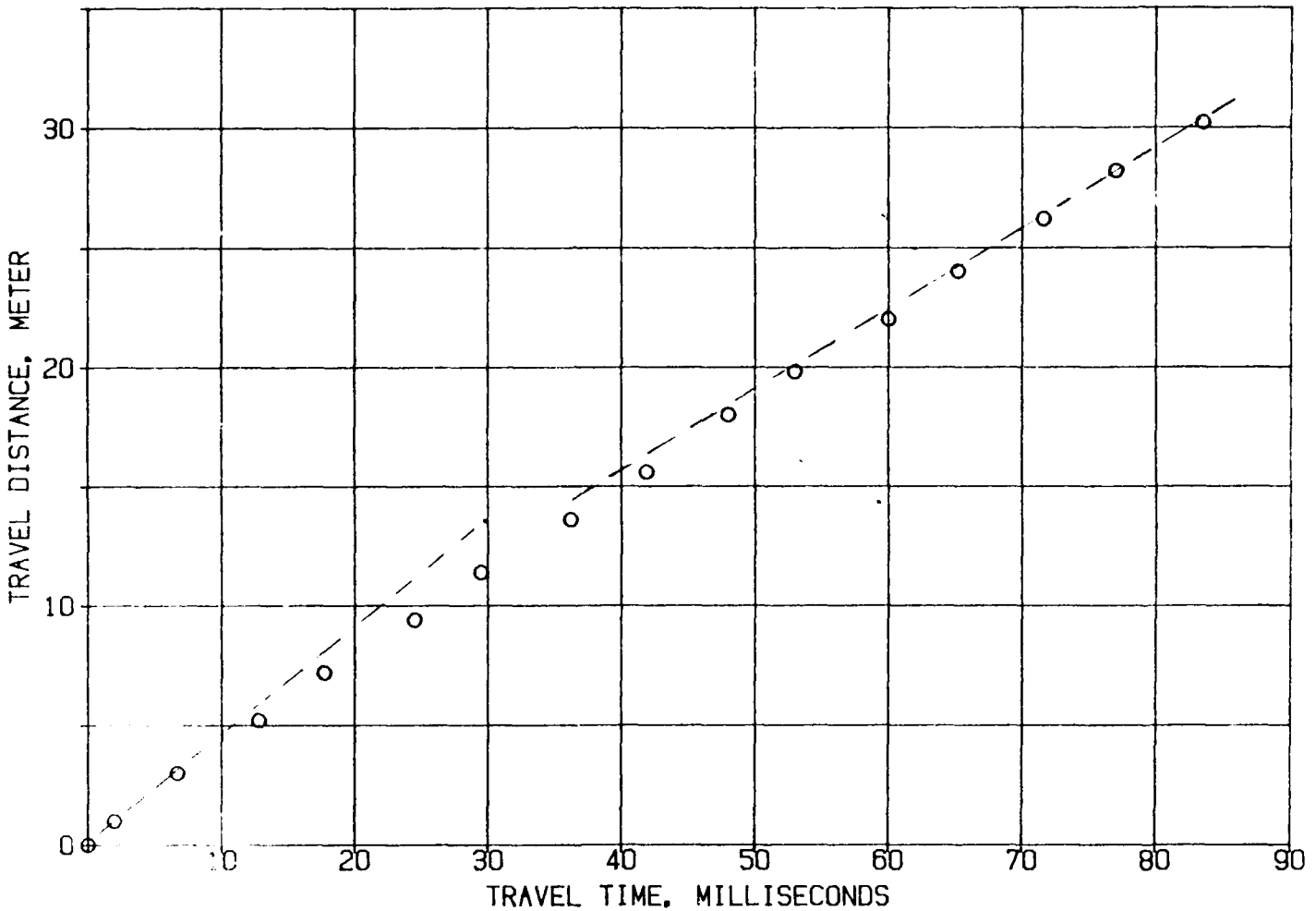


Fig. V 2.
GRAPH OF DISTANCE VERSUS TIME FOR A PULSE WAVE IN A SHOCK TUBE.
DATA: Peak pressure of pulse at x = 1 m, p
Tube diameter: 5 cm. Gas: Air, atm pressure.

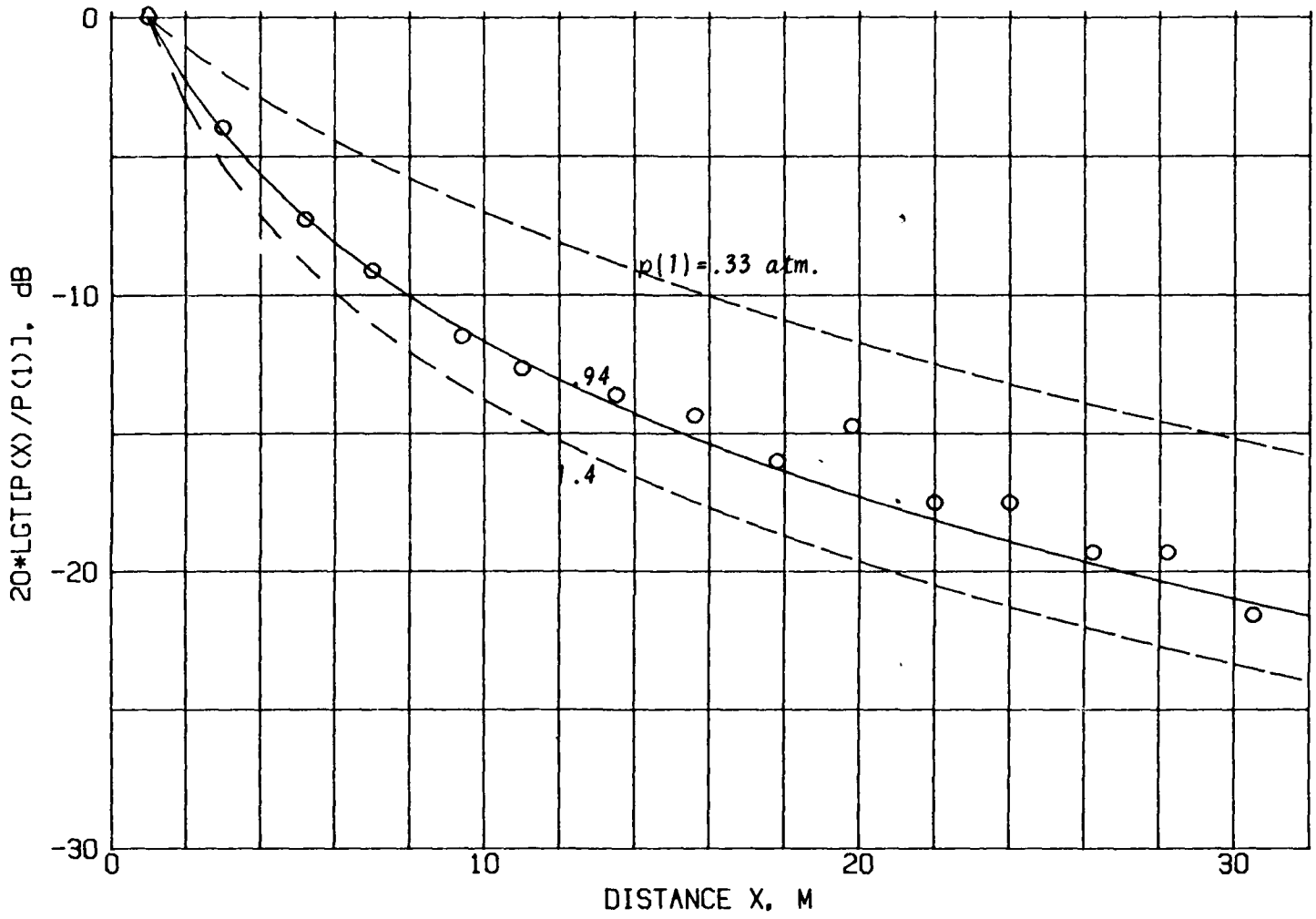


*Fig. V.3.*
NORMALIZED PEAK PRESSURE, p(x)/p(1), OF A PULSE WAVE VERSUS TRAVEL DISTANCE IN A SHOCK TUBE.

*DATA. Peak pressure at x=1 m, p(1)=.33, .94, 1.4 atm.*
*Tube diameter: 5 cm. Gas: Air, atm. pressure.*
*Circles: Experimental data for p(1)=.94 atm.*

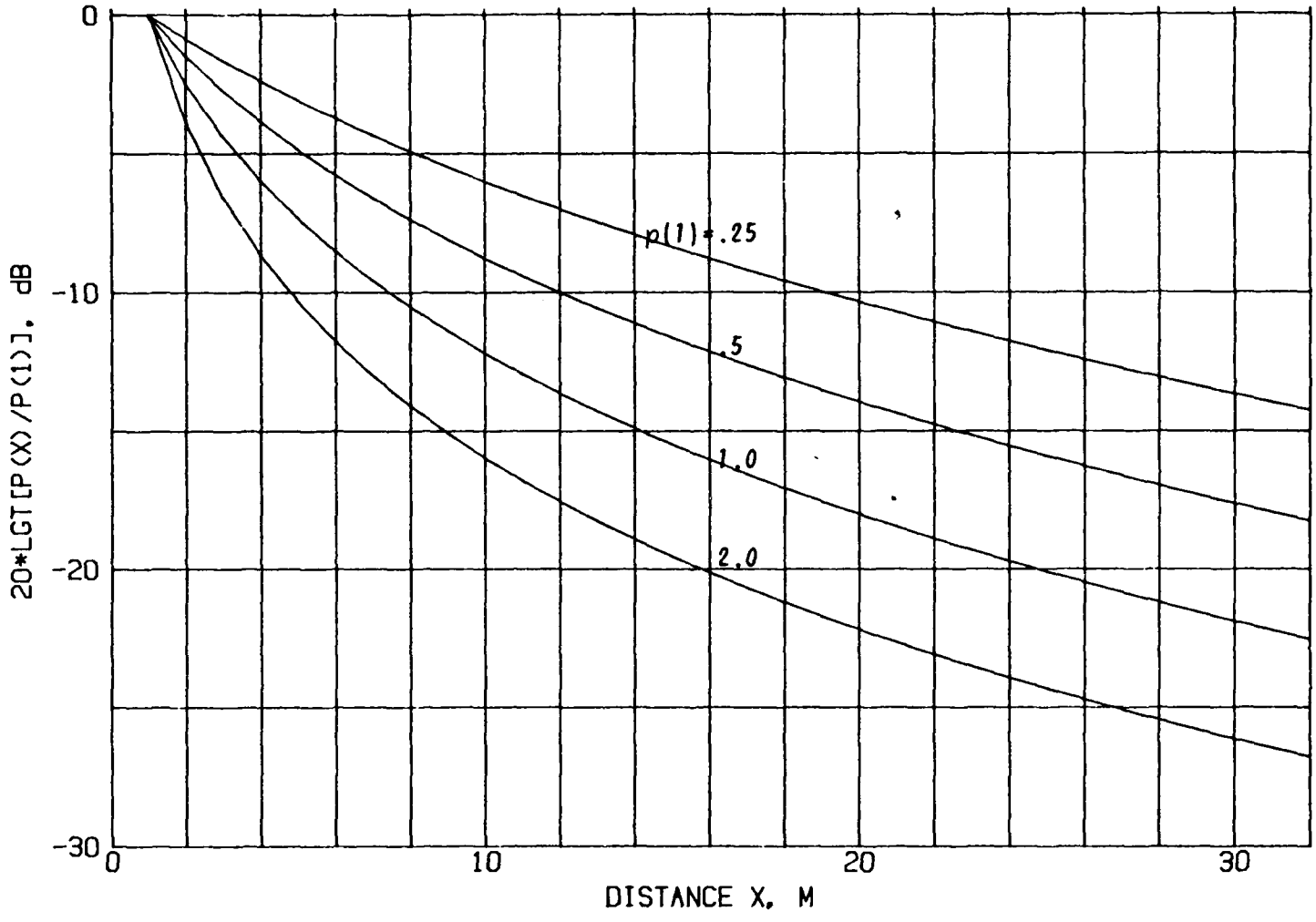


*Fig. V.4.*
COMPUTED X-DEPENDENCE OF THE PEAK PRESSURE OF A WAVE PULSE IN A SHOCK TUBE.

*DATA. Peak pressure at x=1 m, p(1)=.25, .5, 1, and 2 atm.*
*Tube diamter: 5 cm.*
*Gas: Air. Ambient pressure, 1 atm.*

# V. THEORY AND DESIGN OF NONLOCALLY REACTING PARALLEL BAFFLE ATTENUATORS

## 1. Introduction.

The propagation of sound in attenuating ducts have been the subject of numerous studies ranging from routine attenuation measurements to complex mathematical studies. In most of the mathematical analyses, starting with those of Morse (18) and Brillouin (19), the duct liners have been assumed to be locally reacting with a normal acoustic impedance known a priori, expressing a characteristic property of the liner independent of the nature of the sound field, to which it is exposed.

One notable exception is the analysis by Scott (20) of sound propagation in a duct with a rigid porous layer, which did not rely on the assumption of local reaction. The general expression for the dispersion relation was derived and numerical analysis for a few modes was carried out.

In the present study, the general analysis is extended to include a flexible porous liner and a uniform mean flow in the duct. Furthermore, and more important from the standpoint of design and system analysis, we derive closed form expressions for the frequency dependence of the attenuation and phase velocity for long wavelengths, which makes a parametric study of the characteristics of the attenuator tractable. For example, simple formulas are given for the optimum design for maximum attenuation at a given frequency.

The results can be applied not only to a lined duct but also to a "parallel-baffle" attenuator, which contains several porous baffles in a duct, as shown in Fig. 1.

## 2. The dispersion relation.

The porous material in the liners or baffles is assumed to be homogeneous and isotropic. To account for the flexibility in a

simple manner, we neglect the structural stiffness and treat the material as "limp" with a mass density M. The results corresponding to a rigid material is then obtained by putting M equal to infinity in the final formulas. The assumption of limpness is valid if the compressional wave speed in the porous structure is considerably smaller than the speed of sound in the surrounding gas.

To analyze wave propagation in a duct lined with a nonlocally reacting porous layer, we consider a two-dimensional duct with a hard wall at y=D and a porous layer of thickness d placed at the wall at y=0. The axis of the duct is in the x-direction.

Ths sound pressure fields in the two regions are then

$$p=A\cos[k_y(D-y)]\exp(ik_x x) \qquad \text{(gas)} \qquad (2.1)$$

$$p'=B\cos(q_y y)\exp(ik_x x) \qquad \text{(porous material)} \qquad (2.2)$$

where

$$k_x^2+k_y^2=k^2=(\omega/c)^2 \qquad (2.3)$$

$$q_x^2+q_y^2=q^2=(\omega/\hat{c})^2=(\omega/c)^2(\hat{\rho}/\rho)(\hat{\varkappa}/\varkappa) \qquad (2.4)$$

The quantities $\hat{c}$ and $\hat{\rho}$ are the complex sound velocity and the complex inertial mass density in the gas in the porous material, as defined in Appendix . We have

$$\hat{\rho}/\rho=H+iz/\omega\rho \qquad (2.5)$$

$$\hat{z}=z/(1+iz/\omega M)$$

$$z=r-i\omega gH\rho \qquad (\varkappa=1/\rho c^2,\ \hat{\varkappa}=1/\hat{\rho}\hat{c}^2)$$

where H is the porosity, M the mass density, and r the flow resistance per unit length of the porous material. The factor g is the induced mass factor defined in Appendix .

The y-component of the velocity in each of the two regions follows from Eqs. 2.1 and 2.2,

$$u_y=(1/i\omega\rho)\partial p/\partial y=(A/i\rho c)K_y \sin[k_y(D-y)]\ \exp(ik_x x) \quad (2.6)$$

$$u'_y=(1/i\omega\rho')\partial p'/\partial y=-(B/i\rho c)[Q_y/(\hat{\rho}/\rho)]\sin(q_y y)\ \exp(ik_x x) \quad (2.7)$$

Continuity of pressure and normal mass flow at the boundary of the porous material require, that $p=p'$ and $u_y=Cu'_y$ for $y=d$, where $C=(H+i\,z/\omega M)/(1+i\,z/\omega M)$. Applying these conditions on the expressions for pressure and velocity above, we obtain

$$K_y \tan[K_y k(D-d)]=-C(\rho/\hat{\rho})Q_y \tan(Q_y kd) \quad (2.8)$$

$K_y=k_y/k$, $Q_y=q_y/k$, $k=\omega/c$

Having obtained $K_y$ from this equation, we determine the progation constant of interest

$$K_x=\sqrt{1-K_y^2} \qquad \text{(See Eq. 2.3)} \quad (2.9)$$

From the real and imaginary parts of this propagation constant, we obtain the phase velocity along the axis of the duct

$$v_p=(k/K_r)c \quad (2.10)$$

c=free space sound speed. $K_x=K_r+iK_i$

and the x-dependence of the wave amplitude, $\exp(-K_i kx)$, corresponding to an attenuation in dB per unit length

$$A=20\cdot\log(e)\cdot K_i k\approx 8.7\ K_i k \quad (2.11)$$

These results are valid also for a two dimensional duct with both walls lined if we consider the wave modes symmetrical with respect to the center plane of the duct. The dimension D is then half of the duct width, and the fraction open area of the duct is $S=(D-d)/d$.

For modes, which are anti-symmetrical with respect to the center plane of the duct (a nodal plane for pressure), Eq. 2.8 has to be replaced by

$$K_y \cos[K_y k(D-d)] = (\rho/\hat{\rho}) Q_y \tan(Q_y kd) \qquad (2.12)$$

If several ducts lined on both sides are arrange in parallel we obtain a "parallel-baffle" attenuator, each baffle having a thickness 2d and with a separation between adjacent baffles of 2D. The fraction open area of the attenuator is S=(D-d)/D, as before.

## 3. Optimum design.

It is clear, tht for the two limiting values of the flow resistance, zero and infinity, the attenuation will be zero. Consequently, there exists an optimum value for the flow resistance, for which the attenuation is a maximum. This optimum value is expected to depend on frequency. To determine it in the general case requires extensive numerical parameteric studies.

On the other hand, it is of considerable practical importance to determine the attenuation at long wavelengths, which is most cases play the most important part in the design of the attenuator. In this long wavelength regime, it is possible to simplify the dispersion relation considerably.

Thus, if we assume, that both d and D are much smaller than a wavelength, so that both kD and kd are small compared to unity, Eq. 2.9 can be written

$$K_x^2 = aZ/(Z+b) \qquad (3.1)$$

$K_x = k_x/k \qquad k=\omega/c$

$Z=\hat{\rho}/\rho$ (See Eq. 2.5)

$a=[1+(\hat{\varkappa}/\varkappa)CS']=1+HS'$

$b=CS', \quad C=(z-iH\omega M)/(z-i\omega M)=H(\varkappa/\hat{\varkappa})$

$S'=(1-S)/S$. $S=(D-d)/D$=fraction open area of the attenuator.

We note, that for S=0 we obtain $K_x=\sqrt{(\hat{\rho}/\rho)(\hat{\varkappa}/\varkappa)}$, the result for a porous material, and for S=0 we get $K_x=1$, which is consistent with the value for propagation in the gas.

The right hand side of Eq. 3.1 is a complex number A+iB, which readily can be determined in terms of the physical parameters of the porous material and the duct system. The corresponding expressions for the real and imaginary parts of the propagation constant $K_x=K_r+iK_i$ are then

$$K_r=(1/\sqrt{2})(\sqrt{A^2+B^2}+A)^{\frac{1}{2}} \tag{3.2}$$

$$K_i=(1/\sqrt{2})(\sqrt{A^2+B^2}-A)^{\frac{1}{2}} \qquad (K_x^2=A+iB) \tag{3.3}$$

As already indicated, the corresponding values for the phase velocity of the fundamental mode in the duct system is then

$$v_p=(k/K_r)c \tag{3.4}$$

and the attenution in dB per unit length of the duct is

$$A\approx 8.7kK_i\approx 54.6K_i f/c \tag{3.4}$$

where f is the frequency.

Examples of the frequency dependence of the phase velocity, computed from Eq. 3.4, are shown in Fig. B.1. In this particular case the porous material is assumed to be rigid. But even for a comparatively light limp material, with M=.05 g/cm$^3$, for example, the results are approximately the same. The motion of the porous material reduces the friction coupling slightly, and the phase velocity becomes somewhat higher. The difference increases with increasing flow resistance, however.

Of more interest in this context is the attenuation and its frequency dependence. Examples of computed attenuation curves A versus f for some different values of the flow resistance and

the open area fraction are shown in Figs. 3-6 .. It can be seen from these curves, that for given values of frequency and open area fraction, the attenuation has a maximum for a certain value of the flow resistance.

In order to see this dependence on R more clearly, we have plotted the attenuation versus R with frequency as a parameter, as shown in Figs. 7-10 . By comparing Figs. 7 and 8 we get an idea of the difference in attenuation between limp and rigid baffles. For the particular open area fraction involved, S=.2 and the mass density, corresponding to m=38, the difference is small. The rigid baffle yields a somewhat higher attenuation and the optimum resistance is slightly larger than for the limp material.

It is interesting in this context to note, that for a rigid porous material, the value of the optimum resistance and the corresponding maximum attenuation can expressed in a simple closed form in terms of the open area fraction and the frequency. This follows, after some algebra, by maximizing the expression for $K_i$ in Eq. 3.3 with respect to the flow resistance. We find, that the optimum flow resistance can be expressed as

$$R=r/\rho c=kH(G+S')[(4G+S')/(4G+3S')]^{\frac{1}{2}} \qquad (3.5)$$

$S'=(1-S)/S$

$G=1+g$=structure factor of porous material

The correspnding expressions for the maximum value of $K_i$ and the corresponding attenuation in dB per unit length are

$$K_i==(1/2\sqrt{2})S'[(1+HS')/(G+S')(2G+S')]^{\frac{1}{2}} \qquad (3.6)$$

$A\approx 8.7\ kK_i \approx 54.6\ K_i f/c$

$k=2\pi f/c$

f=frequency

c=sound speed in gas

H=porosity

Thus, for an acoustically compact duct or baffle attenuator with nonlocally reacting porous material, the optimum flow resistance, as well as the corresponding maximum attenuation, is proportional to the frequency, and the constants of proportionality are functions of the open area fraction, as shown in Figs. 11-12.

These results have been derived for a rigid porous material, but in most cases they are good approximations for the optimum design of flexible porous baffles. The flexibility reduces somewhat the values of both the optimum resistance and the maximum attenuation.

It is significant, that for the nonlocally reacting baffles considered here, the dependence of the geometry of the attenuator on the attenuation is expressed by the single parameter S, the open area fraction. This means, that for a given value of S, we can make the baffles quite thin without reducing the low frequency attenuation. The corresponding width of the channel between two adjacent baffles then will be small also, which reduces the effect of the "beaming" of sound and the corresponding loss in attenuation at high frequencies. In the selection of a baffle thickness, nonacoustical factors must be considered also, such as the pressure drop in the presence of a mean flow.

## 4. Effect of mean flow.

Again, we consider the two dimensional duct with a rigid wall at y=D and a porous, nonlocally reacting porous layer of thickness d applied to the wall at y=0. Uniform flow in the duct is assumed with a velocity U and the corresponding Mach number M=U/c, not to be confused with the mass density M of the porous material.

The determination of the dispersion relation is quite similar to what we did earlier in the absence of flow. The difference can be expressed simply by assigning a different value for the constant C, which was defined in the discussion of Eq. 2.8.

The factor C now contains the propagation constant $k_x$

through the additional factor $(1-MK_x)^n$, where n is 1 or 2 depen- on whether continuity of particle velocity or displacement is assumed just outside the boundary layer of the porous material. Which boundary condition to use is an open question. In a special case, involving flow over a side branch cavity in a duct, a transition from n=2 to n=1 with increasing flow speed was found to be consistent with experimental data (4).

Thus, for an acoustically compact parallel baffle attenuator, the dispersion relation can be expressed as

$$K_x = a'Z/(Z+b') \tag{4.1}$$

$K_x = k_x/k$, $k=\omega/c$

$Z=\hat{\rho}/\rho$

$b'=C(1-MK_x)^n$, $a'=1+b'$

$M=U/c$, U=mean flow velocity.

## 5. Pressure reflection coefficient.

In most engineering problems involving mufflers, the reduction of the transmitted sound is of primary interest. In the application considered in this report, howeer, the pressure pulses reflected from an attenuator (or any other discontinuity in the duct loop) is an equally important factor to consider.

To determine the reflection coefficient at the entrance to a parallel baffle attenuator or lined duct, we start by determining the characteristic wave impedance. In the long wavelength approximation it is the ratio between the complex pressure amplitude and the amplitude of the average velocity across the duct.

With the pressure field given by Eqs. 2.1 and 2.2, the x-component of the velocity in the gas and in the porous material are

$$u_x = (1/\omega\rho)k_x A\cos[k_y(D-y)]\exp(ik_x x) \tag{5.1}$$

$$u_x' = (1/\omega\hat{\rho})k_x B\cos(q_y)\exp(ik_x x)$$

The average value of the velocity across the duct is

$$\underline{u}=Su_x+(1-S)u'_x \tag{5.2}$$

With A B, the normalized wave impedance becomes (see Fig. 13)

$$Z_0=(1/\rho c)p/\underline{u}=(1/K_x)Z/(SZ+1-S) \tag{5.3}$$

$Z=\hat{\rho}/\rho$

S=open area fraction=(D-d)/D

To obtain the input impedance of the attenuator, we must modify the average flow velocity somewhat to account for the boundary condition at the leading edge of the porous baffles. As explained in Section A4, the flow velocity in the gas outside the porous material is $Cu'_x$, where C is given in Eq. 3.1. This modification applies only to the part of the duct occupied by the baffles, and the input impedance becomes

$$Z_1=(1/K_x)Z/[SZ+C(1-S)] \tag{5.4}$$

Comparing this with the expression for $K_x$ in Eq. 3.1, we obtain

$$Z_1=K_x/[H+S(1-H)] \tag{5.5}$$

The pressure reflection coefficient at the entrance to the attenuator then can be expressed as

$$R_p=(Z_1-1)/(Z_1+1) \tag{5.6}$$

Fig. 14 shows the results of the computed frequency dependence of the reflection coefficient for some different values of the open area fraction S for rigid baffles. For a solid baffle,

we have $K_x=1$, and with H=1, the reflection coefficient reduces to the value (1-S)/(1+S), corresponding to the change in the area of the duct.

It should be emphasized, the the reflection coefficient in Eq. 5.6 refers to the reflection from the front end of the attenuator. There will be a reflection also at the other end, but the corresponding reflected wave will be attenuated by an amount corresponding to a travel distance equal to twice the length of the attenuator.

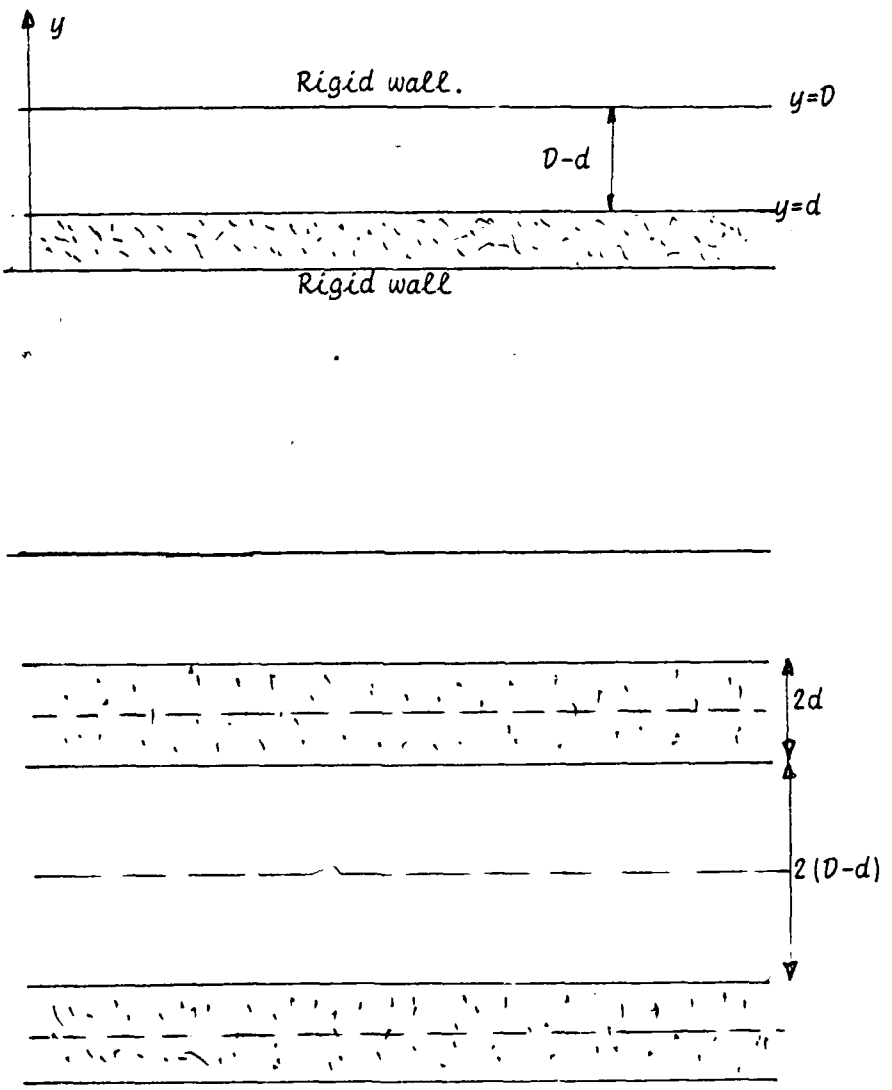


Fig. VI.1.
DUCT WITH ONE WALL LINED WITH A POROUS LAYER AND THE CORRESPONDING PARALLEL BAFFLE ATTENUATOR.

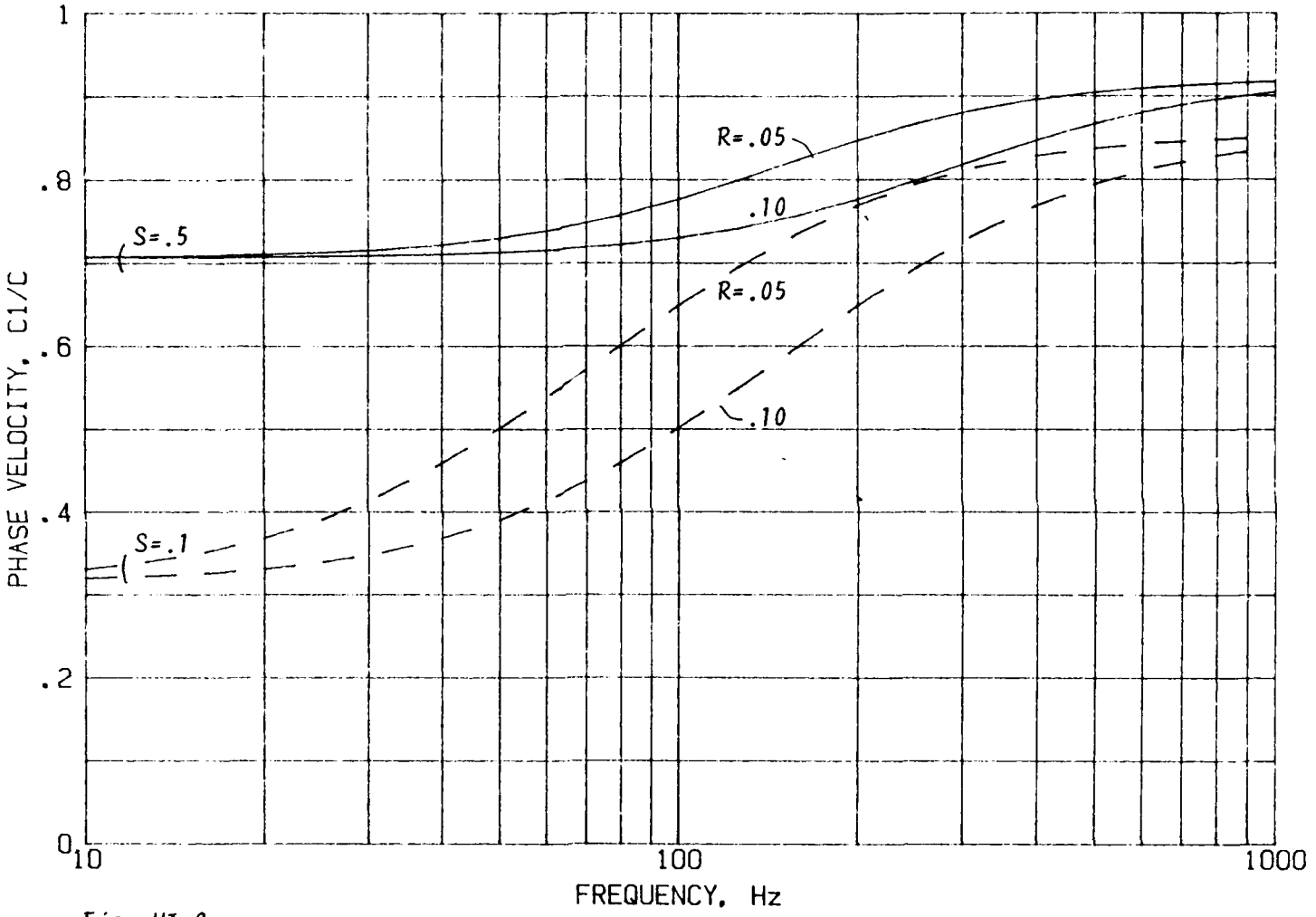


*Fig. VI.2.*
ACOUSTIC PHASE VELOCITY RATIO: C1=PHASE VELOCITY IN PARALLEL-BAFFLE ATTENUATOR, C=PHASE VELOCITY IN GAS.

*DATA. Porous baffle: Rigid and nonlocally reacting. Flow resistance, R=.05, .10 ro-ce units/cm. Porosity, H=.95. Structure fctr, G=1.5. Fraction open area of attenuator, S=.1, .5.*

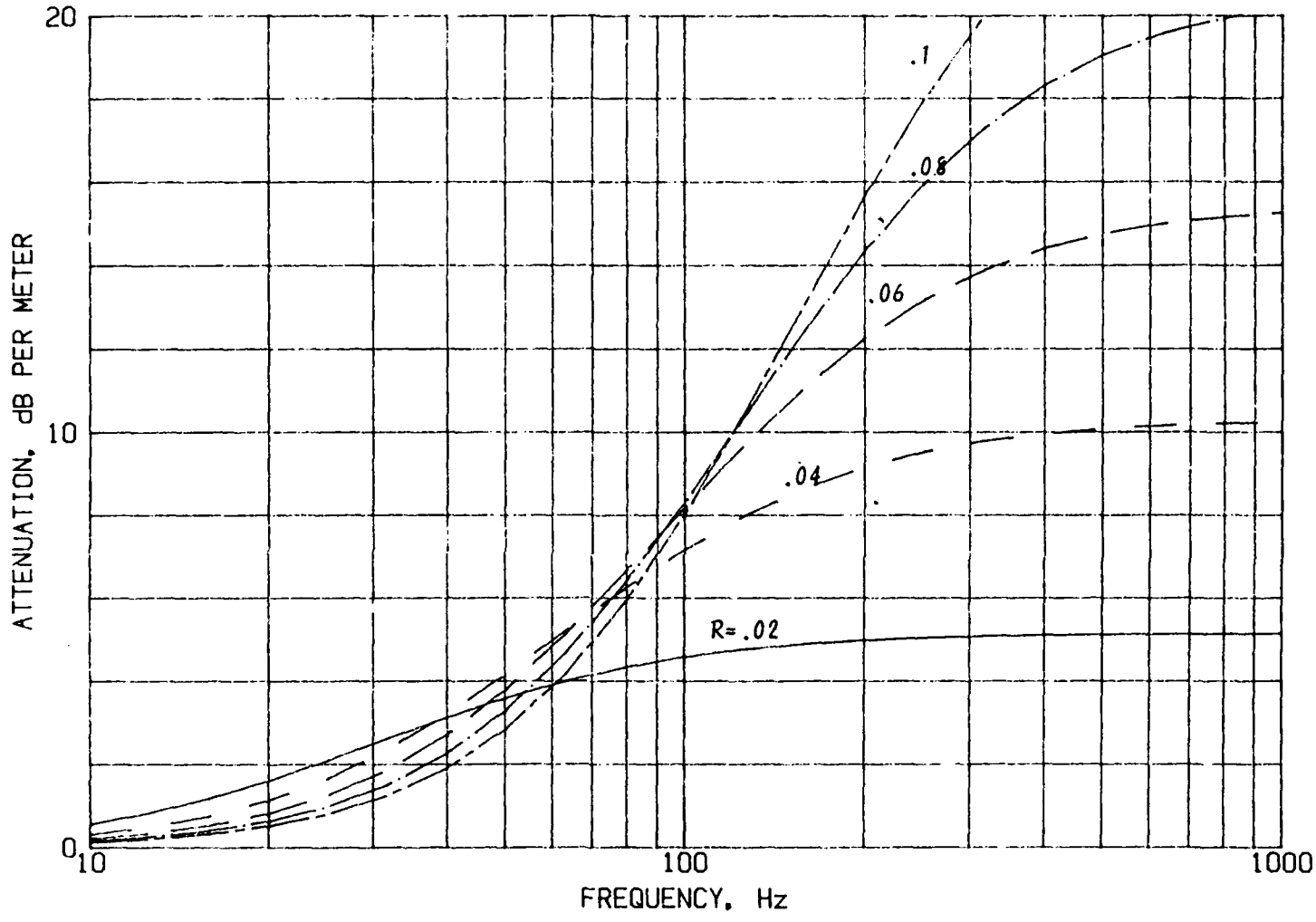


*Fig. VI.3.*
*ATTENUATION OF SOUND IN A POROUS PARALLEL-BAFFLE ATTENUATOR (NON LOC. REACTING, ACOUST. COMPACT).*

*DATA. Porous material (assumed rigid): Flow resistance, R=.02, .04, .06, .08, .10 rayls/cm. Porosity, H=.95. Structure factor, G=1.5. Fraction open area of attenuator, S=.20.*

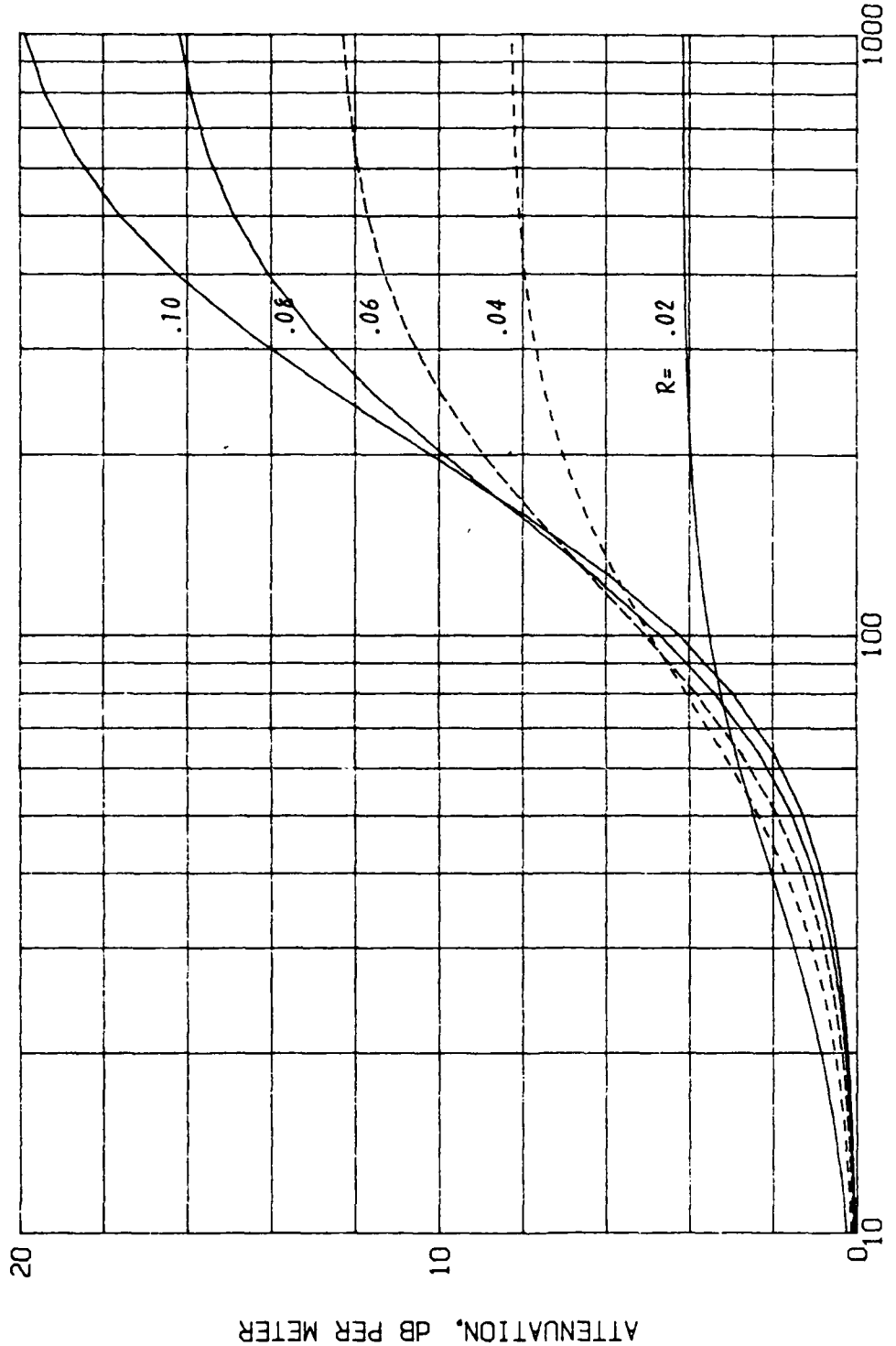


*Fig. VI.4.*
ATTENUATION OF SOUND IN A POROUS PARALLEL-BAFFLE ATTENUATOR (NON LOC. REACTING, ACOUST. COMPACT).

*DATA. Porous material (assumed limp): Flow resistance, R=.02, .04, .06, .08, .10 mks units/cm. Porosity, H=.95. Structure factor, G=1.5. Ratio between mass density and gas density, m=38. Fraction open area of attenuator, S=.30.*

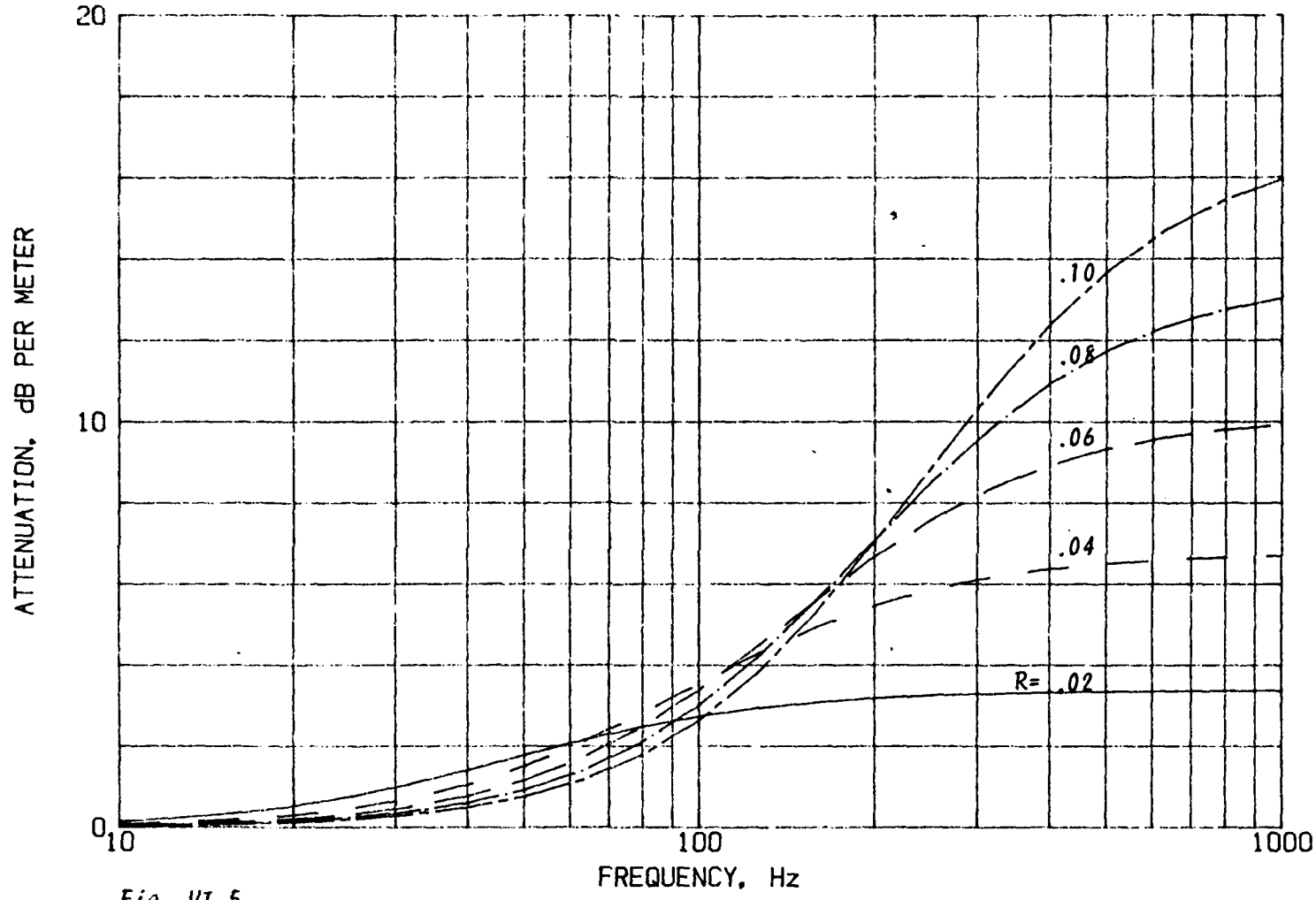


*Fig. VI.5.*
ATTENUATION OF SOUND IN A POROUS PARALLEL-BAFFLE ATTENUATOR (NON LOC. REACTING, ACOUST. COMPACT).

DATA. Porous material (assumed limp): Flow resistance, R=.02, .04, .06, .08, .10 ro-ce units/cm. Porosity, H=.95. Structure factor, G=1.5. Ratio betweeen mass density and gas density, m=38.
Fraction open area of attenuator, S=.40.

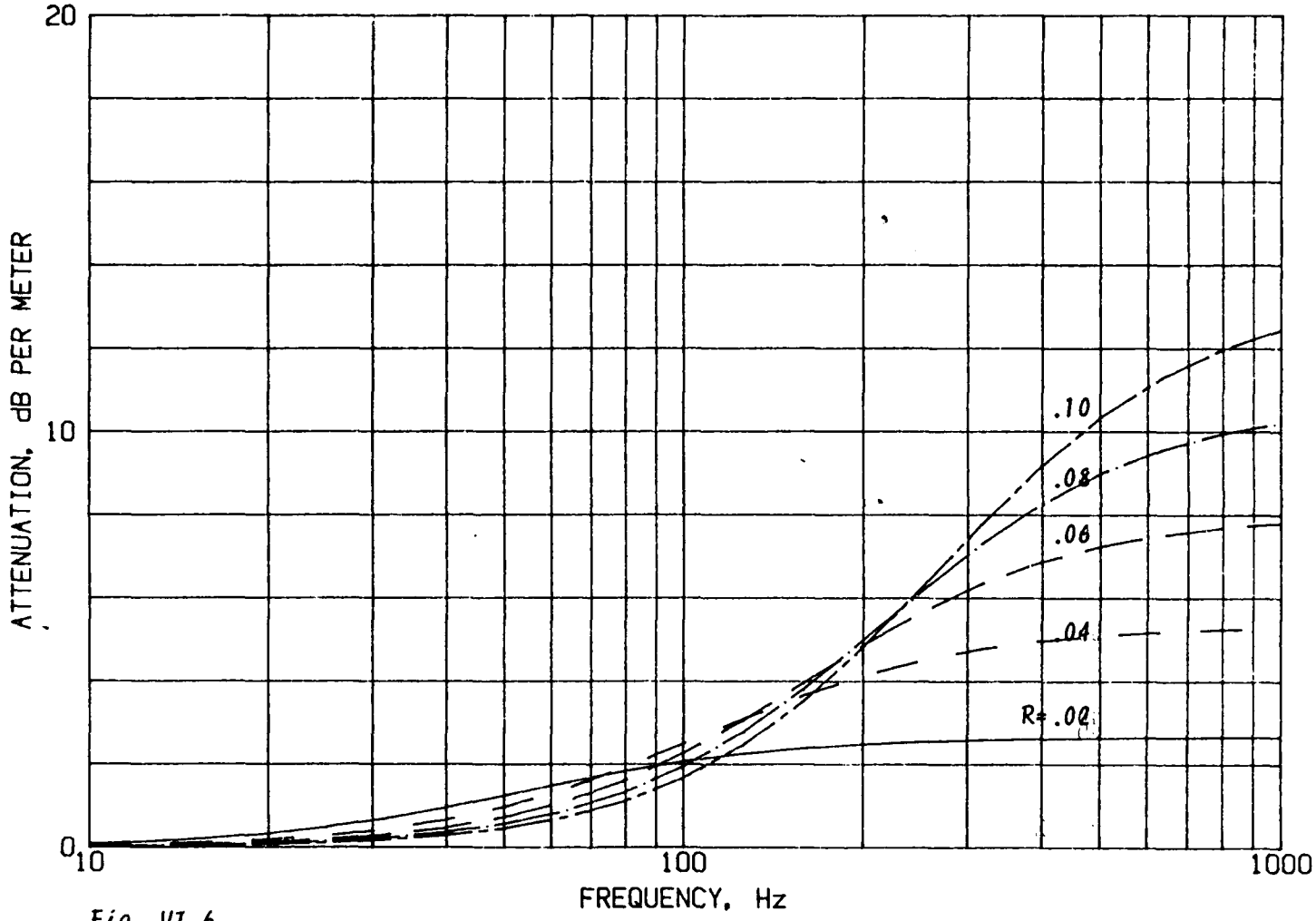


*Fig. VI.6.*
ATTENUATION OF SOUND IN A POROUS PARALLEL-BAFFLE ATTENUATOR (NON LOC. REACTING, ACOUST. COMPACT).

*DATA. Porous material (assumed limp): Flow resistance, R=.02, .04, .06, .08, .10 ro-ce units/cm. Porosity, H=.95. Structure factor, G=1.5. Ratio betweeen mass density and gas density, m=38.*
*Fraction open area of attenuator, S=.50.*

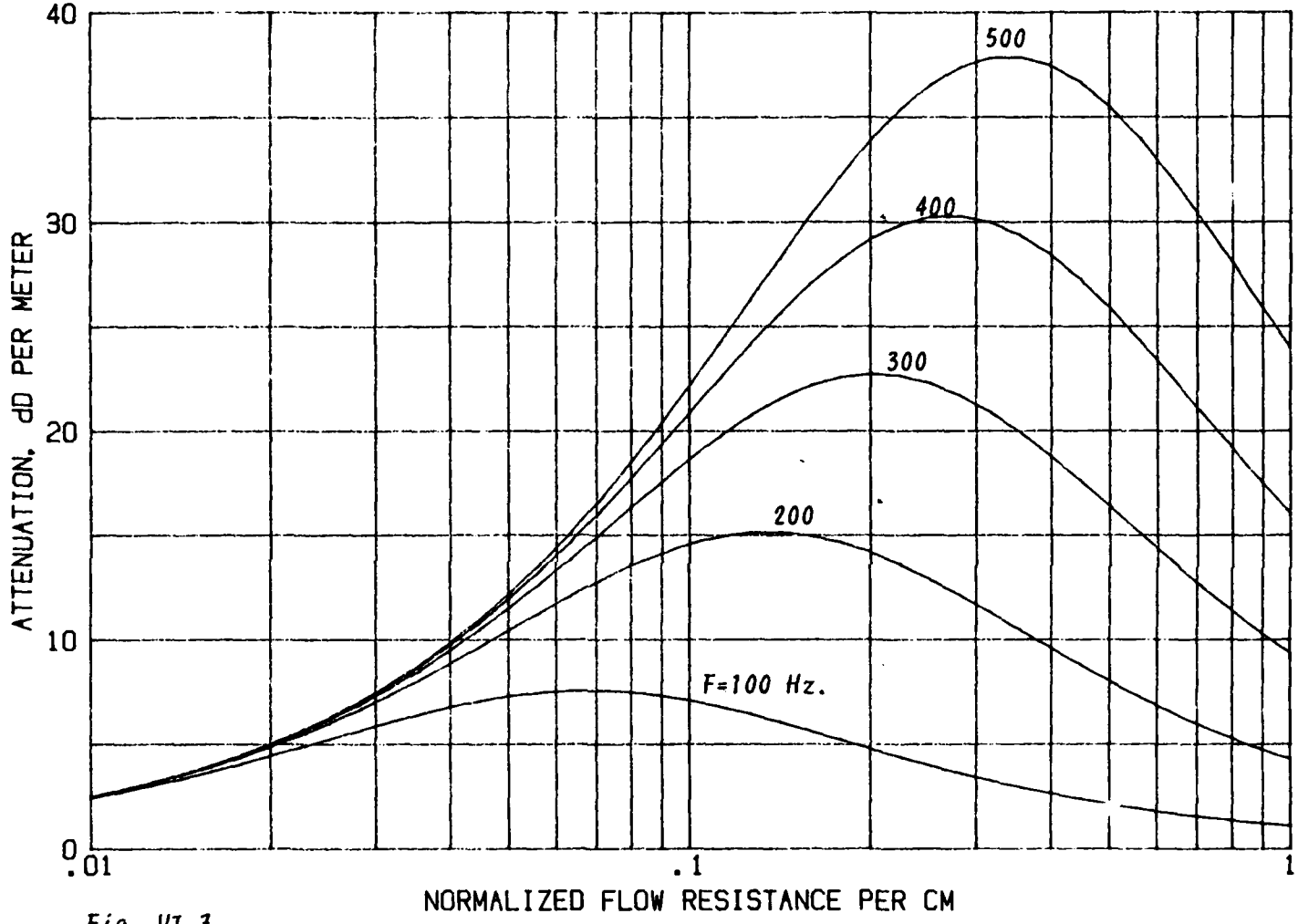


*Fig. VI.7.*
ATTENUATION IN POROUS PARALLEL-BAFFLE ATTENUATOR AS A FUNCTION OF THE FLOW RESISTANCE (NORMALIZED WITH RESPECT TO RO CE) OF THE POROUS MATERIAL.

*DATA: Porous material (assumed limp): Porosity, .95. Structure factor, G=1.5. Ratio of mass density and gas density m=38.*
*Frequency, F=100, 200, 300, 400, 500 Hz.*
*Fraction open area of attenuator, S=.20.*

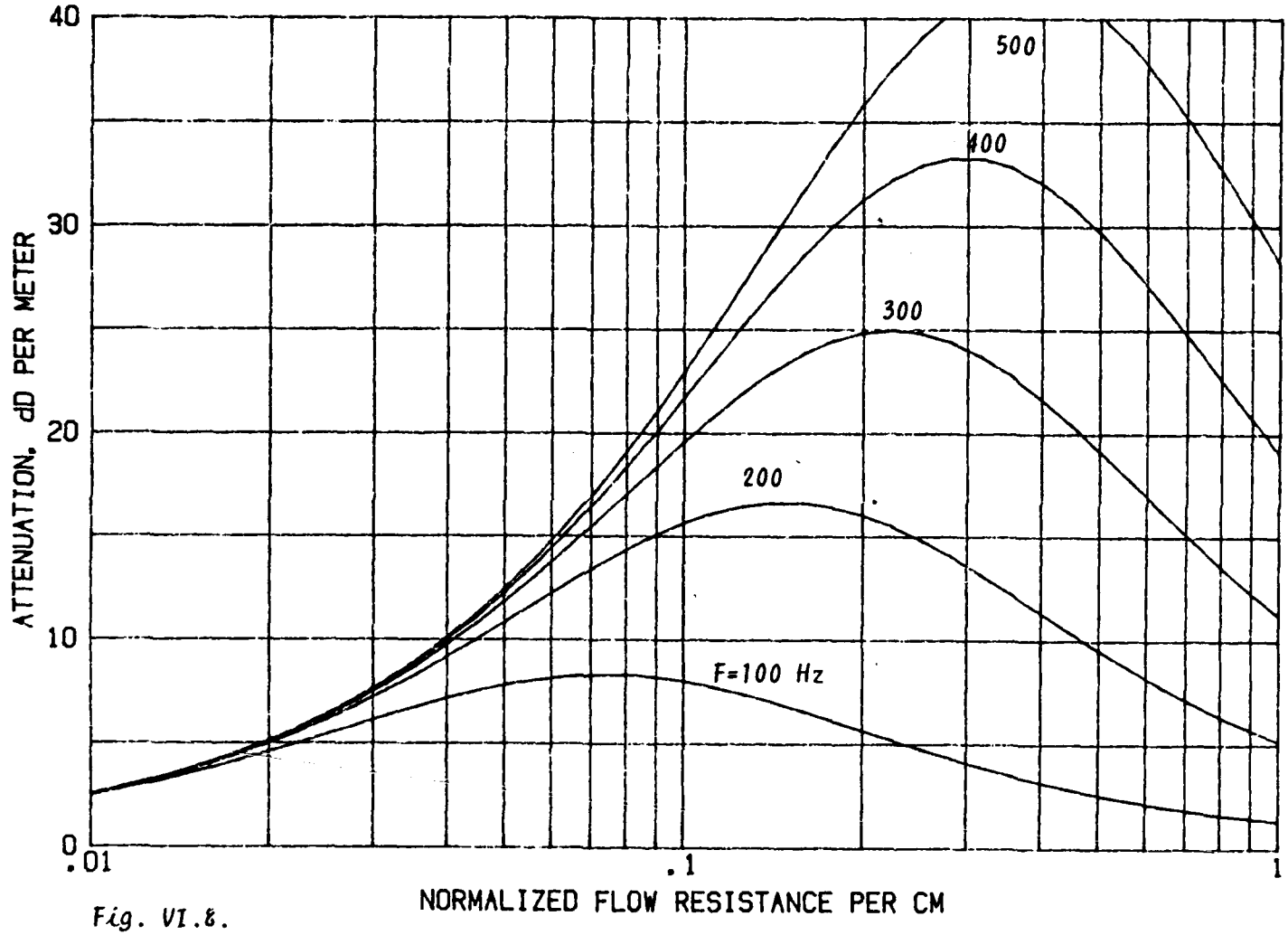


*Fig. VI.8.*
ATTENUATION IN POROUS BAFFLE ATTENUATOR AS A FUNCTION OF THE FLOW RESISTANCE (NORMALIZED WITH RESPECT TO RO CE) OF THE POROUS MATERIAL.

DATA. *Porous baffles: Rigid and non-locally reacting. Porosity, H=.95. Structure factor, G=1.5. Frequency, F=100, 200, 300, 400, 500 Hz. Fraction open area of attenuator, S=.20.*

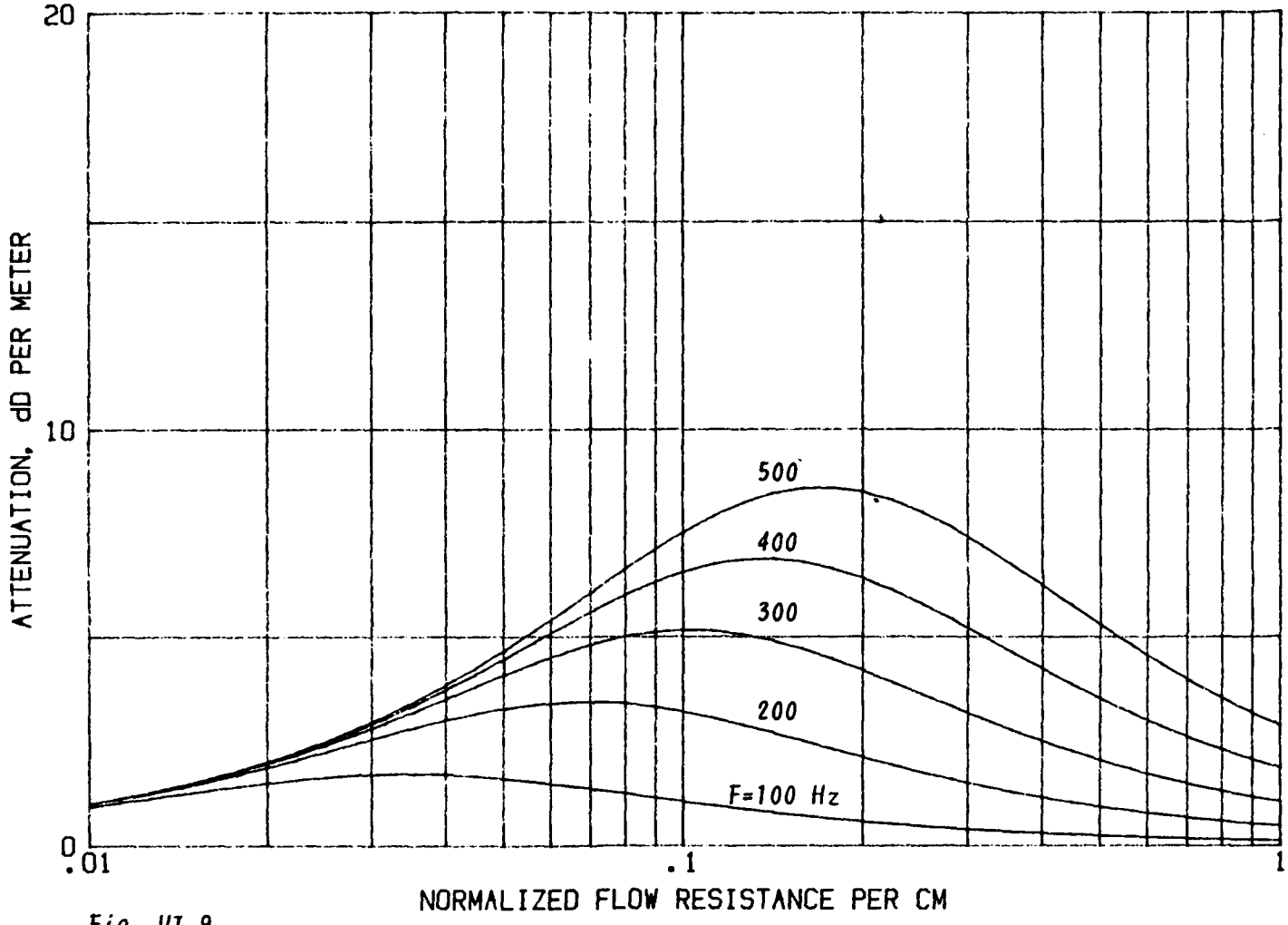


*Fig. VI.9.*
ATTENUATION IN POROUS PARALLEL-BAFFLE ATTENUATOR AS A FUNCTION OF THE FLOW RESISTANCE (NORMALIZED WITH RESPECT TO RO CE) OF THE POROUS BAFFLE MATERIAL.

DATA: *Porous material (assumed limp): Porosity, H=.95. Structure factor, G=1.5. Ratio of mass density and gas density m=38. Flow resistance, R=.01 to 1. Frequency, F=100, 200, 300, 400, 500 Hz. Fraction open area of attenuator, S=.60.*

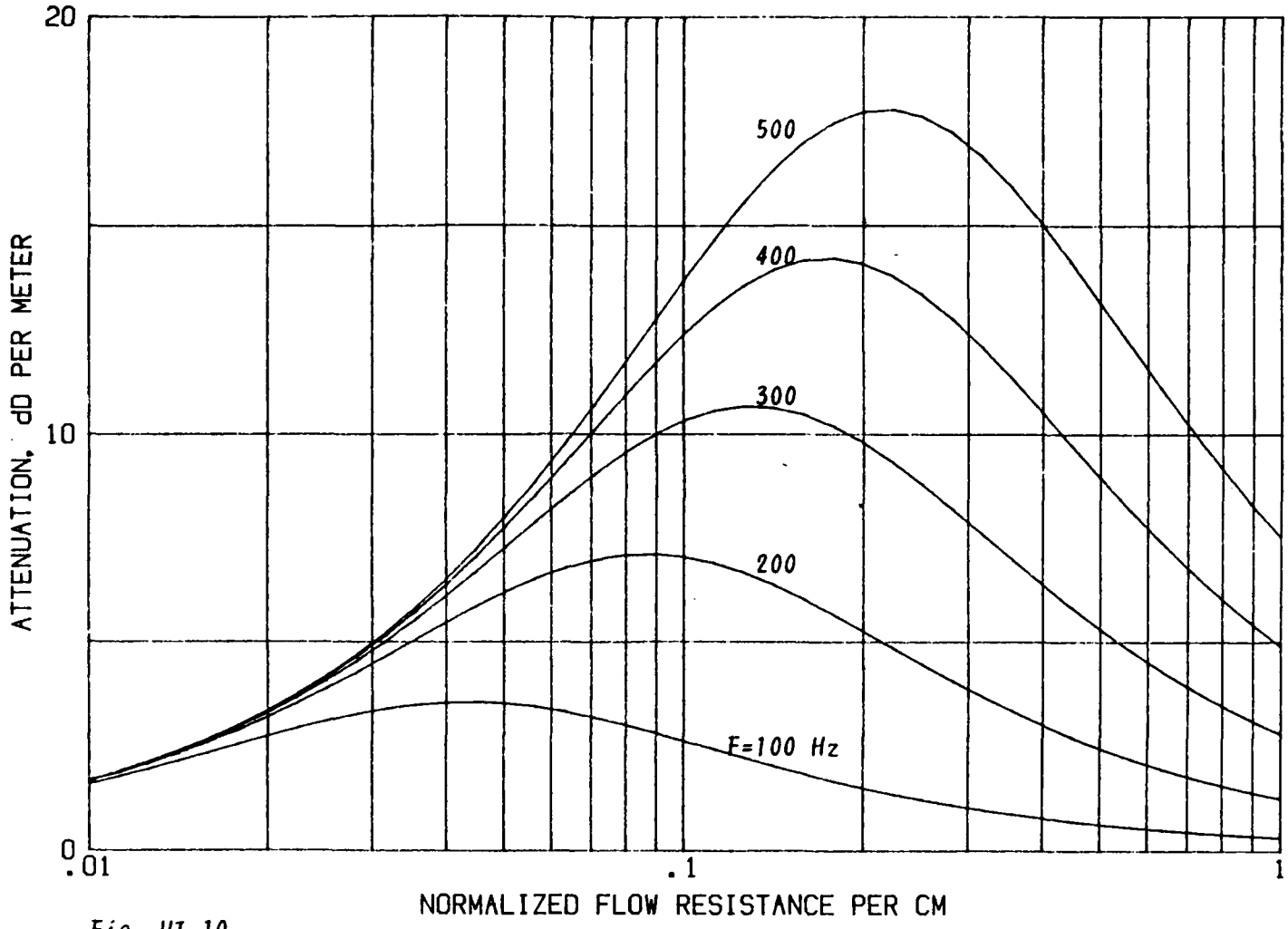


*Fig. VI.10.*
ATTENUATION IN POROUS PARALLEL-BAFFLE ATTENUATOR AS A FUNCTION OF THE FLOW RESISTANCE (NORMALIZED WITH RESPECT TO RO-CE) OF THE POROUS BAFFLE MATERIAL.

*DATA: Porous material (assumed limp): Porosity, H=.95. Structure factor, G=1.5. Ratio of mass density and gas density m=38. Flow resistance, R=.01 to 1. Frequency, F=100, 200, 300, 400, 500 Hz. Fraction open area of attenuator, S=.40.*

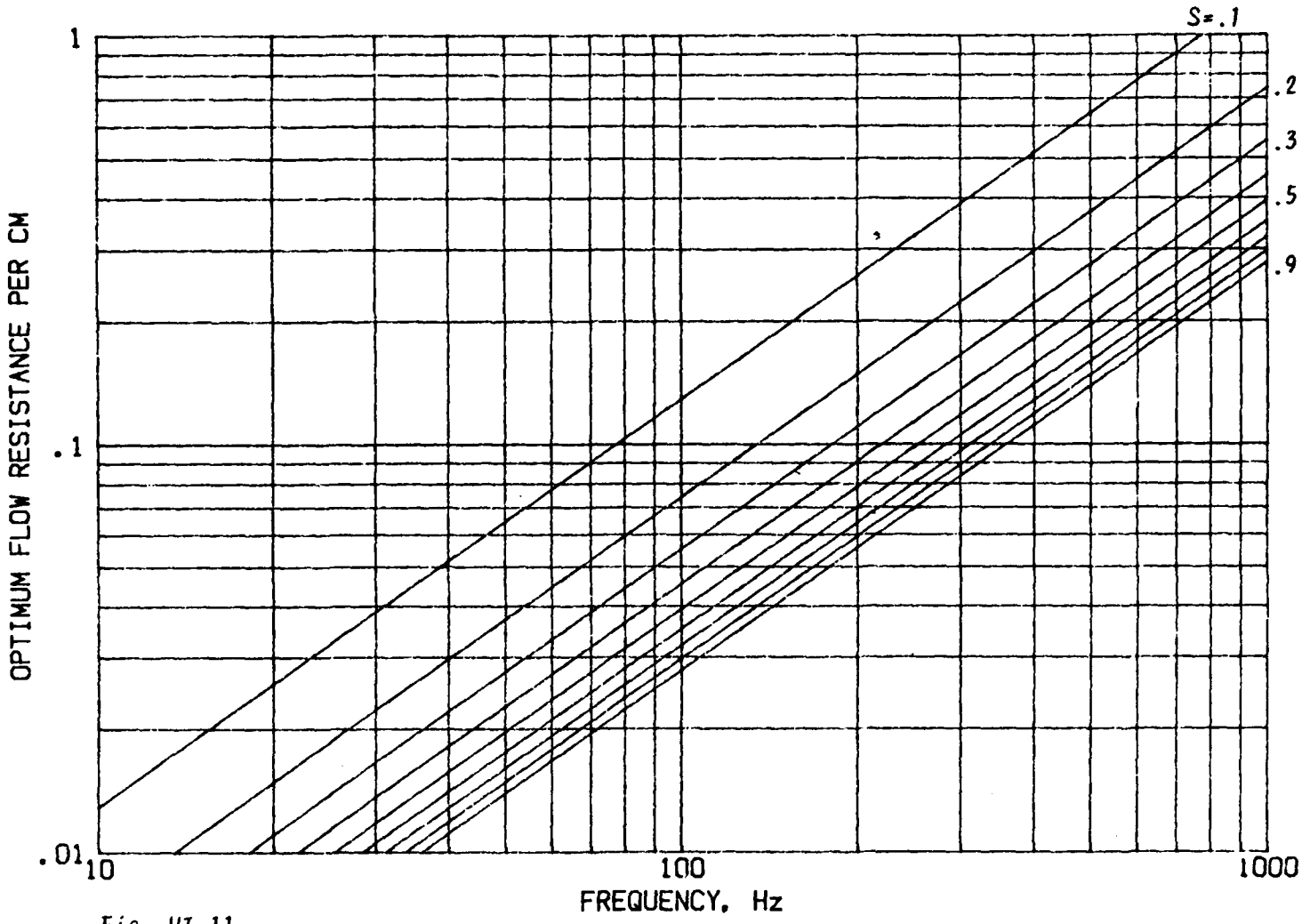


*Fig. VI.11.*
OPTIMUM FLOW RESISTANCE OF THE POROUS MATERIAL FOR MAXIMUM ATTENUATION IN A PARALLEL-BAFFLE ATTENUATOR.

DATA. *Porous baffles: Rigid and non locally reacting. Porosity, H=.95. Struct. fctr., G=1.5. Flow resistance R in ro-ce units/cm. Attenuator is acoustically compact. Open area fraction, S=.1 to .9.*

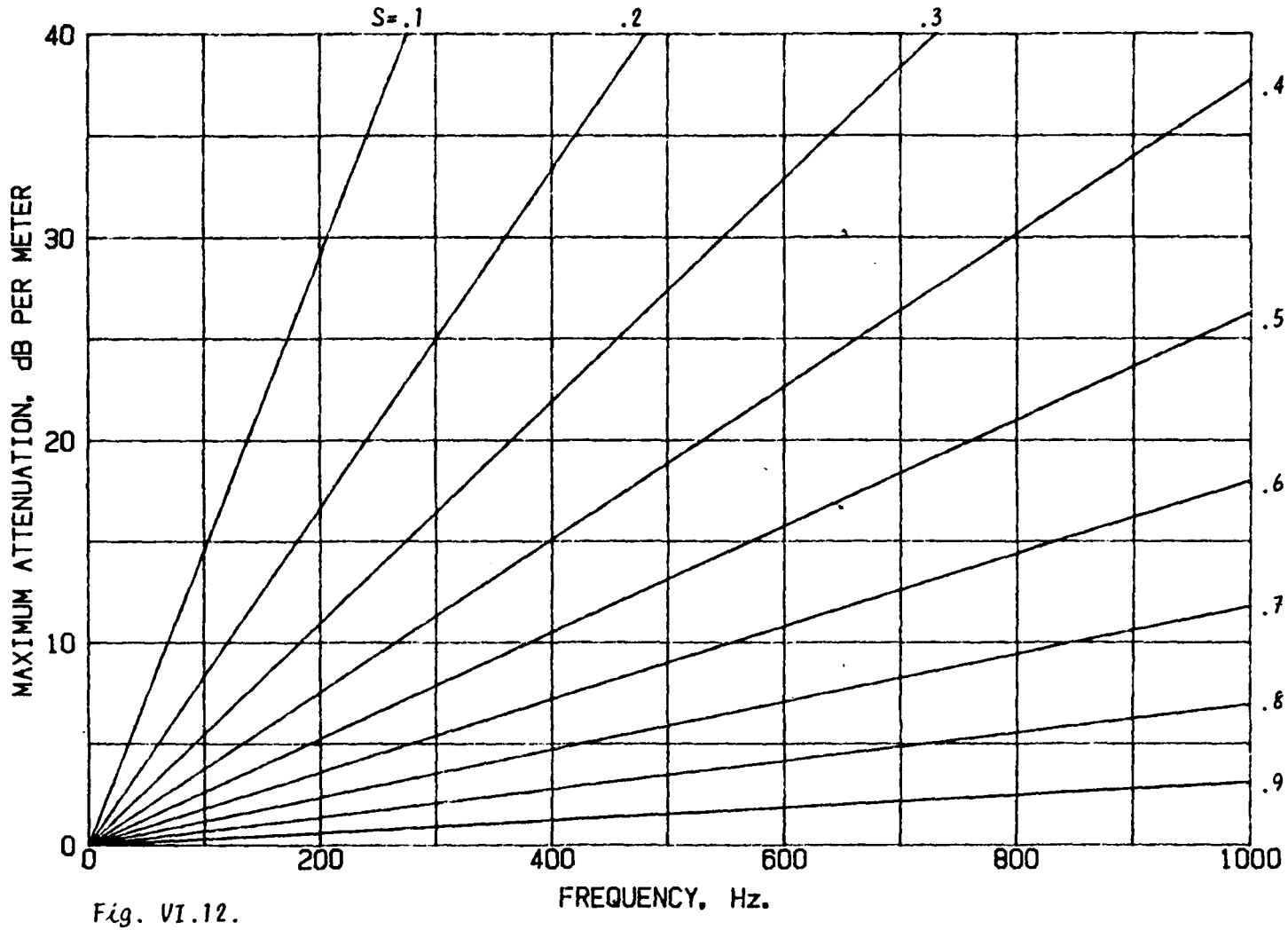


*Fig. VI.12.*
MAXIMUM ATTENUATION OF POROUS PARALLEL-BAFFLE ATTENUATOR.

*DATA. Porous baffles: Rigid and non locally reacting. Porosity, H=.95. Structure factor, G=1.5.*
*Attenuator is acoustically compact. Open area fraction, S=.1 to .9.*

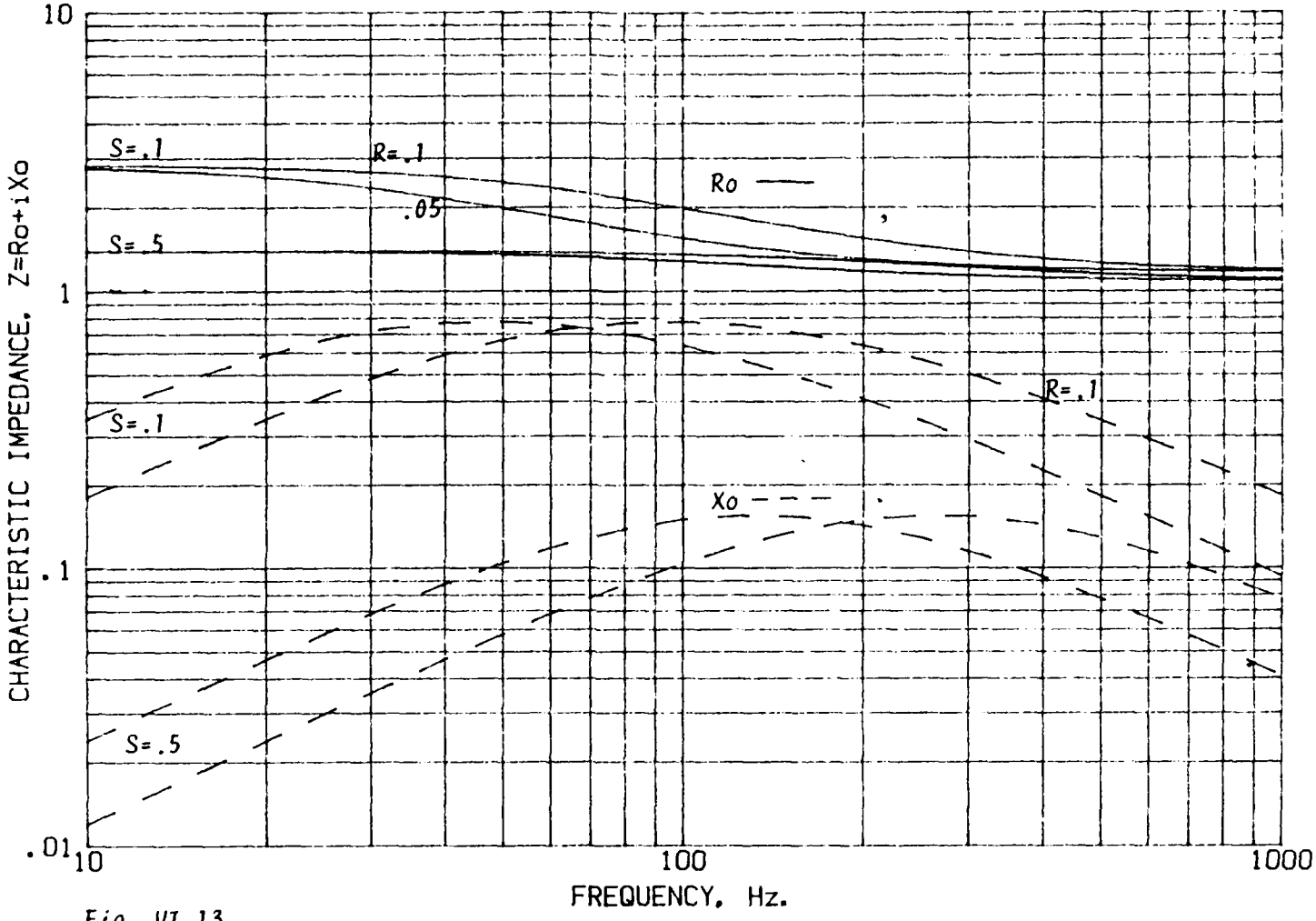


Fig. VI.13.
REAL (Ro) AND IMAGINARY (Xo) PART OF THE CHARACTERISTIC IMPEDANCE OF A POROUS PARALLEL-BAFFLE ATTENUATOR.

DATA. Porous baffles: Limp and nonlocally reacting.
Flow resistance, R=.05, .10 ro-ce units/cm. Porosity, H=.95. Structure fctr., G=1.5
Ratio of mass density and gas density, m=38.
Fraction open area of attenuator, S=.1, .5.

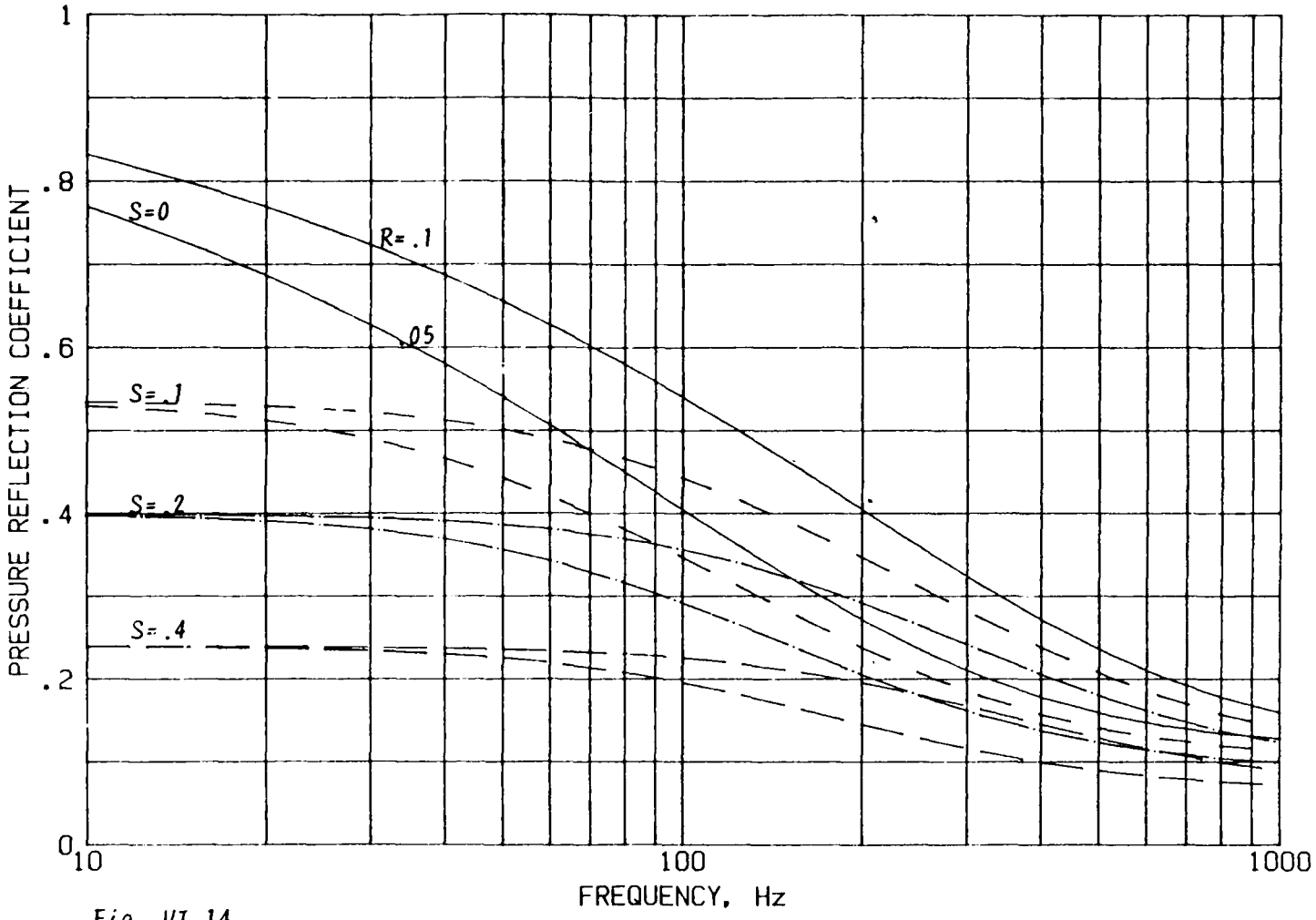


*Fig. VI.14.*
PRESSURE REFLECTION COEFFICIENT AT THE ENTRANCE OF A POROUS PARALLEL-BAFFLE ATTENUATOR.

*DATA. Porous material: Rigd. Flow resistance, R=.05, .10 ro-ce units/cm. Porosity, H=.95. Structure factor, G=1.5. Fraction open area of attenuator, S=0, .1, .2, .4.*

## VI. PRESSURE DROP IN A PARALLEL-BAFFLE ATTENUATOR

The pressure drop in a parallel baffle attenuator is due to the friction loss at the baffle surfaces and to the entrance and exit flow losses. In expressing these contributions to the pressure drop in terms of the attenuator parameters, we shall assume first, that the flow through the baffles themselves can be neglected.

Then, in the mean flow velocity in the main duct is U, the velocity in the channels between the baffles will be $U'=U/S$, where S is the fraction open area of the attenuator.

The total wall area in a channel between two baffles is 2HL, where H is the height and L the length of a baffle. The cross sectional area of the channel is HD, where D is the width of the channel, and the ratio between the two areas is then 2L/D.

The pressure drop in a length L due to wall friction can then be expressed as $f(\rho U'^2/2)(2L/D)$, where f is the friction coefficient ($f\rho U'^2/2$ is the shear stress). At sufficiently large Reynolds numbers, f is approximately independent of the Reynolds number and dependent only on the wall roughness parameter $\varepsilon/D$, where $\varepsilon$ is the average size of the wall roughness, i.e. the protusions of the wall. For $\varepsilon/D$ equal to .01 and .1, the values of the friction coefficient are approximately .01 and .025. In our computations we shall use .015 as a typical average.

The pressure drops due to the flow losses at the entrance and the exit of the attenuator depend on the open area fraction S, and we shall use the approximate expressions $.4(1-S)P'_d$ and $(1-S)P'_d$ for these contributions, where $P'_d=\rho U'^2/2$ is the "dynamic" pressure of the channel flow.

Normalizding the the toral pressure drop with respect to the dynamic pressure $P_d=\rho U^2/2$ of the flow in the main duct, we obtain

$$\Delta P/P_d=(1/S^2)[2fL/D+.4(1-S)+(1-S)^2] \qquad (1)$$

$$P_d=\rho U^2/2$$

AD-A136 538 REPETITIEELY PULSED ELECTRIC LASER ACOUSTIC STUDIES 2/2
VOLUME 1. (U) MASSACHUSETTS INST OF TECH CAMBRIDGE DEPT
OF AERONAUTICS ANDAA.. K U INGARD ET AL. SEP 83
UNCLASSIFIED AFWAL-TR-83-2058-VOL-1 F33615-80-C-2040 F/G 20/5 NL

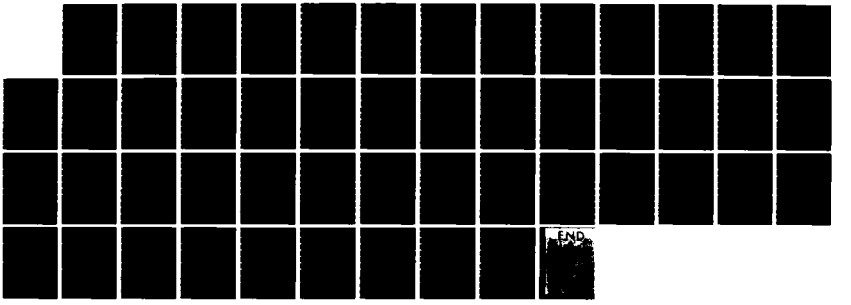

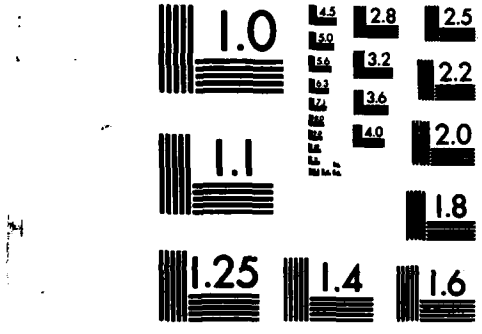

We do not expect this result to be valid for arbitrarily small values of S, since at some point, the flow through the porous material itself will become significant. The value of S, for which this occurs will depend on the flow resistance of the porous material. Actaully, in the limit S=0, the pressure drop will be $\Delta P = rUL$, where r is the flow resistance of the material per unit length.

To account for the flow through the porous material, we start by expressing the total average flow velocity U in the main duct in terms of the velocities U' and U" in the channel and in the porous material, respectively,

$$U = SU' + (1-S)U" \tag{2}$$

The pressure drop per unit length in the channel and in the porous material must be the same, i.e.

$$rU" = (2f/D)(\rho U'^2/2) \tag{3}$$

where r is the flow resistanc per unit length in the porous material, r=R c.

With the thickness of a baffle denoted by d and the width of the channel between two baffles by D, the fraction open area of the attenuator is S=D(D+d). The normalized flow resistance per unit length is R, as before, and the Mach number of the flow in the main duct is M=U/c. From Eqs. 2 and 3 we then can express the velocity of the channel flow as

$$U'/U = (\gamma/2)[\sqrt{1+4(/\gamma S)} - 1] \tag{4}$$

$$\gamma = (Rd/fM)S^2/(1-S)^2$$

and the total pressure drop is

$$\Delta P/P_d=(U'/U)^2[2fL/D+.4(1-S)+(1-S)^2] \quad (5)$$

$$P_d=\rho U^2/2$$

As an example, we have computed $\Delta P/P_d$ as a function of L/D with S as a parameter for the values Rd=.2 c units and f=.015, which can be considered rather typical. For comparison, we have included the result in Eq. 1, which was obtained on the assumption of no flow through the baffles. The results are given in Fig. 1. We note, that the two results, corresponding to Eqs. 1 and 5, deviates significantly only for values of S less than .2.

It should be emphasized, that the dynamic pressure $P_d$ refers to the average flow speed in the duct before the area contraction created by the attenuator. With the attenuator mounted in a duct section with an area larger than that of the main duct, the velocity U and the pressure drop can be reduced accordingly.

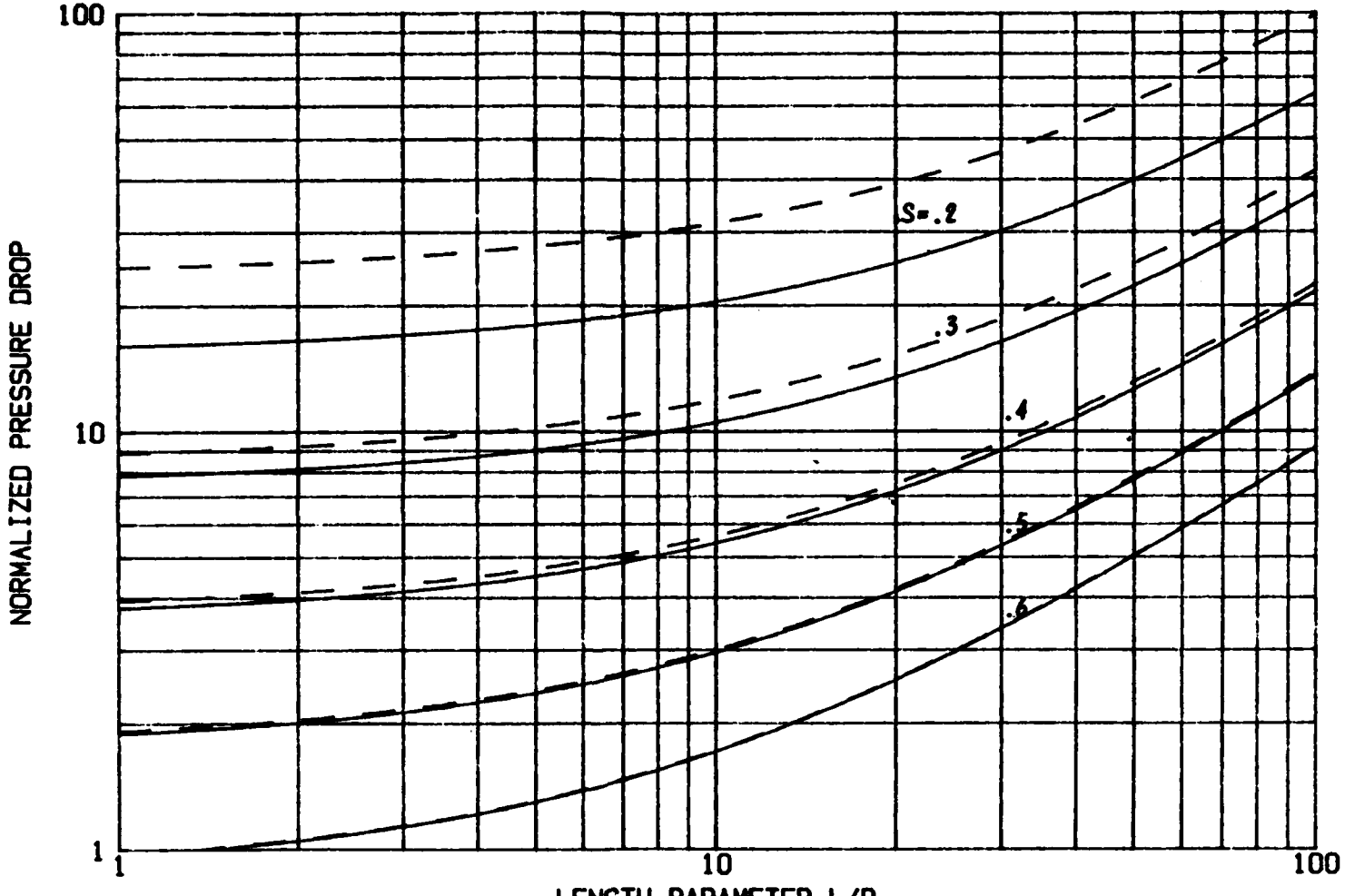


Fig/ VII.1.
PRESSURE DROP IN A PARALLEL-BAFFLE ATTENUATOR, $\Delta P/P_d$, WHERE $P_d=\rho U^2/2$ AND U THE MEAN FLOW VELOCITY IN THE DUCT AHEAD OF THE ATTENUATOR.

DATA. Baffles: Thickness d, total flow resistance Rd=.2 c units.
Mach number, M=U/c=.05. Wall friction factor, f=.015. Open area fraction, S=.2-.6.
Solid lines: Flow through baffles accounted for (Eq. 5).
Dashed lines: No flow through baffles. (Eq. 1).

## VII. INTERACTION OF SHOCK WAVES WITH A FLEXIBLE POROUS LAYERS

In our experimental studies of transmission of sound pulses in duct line with a flexible porous layer or containing a flexible porous baffle, the attenuation generally was found to be significantly dependent on the peak pressure of the pulses. Often the attenuation decreased with increasing pressure, a rather unexpected result.

In order to gain some insight into the mechanism, which might be responsible for this effect, we carried out some experiments on the reflection of the pulse waves from a porous flexible layer, placed at the end of our shock tube and backed by a rigid termination.

The waves involved had peak pressures ranging from .33 to 1.4 atm., as measured at a distance 1 m from the source. Of particular interest is a series of measurements involving a porous flexible material (Solimide) with layer thicknesses from 2 to 8 inches. The recorded time dependence of the incident and reflected wave pulses are shown in Figs. 1-3.

Fig. 1 refers to a layer thickness of 2 inches. For comparison is shown in the same figure the result obtained with a rigid termination. The pressure patterns obtained in the two cases are barely distinguishable, except for the somewhat larger value of the peak pressure of the pulse reflected from the porous material. This may be somewhat unexpected, at first, but it will be explained shortly.

First we analyze the data obtained for the 4 inch sample. Again we have shown the reflection, labelled A, from a rigid termination. With the incident amplitude being .9 atm., the amplitude of the reflected wave is in good agreement with the value predicted by our nonlinear acoustic analysis, given elsewhere in this report.

The pressure pulse labelled B is the reflection from the

front surface of the porous material, and B' is the reflection from the rigid backing wall. By comparison with A, we can estimate the reflection coefficient at the surface, but to do this accurately, we have to account for the difference in the nonlinear attenuation of the waves A and B along the path from the termination to the transducer (in this case 1 m long).

The wave B', reflected from the rigid backing, has travelled back and forth through the porous layer, and from the difference in amplitude of A and B', we can estimate the attenuation of the wave in the porous material. Again, to do this correctly, we have to account for the difference in the nonlinear attenuation of the waves A and B'.

The pressure waves labelled A, B and B' in the same figure, refer to the waves reflected from the rigid wall of the source end of the tube. An interesting observation is, that along the path of propagation from the transducer to the source end and back again (path length=2.2 m), the pressure peak B' has almost overtaken B, because of the difference in wave speed of the two pulses. As a result, the resulting total wave peak is somewhat larger than the peak A obtained in the case of a rigid termination. Thus, at this point of observation, the effect of the porous termination actually is a slight increase of the peak pressure.

Going back to Fig. 1 and the results obtained for the 2 inch porous layer, we can explain the larger amplitude B' of the wave reflected from the porous layer. In this case the wave reflected from the rigid backing has already overtaken the wave reflected from the front, resulting in a total peak, which is larger than the peak A reflected from the rigid wall.

The results obtained for the 8 inch sample are shown in Fig. 3. Here the reflections B and B' from the porous surface and from the rigid backing, respectively, are clearly separated. Their amplitudes are about the same, so that there is little

difference in their wave speeds. Thus, after reflection from the source end, they return with approximately the same separation. The subsequent reflections will be more difficult to separate, since the reflections from the surface of the porous material and from the rigid backing of the incident "doublet" pulse tend to overlap. This can be seen also in Fig. 4, where the reflections are recorded over a longer time span. It should be mentioned, that the results obtained with a porous layer with a higher flow resistance, R=.61 ρc units/cm, were essentially the same.

Amplitude dependence of reflectfons coefficients. Using the 8 inch thick sample of the porous material as a termination of the shock tube, we studied next the reflection as a function of the peak pressure of the incident pulse. Examples of the measured reflected waves are shown in Figs. 5-7.

As before, the peak pressures of the incident waves refer to the location $x_o$=1 m from the source and .8 m from the surface of the porous sample. In each case the reflected wave consists of a "doublet" B, B', where B refers to the reflection from the surface of the porous layer and B' to the reflection from the rigid backing. The range of pressures of the incident pulse was .33 to 1.4 atm. At .33 atm. the amplitude of B' is considerably smaller than the amplitude of B, but as the incident peak pressure increases, the amplitude decreases for B but increases for B'. At an incident pressure of 1.4 atm. the amplitude of B' is larger than that of B.

To describe this effect quantitatively, we introduce two pressure reflection coefficients C=B/A and C'=B'/A, where the reflected pressures and the incident pressure A refer to the location of the surface of the porous material. The pressures are measured at a distance .8 meter from the surface of the porous material, however, and to determine C and C', we have to account for the nonlinear attenuation of the waves in the

tube to determine the pressure amlitudes at the surface of the material. This is doen by using the results of our theoretical analysis of the x-dependence of the pressure, given elsewhere in the report. We find, for example, that for the measured incident amplitudes .33, .54, .95, and 1.4 atm., the corresponding amplitudes at the surface of the material will be .30, .47, .75, and 1.05 atm., respectively. The measured reflected ampliutdes are corrected in similary manner.

The amplitude dependence of each of the reflection coefficients thus obtained is shown in Fig. 8. The reflection coefficient R decreases with amplitude, whereas the opposite holds true for R'. At a certain value $p^*$ of the incident amplitude, R and R' will be the same. In the present case this amplitude is approximately .85 atm. at the surface of the material (corresponding to 1.1 atm. a distance .8 in front of the material). This characteristic pressure is expected to decrease with decreasing thickness of the material.

As a result of this interesting nonlinear effect, we note, that as the amplitude increases beyond the pressure $p^*$, the resulting reflected amplitude will increase with increasing amplitude, with a corresponding decrease in the absorption coefficient. This is consistent with the observed reduction of the attenuation with increasing amplitudes.

Deformation of the material. We found, that the pressure dependence of the reflection coefficient is associated with a deformation of the porous material, caused by the incident shock wave. In these exploratory studies, the compression of the material was measured simply by letting the surface of the material leave a mark on a thin rod, which was inserted along the axis of the material. This was achieved by means of a small amount of india ink, which was applied to the surface of the material in contact with the rod, and, upon compression, left a clear record on

the rod of the maximum deformation of the material.

For incident waves with peak pressures .30, .75, .90, and 1.05 atm. at the surface of the material, the peak compressions d of the porous sample (thickness D=8 inches) were 2.5, 4.8, 5.75, and 6.25 inches, respectively. The corresponding relative displacements d/D are plotted in Fig. 9 as as function of the peak pressure at the surface of the material. At the highest pressure involved, 1.05 atm., the thickness of the material at maximum compression is only 1.75 inches.

In the linear regime, without a significant compression of the material, the wave B' reflected from the rigid termination, travels a distance of 2D (16 inches in this case), and its amplitude is reduced accordingly through friction in the material. When the material is compressed, on the other hand, this distance is reduced, as are the friction losses, and the reflection coefficient will be corresponding larger than in the linear regime, as observed. Apparently, the losses due to the compression of the porous material we used were small compared to the friction losses due to the relative motion of the air and the structure. For another material, with a different internal damping, the relative significance of the compression losses may be markedly different, however.

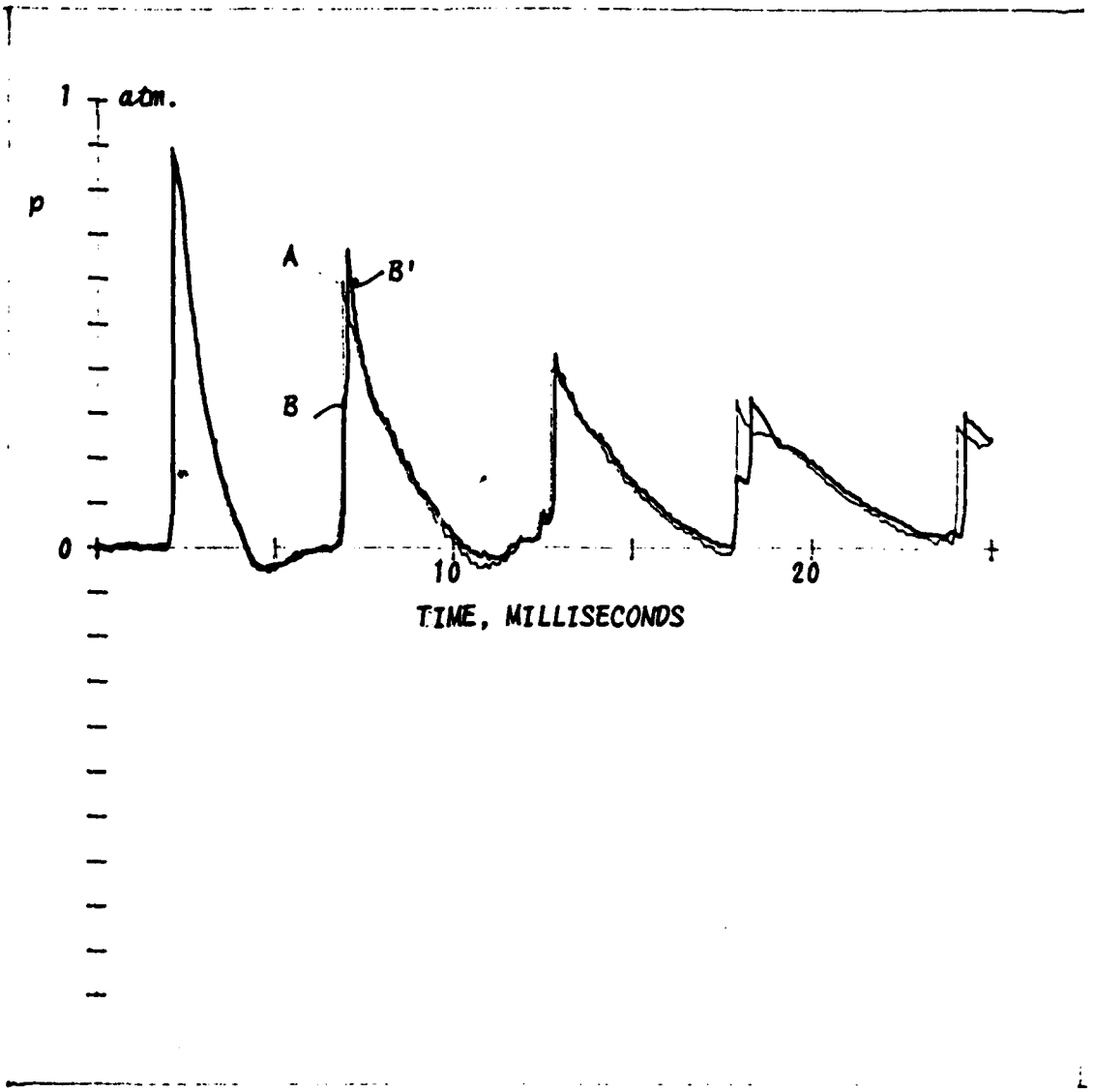


Fig. VIII.1.
SHOCK WAVE REFLECTION FROM A RIGID TERMINATION IN A TUBE AND FROM A POROUS LAYER BACKED BY RIGID TERMINATION.

DATA. Porous material: Solimide. Layer thickness, 2 inches.
Flow resistance, R=.22 ra-ce units/cm.
Mass density, M=.02 g/cubcm
Tube diameter: 5 cm.

A: Reflection from rigid termination.
B: Reflection from surface of porous layer.
B': Reflection from rigid backing.

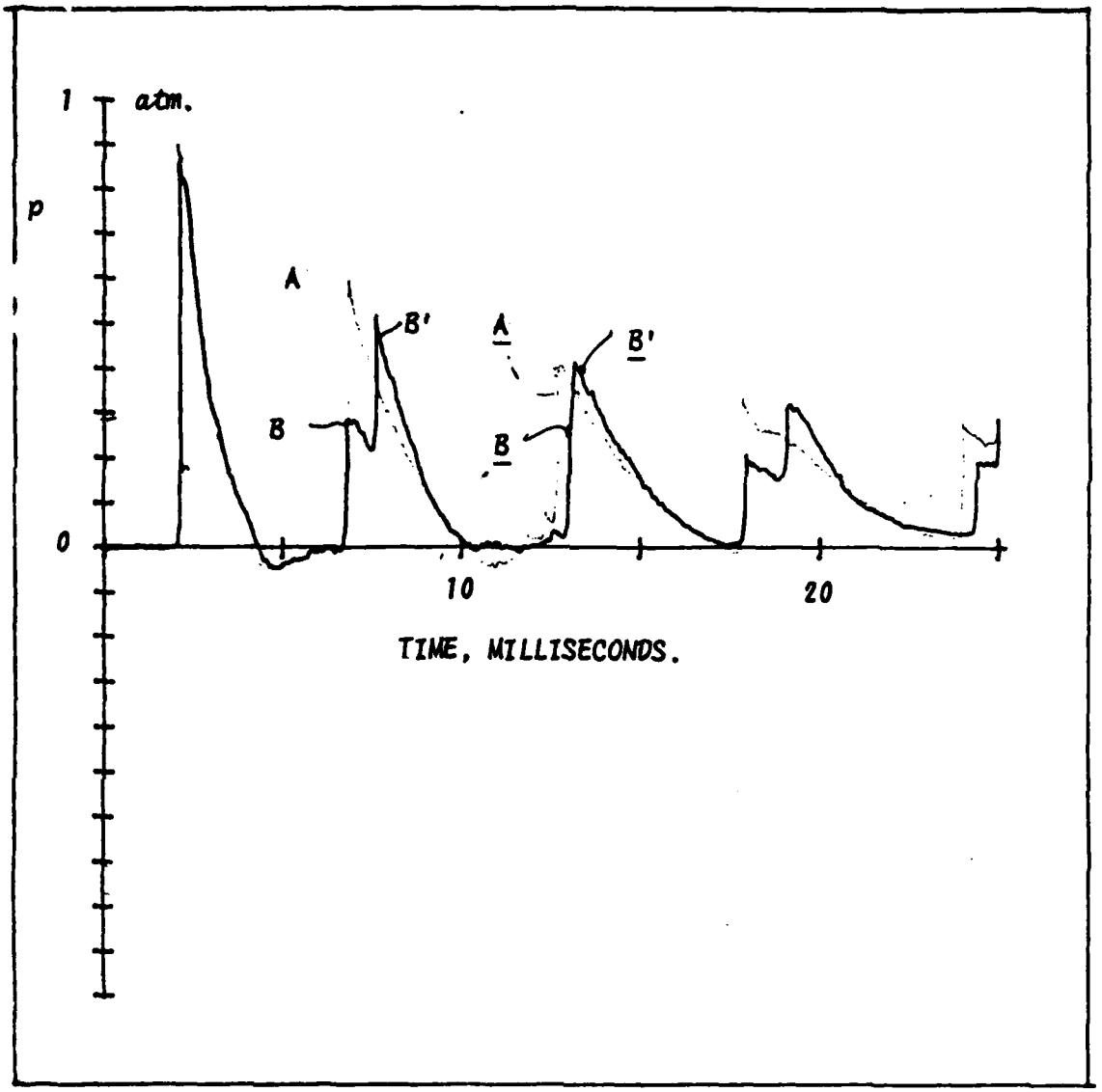


Fig. VIII.2.
SHOCK WAVE REFLECTION FROM A RIGID TERMINATION IN A TUBE AND FROM A POROUS LAYER BACKED BY RIGID TERMINATION.

DATA. Porous material: Solimide. Layer thickness, 4 inches.
Flow resistance, R=.22 ra-ce units/cm.
Mass density, M=.02 g/ cubcm
Tube diameter: 5 cm

A: Reflection from rigid termination.
B: Reflection from surface of porous layer.
B': Reflection from rigid backing.

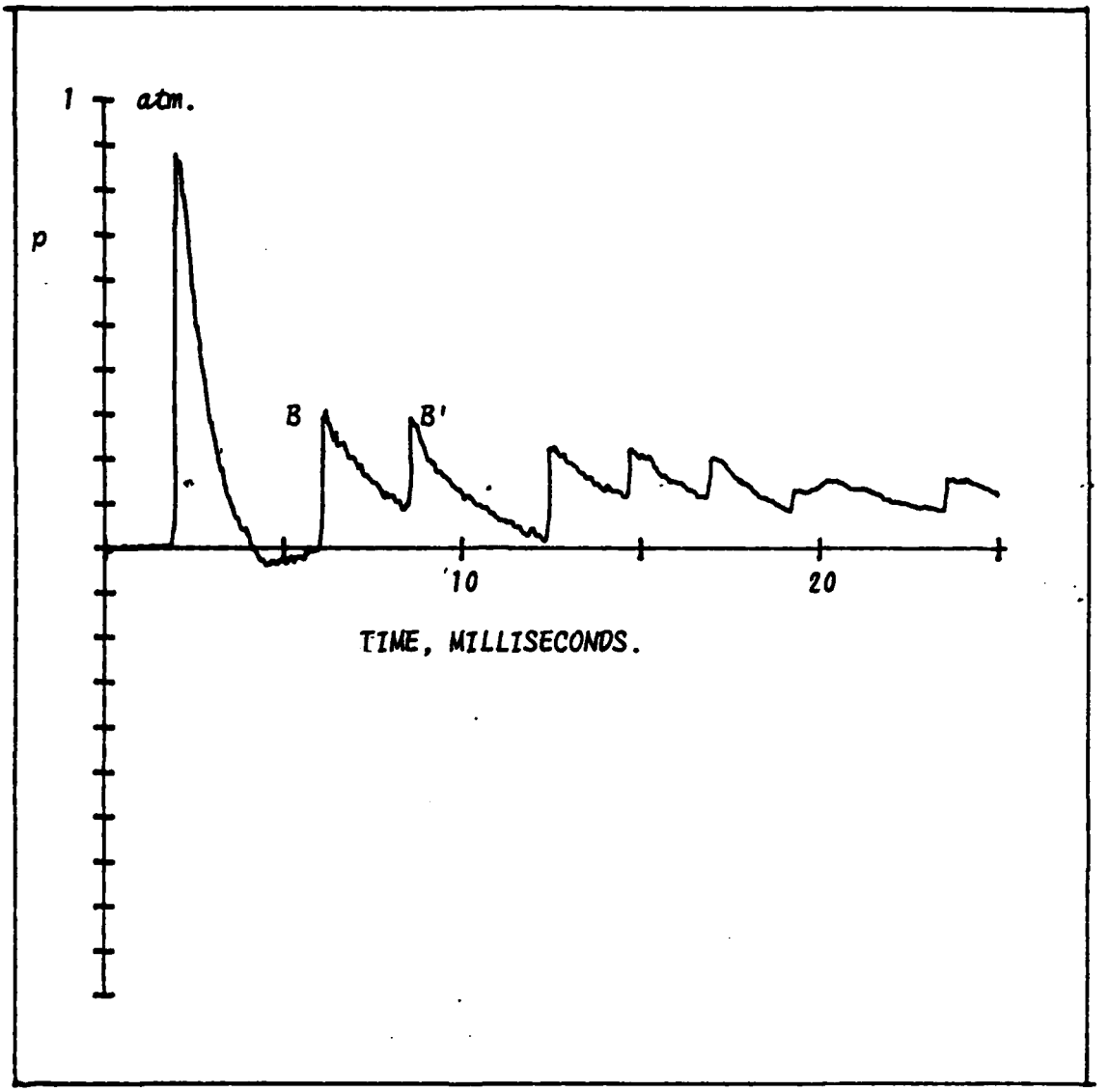


Fig. VIII.3.
SHOCK WAVE REFLECTION FROM A POROUS LAYER BACKED BY RIGID TERMINATION IN A TUBE.

DATA. Porous material: Solimide. Layer thickness, 8 inches.
Flow resistance, R=.22 ro-ce units/cm.
Mass density, M=.02 g/cubcm
Tube diameter: 5 cm

B: Reflection from surface of porous layer.
B': Reflection from rigid backing.

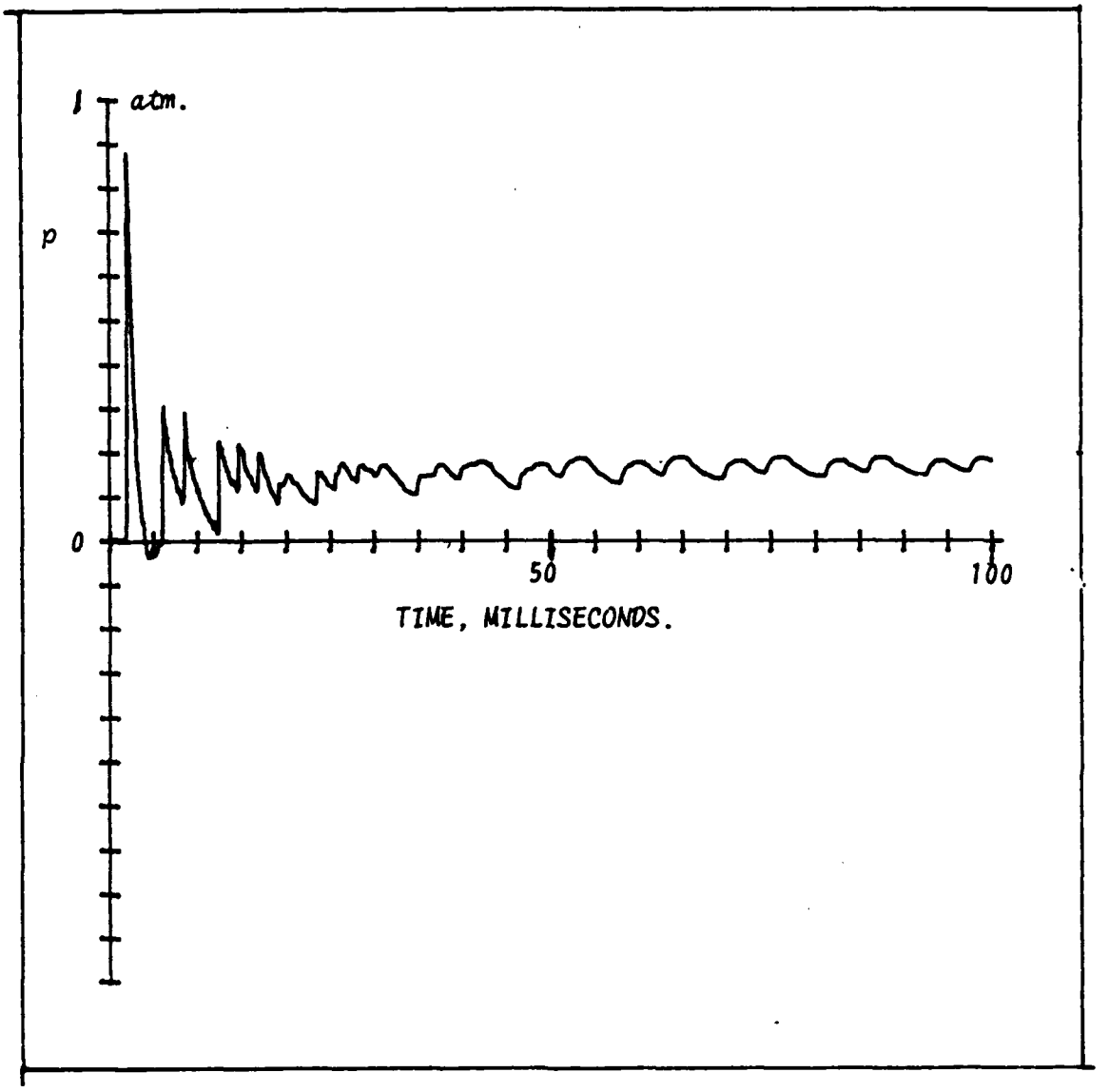


Fig. VIII.4.
SHOCK WAVE REFLECTION FROM A POROUS LAYER BACKED BY A RIGID TERMINATION IN A TUBE.

DATA. Porous material: Solimide. Layer thickness, 8 inches.
Flow resistance, R=.22 ro-ce units/cm.
Mass density, M=.02 g/cubcm
Tube diameter: 5 cm

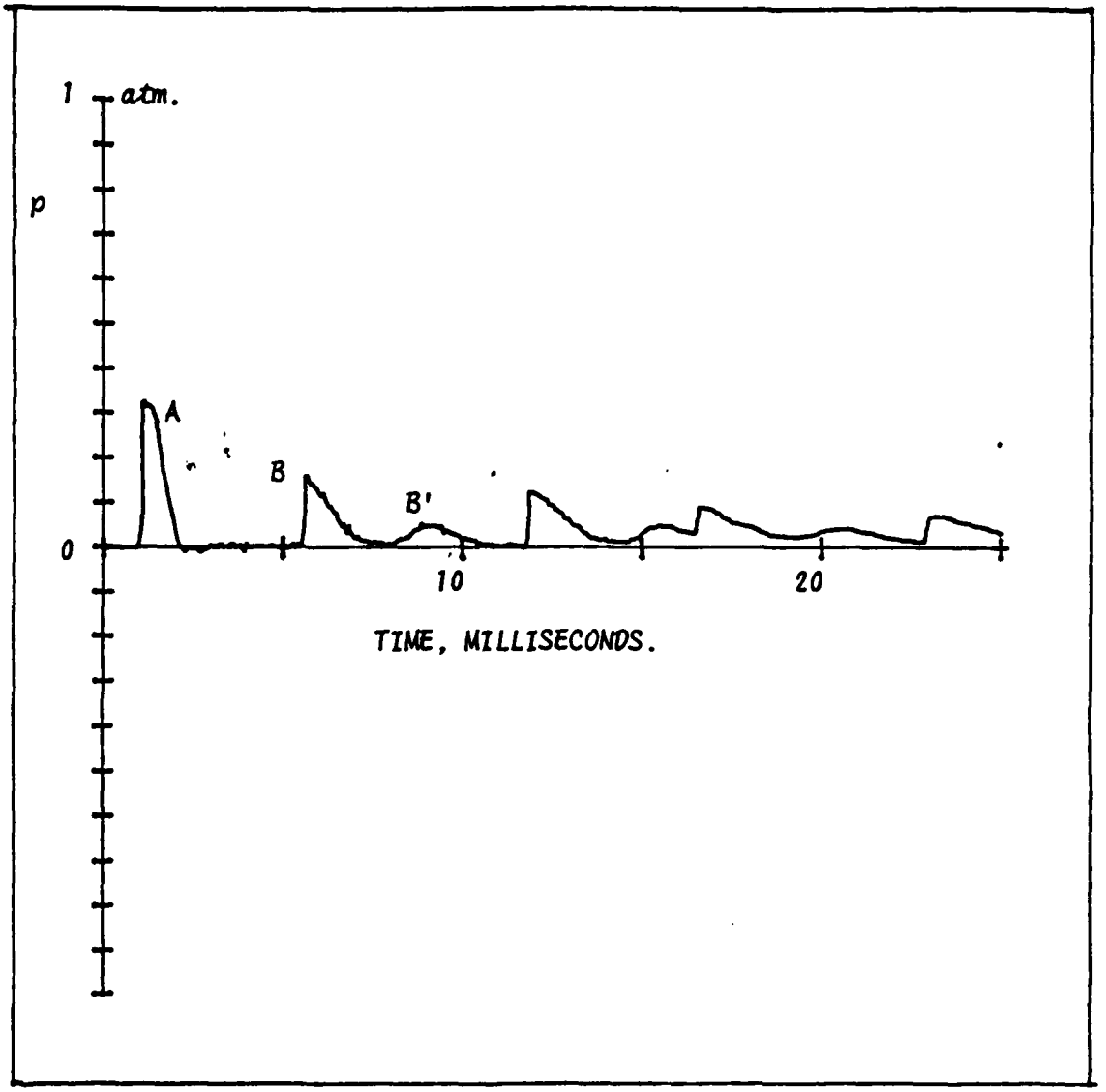


*Fig. VIII.5.*
REFLECTIONS OF A SHOCK WAVE IN A TUBE FROM A FLEXIBLE POROUS LAYER.
B: FROM SURFACE OF MATERIAL. B': FROM THE RIGID BACKING.

*DATA. Porous material. Solimide. Layer thickness, 8 inches. Flow resistance, R=.61 ro-ce units/cm. Mass density, M=.03 g/cubcm.*

*Peak pressure of incident wave at surface of material: .30 atm. (.33 atm. .8 m in front of surface).*

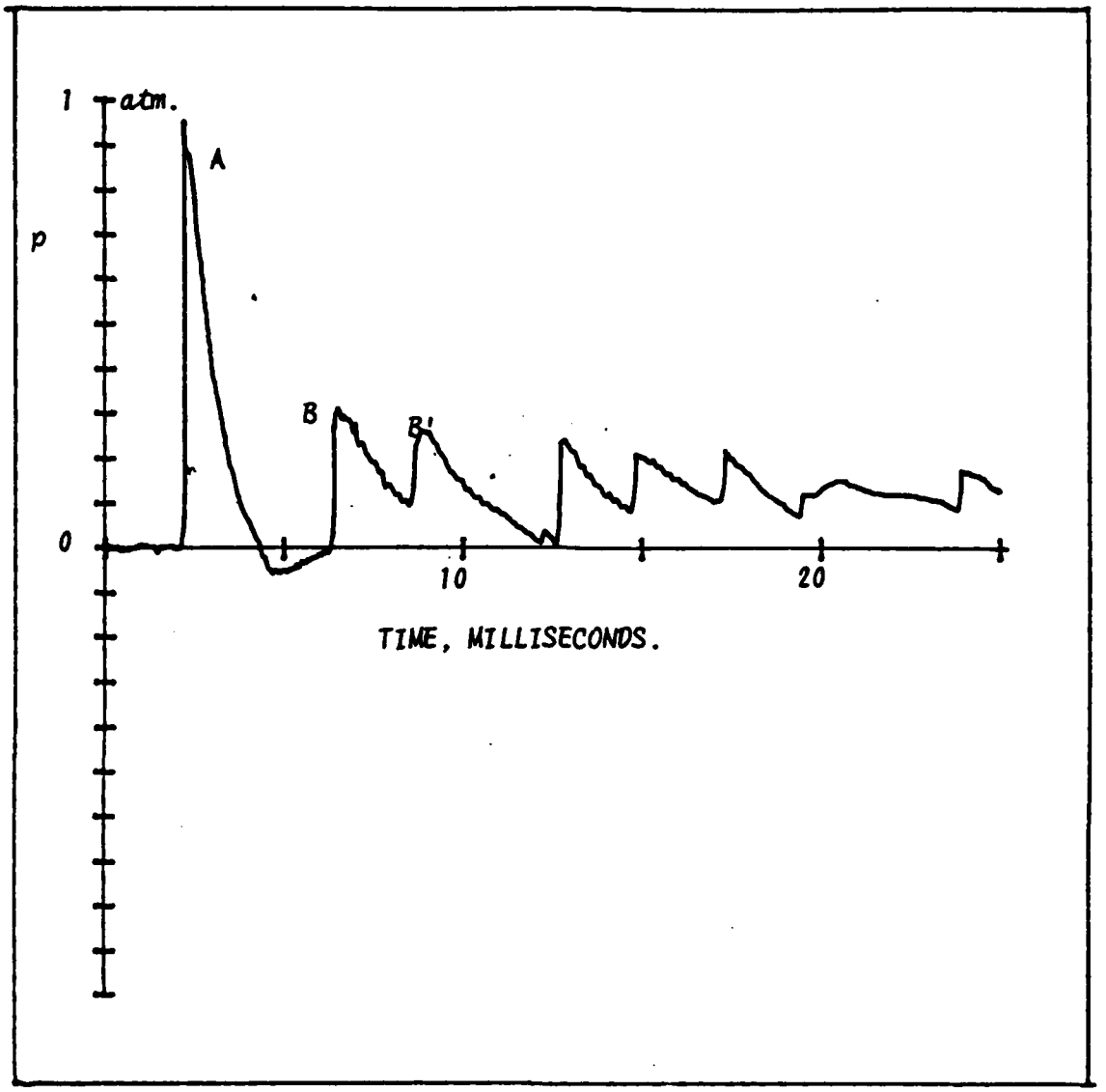


Fig. VIII.6.
REFLECTIONS OF A SHOCK WAVE IN A TUBE FROM A FLEXIBLE POROUS LAYER.
B: FROM SURFACE OF MATERIAL. B': FROM THE RIGID BACKING.

DATA. Porous material. Solimide. Layer thickness, 8 inches.
Flow resistance, R=.61 ro-ce units/cm. Mass density, M=.03 g/cubcm.

Peak pressure of incident wave at surface of material: .47 atm.
(.54 atm. .8 m in front of surface).

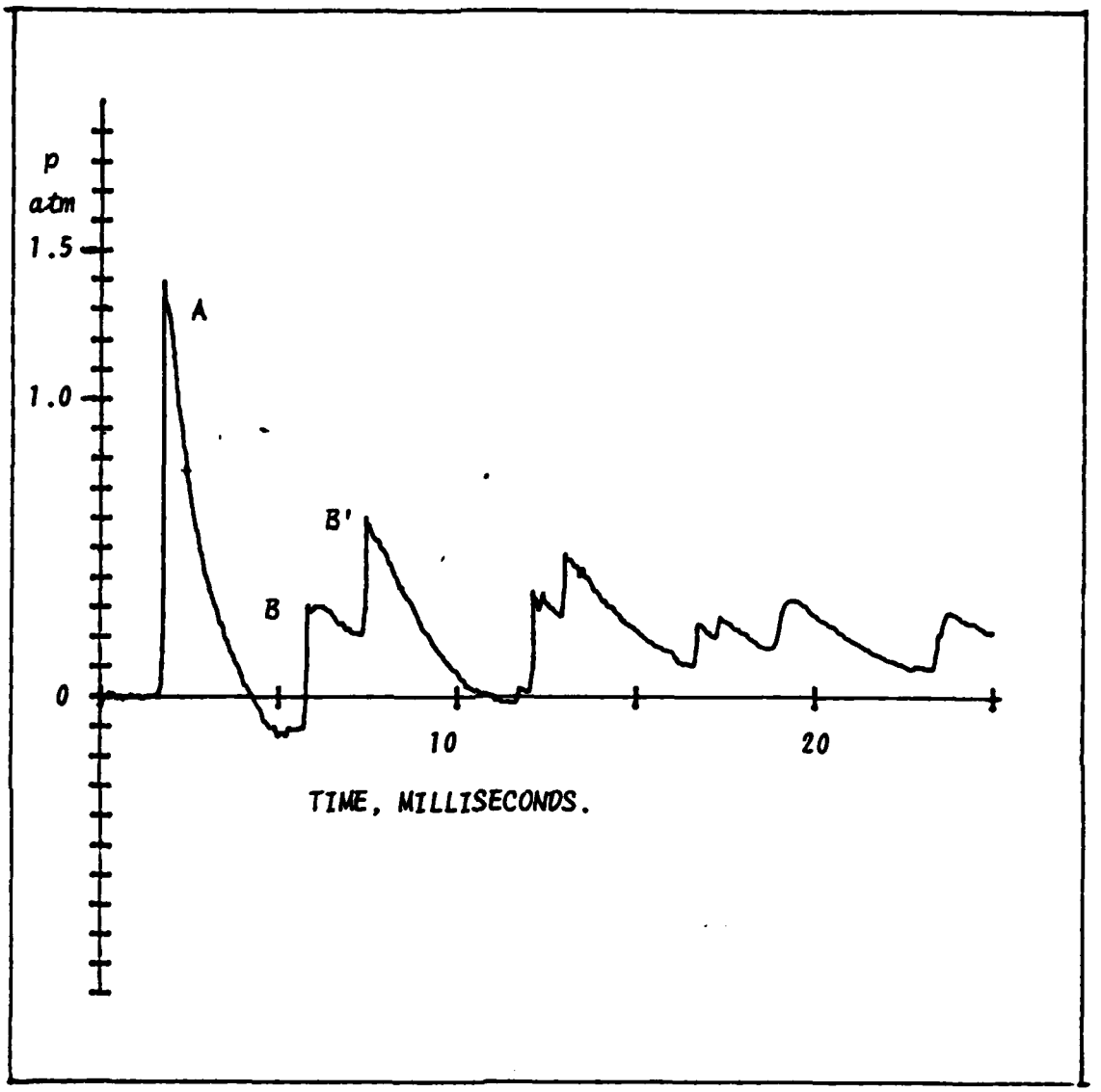


*Fig. VIII.7.*
REFLECTIONS OF A SHOCK WAVE IN A TUBE FROM A FLEXIBLE POROUS LAYER.
B: FROM SURFACE OF MATERIAL. B': FROM THE RIGID BACKING.

*DATA. Porous material. Solimide. Layer thickness, 8 inches. Flow resistance, R=.61 ro-ce units/cm. Mass density, M=.03 g/cubcm.*

*Peak pressure of incident wave at surface of material: 1.05 atm. (1.4 atm. .8 m in front of surface).*

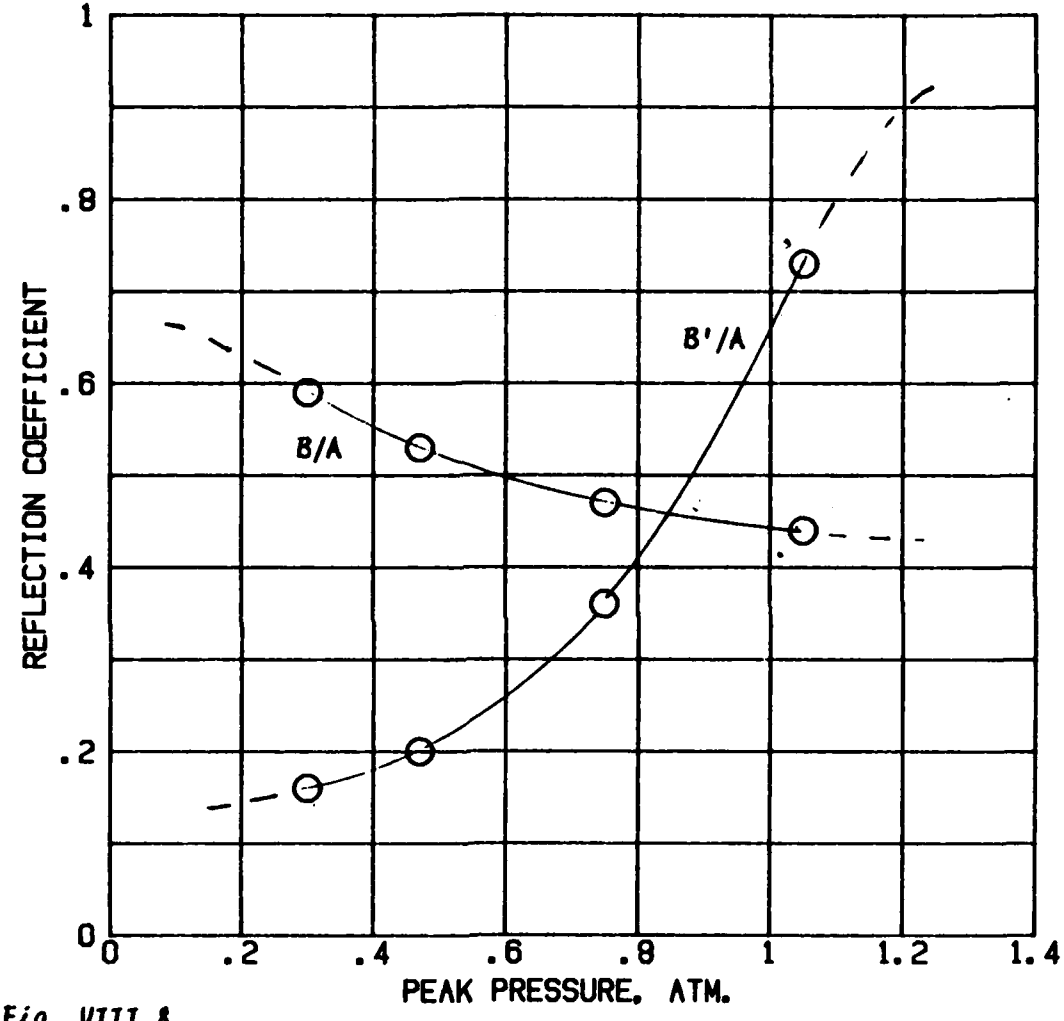


*Fig. VIII.8.*
*PRESSURE REFLECTION COEFFICIENTS, B/A, B'/A. A=PEAK PRESSURE OF INCIDENT WAVE AT SURFACE OF MATERIAL. B,B':REFLECTIONS FROM SURFACE AND FROM RIGID BACKING OF MATERIAL, RESPECTIVELY.*

*DATA. Porous material. Solimide. Layer thickness=8 inches. Flow resistance, R=.61 ro-ce units/cm. Mass density, M=.03 g /cubcm.*

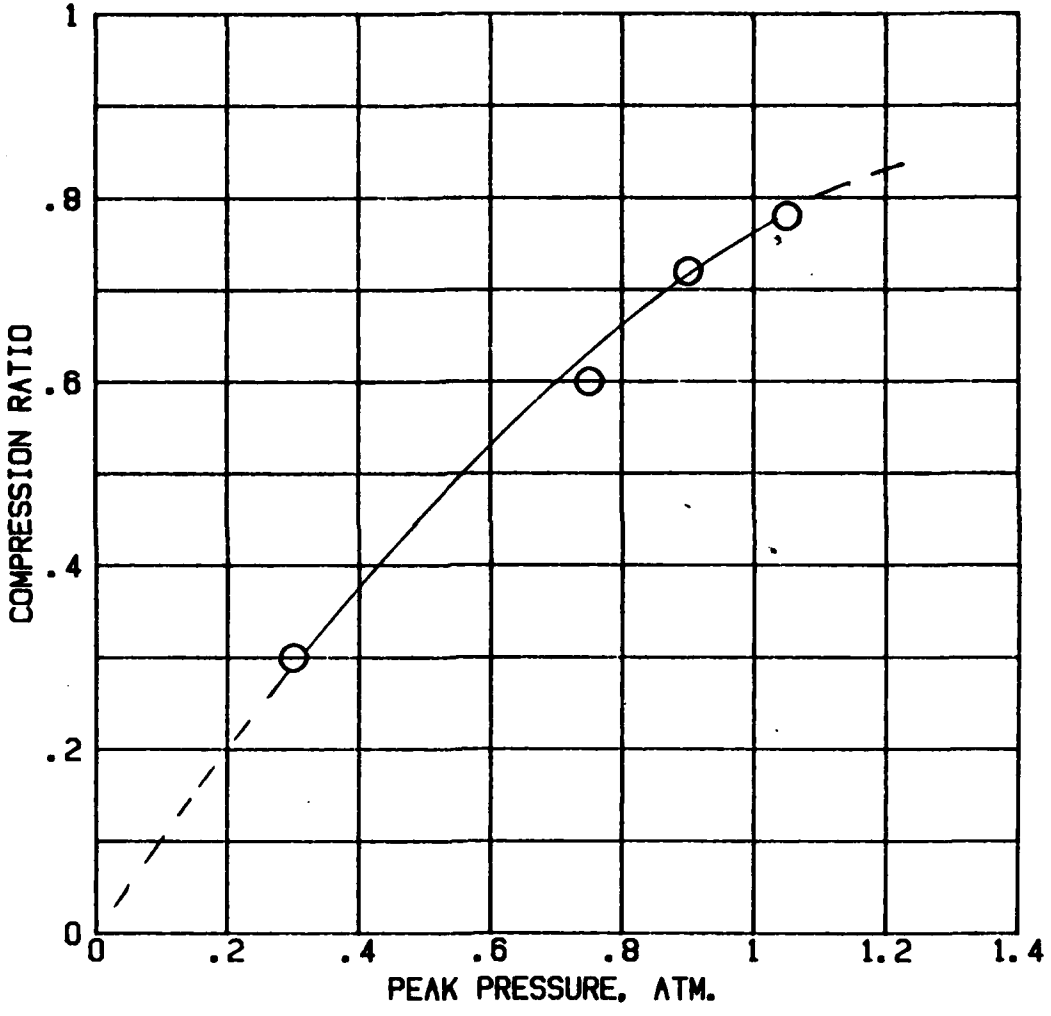


*Fig. VIII.9.*
RELATIVE DEFORMATION d/D OF A POROUS FLEXIBLE MATERIAL PRODUCED BY A SHOCK WAVE IN A TUBE.

*DATA. Porous material. (Solimide). Layer thickness, D=8 inches. Flow resistance, R=.61 ro-ce units/cm. Mass density, M=.03 g/cubcm. Gas: Air at 1 atm.*

## VIII. INSERTION LOSS MEASUREMENTS

The shock tube can be a useful tool also in general acoustic transmission measurements, if it is combinated with a Fourier transform routine for the determination of the power spectrum of the pulses generated. We developed and incorporated such a routine in our data acquisition system, and the related FFT program is included in Appendix C. This enabled us to obtain the power spectrum of our pulses in the frequency range between 18 to 4000 Hz.

The time dependence of a typical pulse wave generated in our shock tube is shown in Fig. 1 and the corresponding power spectrum in Fig. 2. The bulk of the energy of the pulse is in the frequency range below 300 Hz. The duration of the positive portion of the pulse is .0027 sec., the inverse of which corresponds to a frequency of 370 Hz.

It should be mentioned in this context, that in most sound sources used in acoustic laboratory transmission measurements suffer from a low frequency power deficiency, and to get adegquate low frequency power, special large loudspeakers often have to be used. In the shock tube, on the other hand, the bulk of the energy is at low frequencies, and offers a simple means of solving the source problem at low frequencies, when combined with a FFT capability.

The main reason for developing this capability in our case was to make possible studies of the frequency dependence of the attenuation of various attenuators and to check experimentally the theory for sound transmission in parallel baffle attenuators presented elsewhere in this report.

Most of these studies involved insertion loss measurements, i.e. the measurements of the power spectrum of a pulse at a fixed location before and after the attenuator (or other acoustical element) was introduced. It is necessary in such measurements,

that the pulses (and the related spectra) are repeatable. With our experimental procedure, as discussed earlier, repeatability was assured with a high degree of accuracy, as can be seen from Figs. 1 and 2. The curves in these figures actually represent the superposition of the curves for pulses from two experimental runs. It can be stated, that the spectra from one pulse to the next could be reproduced within half a decibel at frequencies up to 1000 Hz.

Measurements of the insertion loss of flexible porous baffles of lengths 1' and 2' and with flow resistances of .75 and 1.5 c units per inch were made. In each case the baffle was inserted in the center of the shock tube (5.1 cm in diameter) and the thickness of the baffle was such, that the open area fraction of the attenuator was 50 %. Insertion loss measurements were made on other elements also, such as orifice plates, lined duct elements, and period structures.

Considering now the results obtained for the porous baffles, we present first the calculated attenuation per foot in such an attenuator. It should be pointed out, that this attenuation is expected to be approximately equal to the insertion loss only at high frequencies, at which the effect of the reflection from the entrance to the attenuator is negligible. (The frequency dependenc of the reflection coefficient has been computed elsewhere in this report). In the frequency range considered here, the computed attenuation curves for the two baffles have the same general behaviour, and do not differ much even quantitatively.

To study the possible amplitude dependence of the insertion loss, we used pulses with two different peak pressures, .2 and .7 atm. These pulses and the their spectra are shown in Figs. 6 and 7.

The measured insertion loss curves for the two attenuators are shown in Figs. 7 and 8. Each figure contains the curves corresponding to the two different peak pressures of the incident

wave. At high frequencies the measured insertion loss follows the same general trend as the computed attenuation. At low frequencies, as expected, the insertion loss is larger than the attenuation, which can be explained on the basis of the reflection from the entrance to the attenuator.

More significant, however, is the unexpected decrease in the insertion loss with frequency, particularly pronounced at the higher incident pressure. For the .7 atm. pulse, the decrease starte approximately at 250 Hz and for the .2 atm. pulse at about 700 Hz. The effect is more pronounced for the baffle with the higher flow resistance.

Initially, we considered the possibility, that the effect might be related to the flexibility of the material, and this led to a study of the compression of a porous material by a shock wave, as described earlier. Although this effect may contribute to some extent to the anomalous behaviour, a more likely explanation involves the flow noise produced by the "jets" discharged from the end of the attenuator (or from the "wake" of the baffle).

The peak frequency of the noise spectrum from the flow is proportional to the flow speed. This is consistent with the observed result, that the frequency, at which the reduction in insertion loss is largest, increases with the incident pressure and hence with the velcoity.

Also supporting this explanation is the fact, that in the measurements of the insertion loss of orifice plates, the same general effect was observed. Furthermore, the weakness of the power spectrum of the incident pulse at high frequencies makes even a relatively low level high frequency flow noise at the attenuator exit dominating, thus reducing the insertion loss. In other words, the flow noise effect on the insertion loss will depend not only on the strength of the incident pulse but also on its spectrum.

In experiments with a periodic baffle attenuator, consisting of 1" long porous elements placed a distance 2" apart, we found that the flow effect on the insertion loss was significantly smaller than for the uniform baffle.

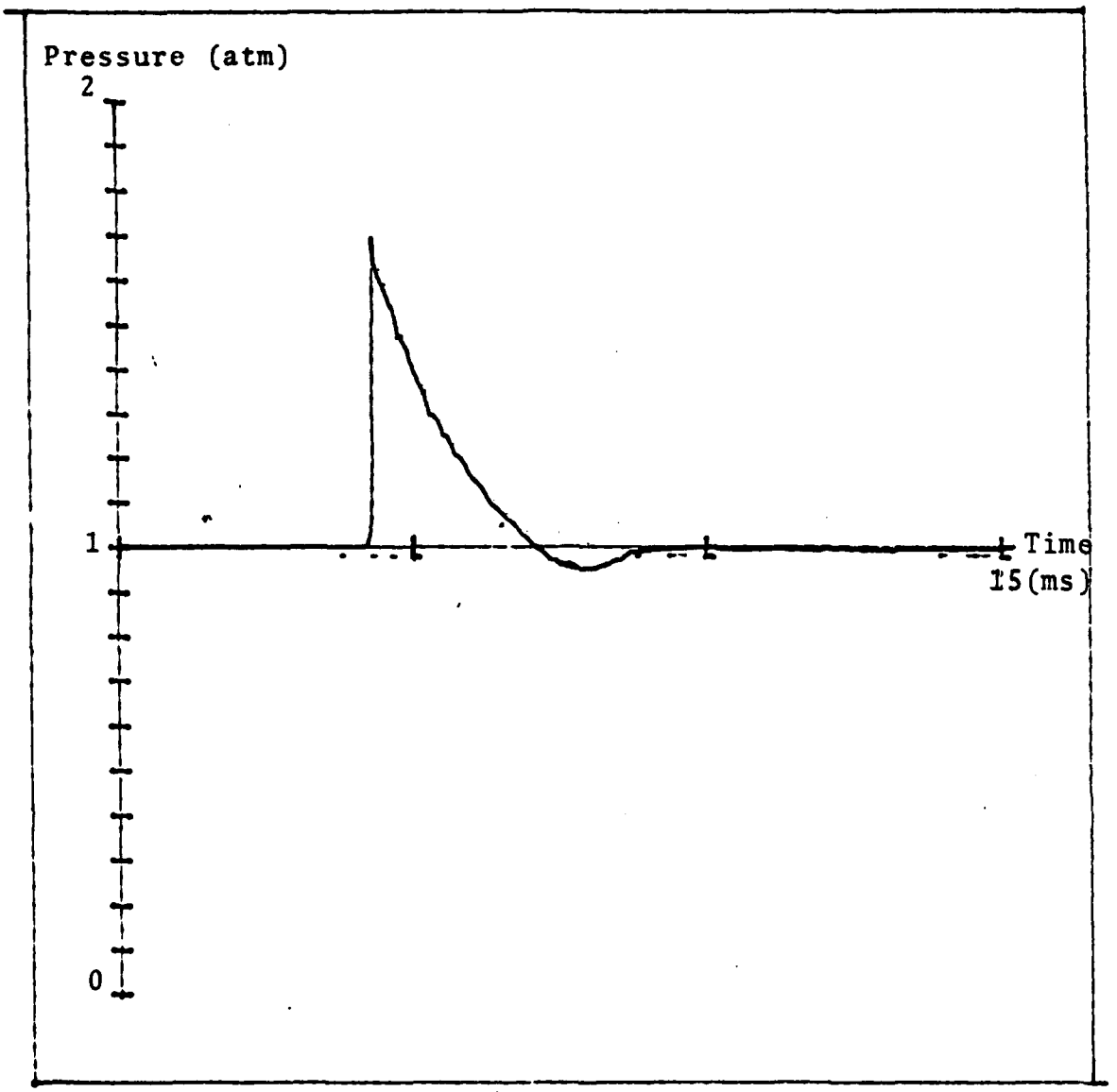


*Fig. IX.1.*
*COMPARISON OF PRESSURE RECORDS FROM TWO DIFFERENT EXPERIMENTAL RUNS IN THE SHOCK TUBE WITH THE SAME DRIVER SECTION PRESSURE. The curves fall almost on top of each other demonstrating reproducibility of pulse wave generation.*

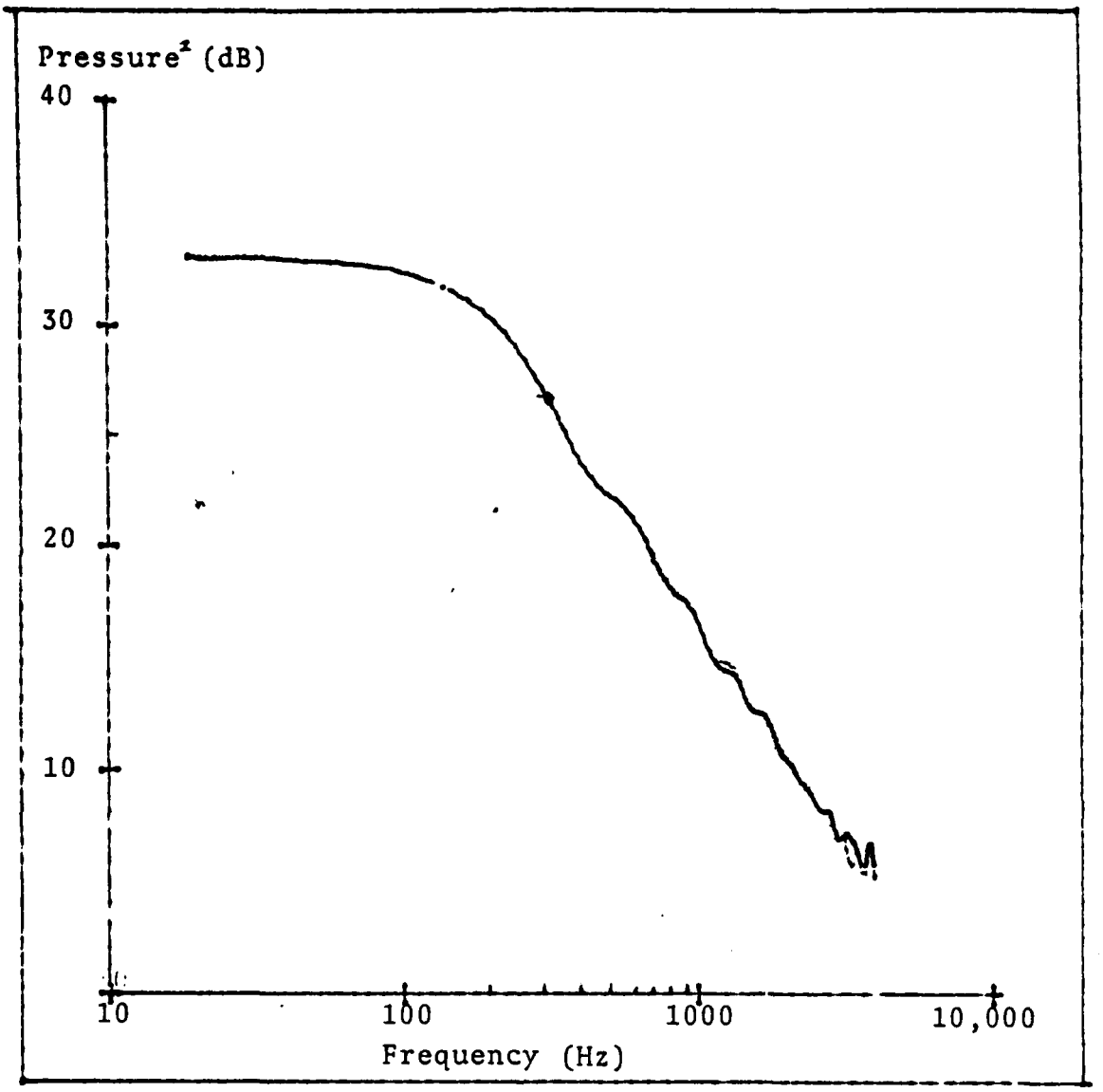


*Fig. IX.2.*
*FREQUENCY SPECTRA OF THE TWO PULSES IN FIG. IX.1.*
*The curves fall almost on top of each other demonstrating reproducibiliy.*

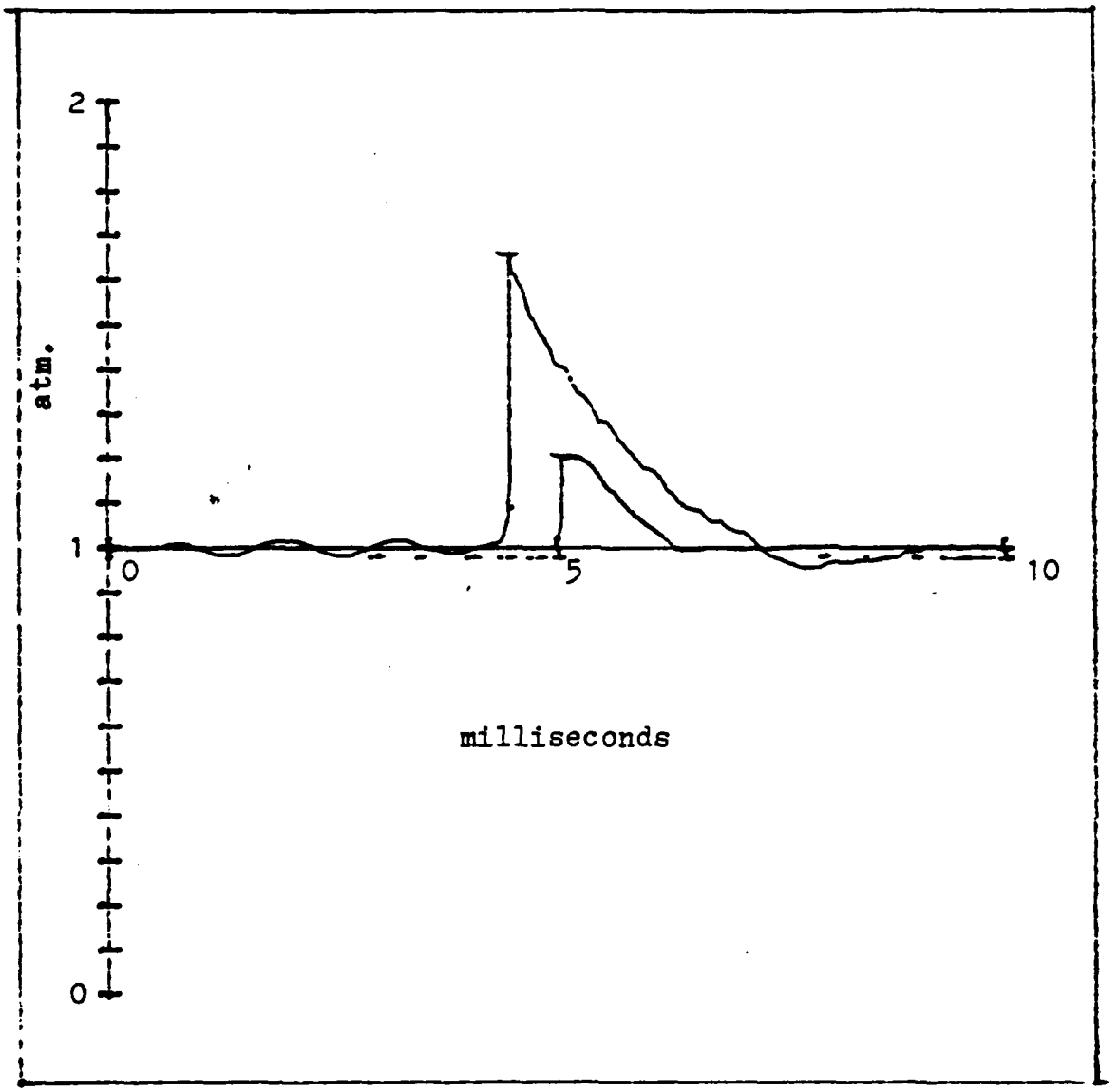


*Fig. IX.3.*
*THE TWO INCIDENT SHOCK WAVES WITH PEAK PRESSURES .7 AND .2 ATM, USED IN THE INSERTION LOSS MEASUREMENTS.*

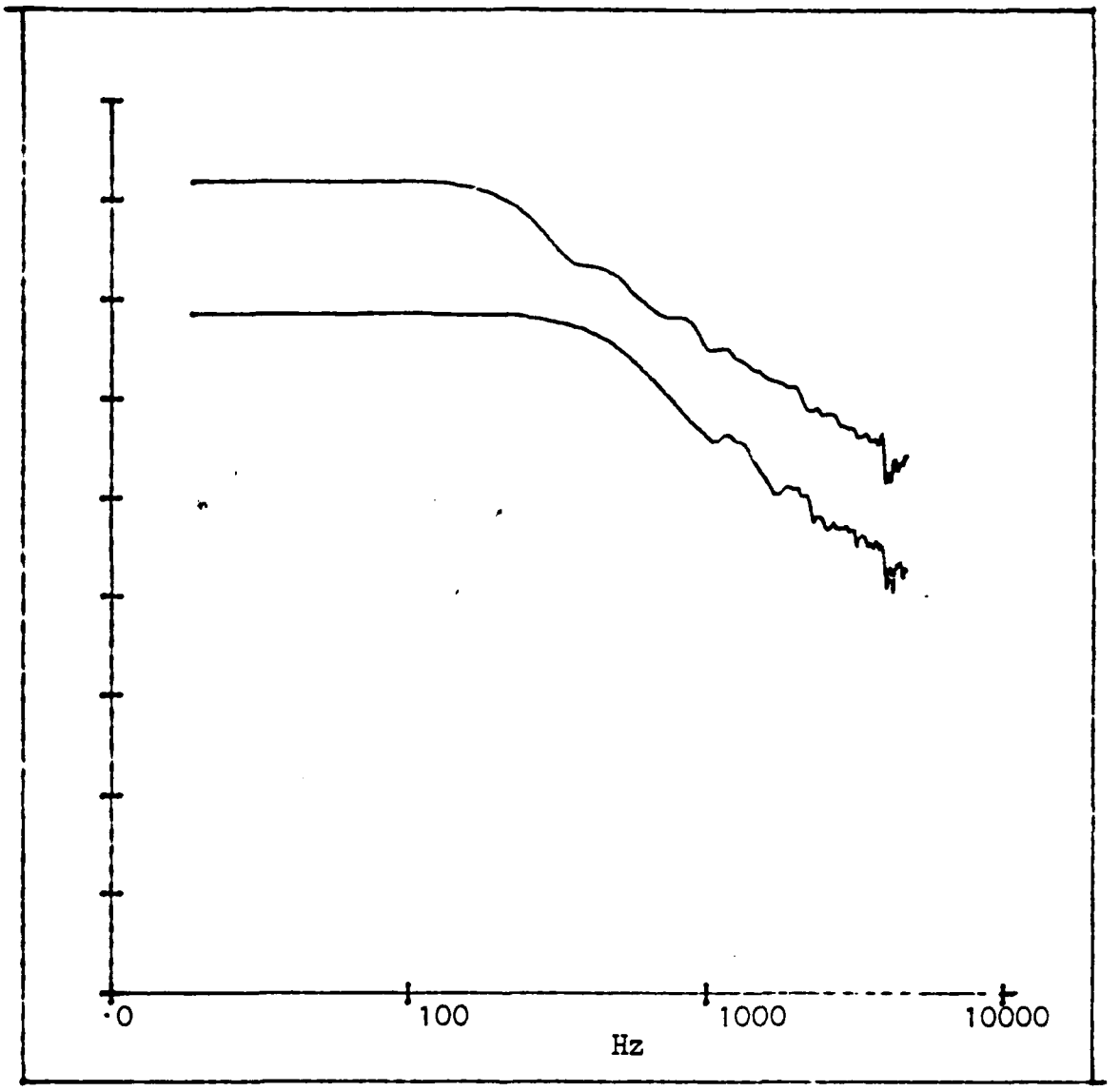


*Fig. IX.4.*
*THE FREQUENCY SPECTRA OF THE TWO PULSES IN FIG. IX.3.*

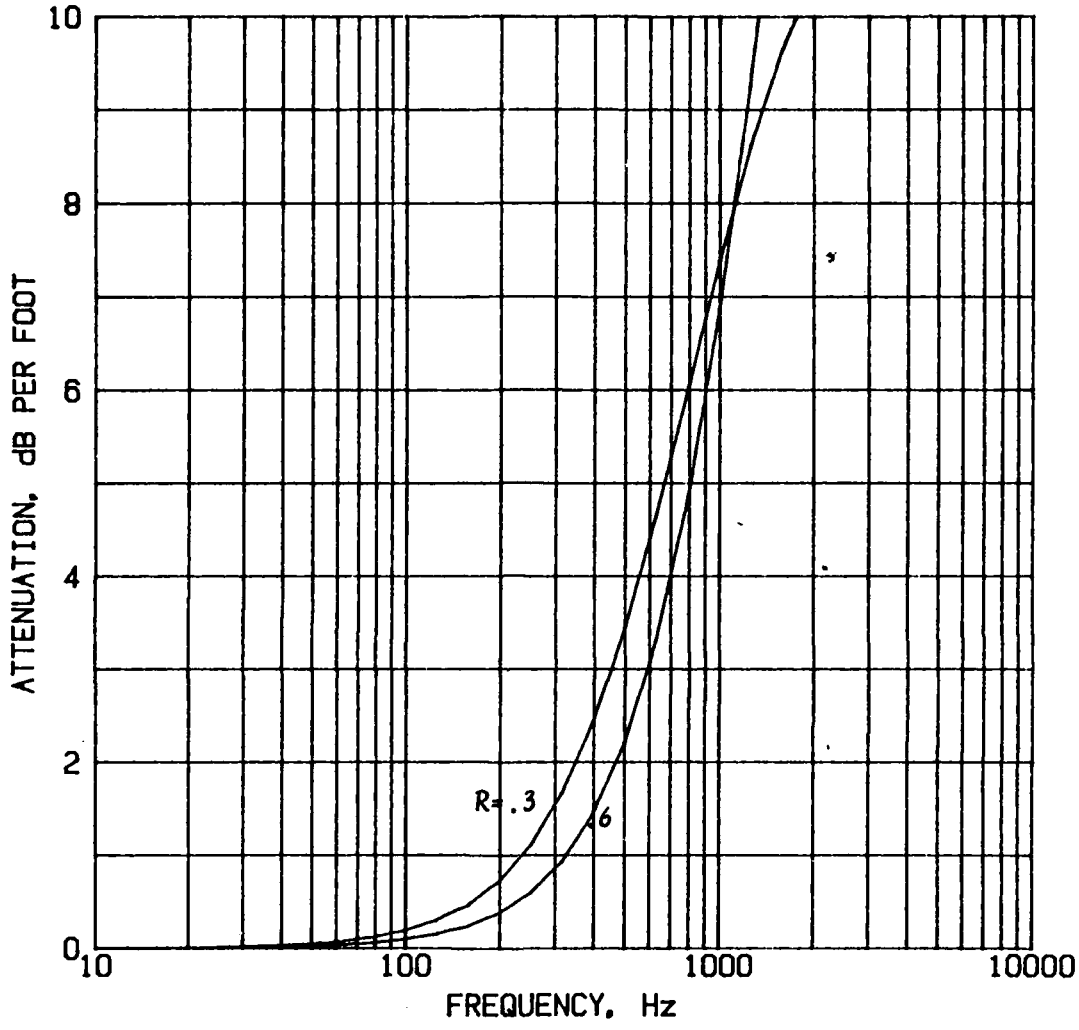


*Fig. IX.5.*
*ATTENUATION OF PARALLEL-BAFFLE ATTENUATOR COMPUTED FROM THE ANALYSIS OF SECTION VI.*

*DATA. Porous baffles: Limp. Mass density, M=.05 g/cubcm.*
*Flow resistance, R=.3, and .6 ro-ce units/cm.*
*Open area fraction of attenuator, S=.5.*

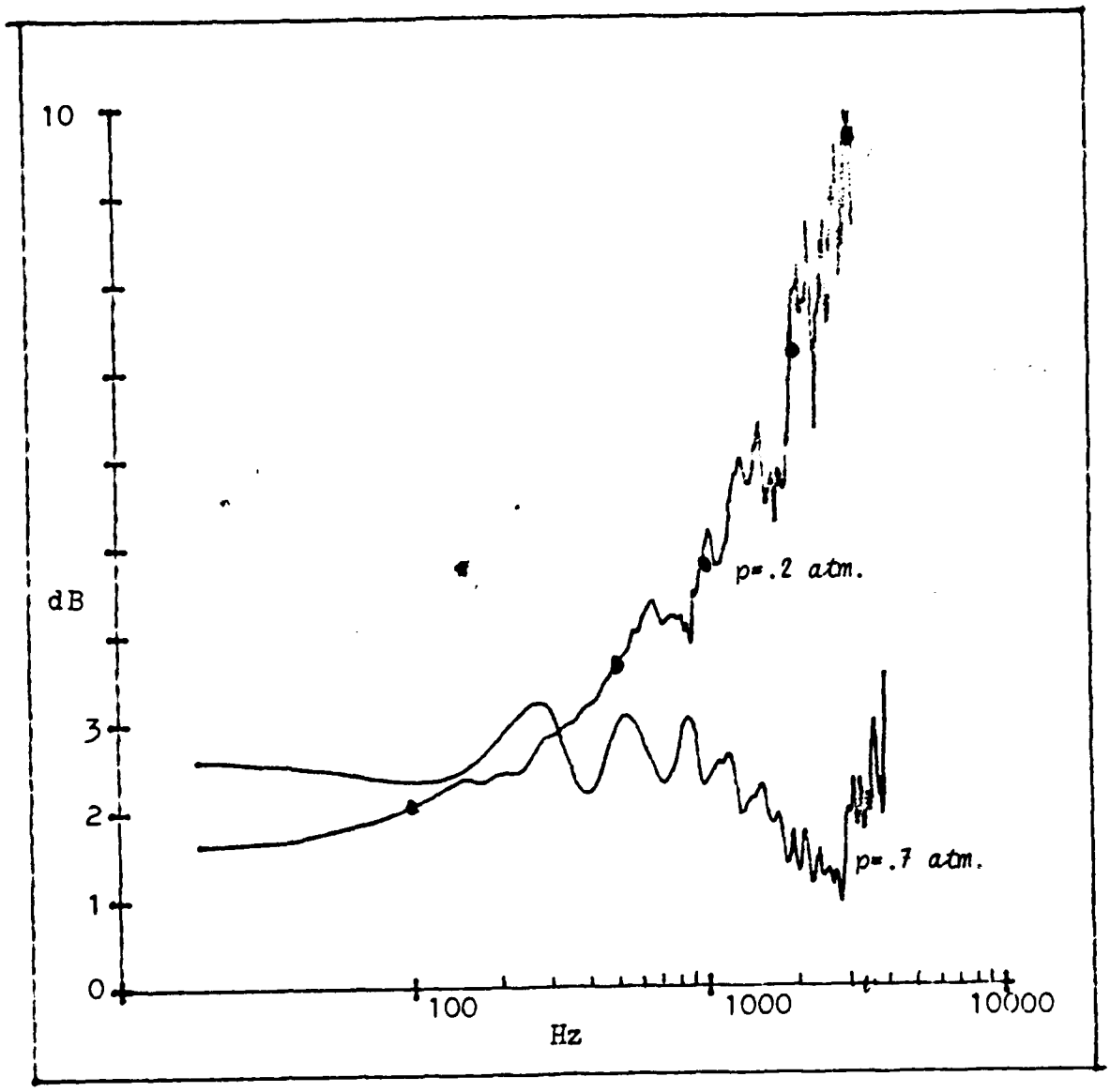


*Fig. IX.6.*
*MEASURED INSERTION LOSS OF BAFFLE ATTENUATOR.*

*DATA. Porous baffle. Flow resistance, R=.3 ro-ce units/cm*
*Mass density, M=.05 g/cubcm.*
*Peak pressure of incident pulse, p/P=.2, and .7. (air, P=1 atm.)*
*Open area fraction of attenuator, S=.5.*

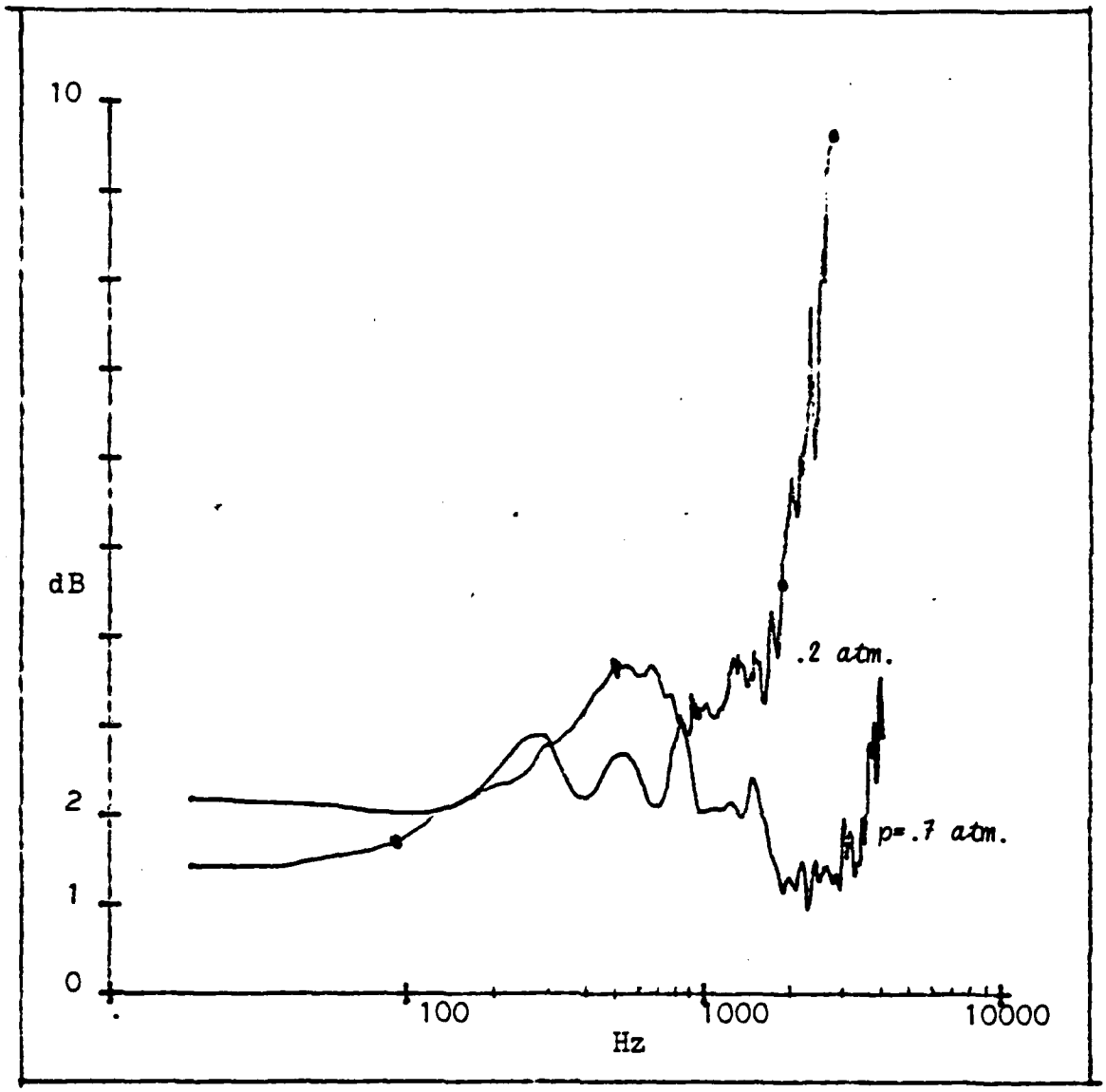


Fig. IX.7.
MEASURED INSERTION LOSS OF BAFFLE ATTENUATOR.

DATA. Porous baffle. Flow resistance, R=.6 ro-ce units/cm
Mass density, M=.05 g/cubcm.
Peak pressure of incident pulse, p/P=.2, and .7. (air, P= 1 atm)
Open area fraction of attenuator, S=.5.

## Appendix A

## ACOUSTICAL PROPERTIES OF FLEXIBLE POROUS MATERIALS.

### 1. Introduction.

We present here a brief discussion of some acoustical properties of flexible porous materials, which have been used on our study of sound attenuation in lined ducts and parallel-baffle attenuators in Section VI.

Although numerous papers have been written on the acoustics of porous materials, few have included the effect of flexibility of the material. This omission is justified at sufficiently high frequencies, when the inertia of the porous structure prevents it from participating in the oscillatory motion in the sound field. In a general analysis, the inclusion of flexibility and the elastic properties of the elastic structure makes it quite complex, and the effect of the various parameters on the acoustical properties of the material cannot be expressed in a simple manner.

On the other hand, most of the porous materials used in acoustical applications have a relatively small elastic modulus, so that the longitudinal wave speed in the structure is small compared to the wave speed in the surrounding gas. Under such conditions, the porous material can be considered to be "limp" (as will be shown), and the effect of flexibility can then be accounted for in a simple manner.

### 2. Physical parameters.

We begin with a brief review of the macroscopic physical quantities, which will be used in our acoustical analysis.

Porosity, H, is the volume fraction of the material occupied by the "voids" in the material. In the present case the voids are filled with the ambient gas, and the average gas density in the

material is then

$$\underline{\rho}=H\rho \qquad (2.1.)$$

where $\rho$ is the ambient gas density. Similarly, if the mass density of the solid constituent (such as fibers) of the material is $\rho'$, the bulk mass density of the porous structure is

$$M=H\rho+(1-H)\rho'\approx(1-H)\rho' \qquad (2.2)$$

For the materials of interest here, the mass density M typically lies in the range from .025 to .25 $g/cm^3$, corresponding to a weight per unit volume of approximately 1 to 15 $lbs/ft^3$, between 20 to 200 times heavier than air.

With a value of $\rho'\approx 1.5\ g/cm^3$, which is typical for most synthetic fibers, the corresponding range of the porosity, as obtained from Eq. 2.2 is .85 to .98. In special cases, considerably smaller values of the porosity are encountered. For example, in studies of sound propagation over ground, the ground material often is treated as a porous material with a porosity between .3 and .5, corresponding to the values for the type of sand normally encountered.

In terms of the average gas density in the porous material, as given by Eq. 2.1, the <u>average mass flux</u> in the material is expressed as $H\rho u$, where u is the average velocity, the averaging beeing made over all directions and magnitudes of the velocities in the pores and channels of the material.

Ordinarily, no distinction is made between mass density and inertial mass density. In the macroscopic description of the momentum balance of the gas in the porous material, however, we must include an "induced" mass density to account for the microscopic tortuous motion of the gas in the pores. (Compare the induced mass of an oscillating sphere in a fluid or the mass end correction of

an open ended pipe). We shall denote the induced mass density by $g\rho$, and the total inertial mass density is the $(1+g)\rho$, where $G=1+g$ usually is called the "structure factor". Included in the structure factor is the (small) effect of the constriction produced by the viscous boundary layers in the flow channels in the material.

The structure factor, which normally has a value between 1.2 and 2, should be regarded as an empirical parameter, which can be measured. Fortunately, the overall acoustical characteristics of a porous layer do not depend strongly on the structure factor.

Flow resistance, r, per unit length of the porous material is defined by the relation $ru"=-gradp$, where u" is the average relative velocity of the gas and the porous material, and gradp the pressure gradient. For small values of u", usually less than 10 cm/sec, the flow resistance is independent of velocity. At higher velocities, flow separation and turbulence may occur within the material, and the relation between u" and gradp then becomes nonlinear.

The flow resistance often is measured by means of a steady flow apparatus, and the DC flow resistance thus obtained is assumed to be applicable also in the description of the acoustic interaction between the gas and the porous material. This is not entirely correct, however; simple microscopic models indicate, that the acoustic flow resistance increases slowly with frequency, and in some cases it can be considerably different from the DC value.

The physical parameters introduced so far are not all independent; their interrelationship depends on the details of the microstructure of the material. For example, it follows from dimensional considerations, that, for a given porosity, the viscous flow resistance is inversely proportional to the square of the fiber diameter (or pore size) and directly proportional to the shear viscosity coefficient. The fiber diameter, in turn,

is related to the porosity and the mass densities M and $\rho'$.

In the limits 0 and 1 for the porosity, the flow resistance should be zero and infinite, respectively. A simple empirical expression for the flow resistance, which meets these conditions, is $r \simeq (\text{const})[(1-H)/H]^n$, where n is positive. If we introduce $1-H \simeq M/\rho'$ and use the fact, that H is close to unity for most materials of interest here, we obtain $r \simeq (\text{const})(M/\rho')^n$. In other words, for a given value of $\rho'$, the flow resistance is proportional to some power of the mass density M. Experimental data indeed are consistent with this relation for most materials over the range of commonly encountered M-values, if n=1.4-1.5.

Making use of this result and the dimensional considerations mentioned above, we arrive at the relation

$$r \simeq (\text{const})(M/\rho')^n(\mu/cd^2) \qquad (2.3)$$

where $\mu$ is the coefficient of shear viscosity of the gas and d the fiber (or pore) diameter.

Since the shear viscosity is independent of the gas density, it follows, that the same holds true also for the flow resistance. In other words, if the flow resistance is measured at atmospheric pressure, the value obtained can be applied also when the material is used (in a closed loop laser, for example) at reduced pressure.

The numerical value of (const) in Eq. 2.3 depends on the geometrical arrangement of the fibers and pores, and, if the material is anisotropic, also on the direction of the flow in the material. For synthetic fibers the diameter d typically is of the order of $10^{-3}$-$10^{-4}$ cm. Using this range in Eq. 2.3 and typical measured values of r, M, and $\rho'$, we find the range of values for (const) to be of the order of 15 to 1500 1/cm, depending on the fiber (or pore) size.

If the porous material is flexible, additional parameters, elastic constants and internal damping must be included in the

description. The general analysis then involves the study of coupled wave motions. Fortunately, for most flexible materials of interest in this context, the longitudinal wave speed in the material is small compared to the speed of sound in the surrounding gas. As we shall show, it is then a good approximation to treat the material as limp.

## 3. Characteristic frequencies.

In the discussion of the acoustical properties of a porous material it is instructive and useful to introduce some characteristic frequencies. The first (angular) frequency is

$$\omega_1 = r/\rho_1 \qquad (3.1)$$
$$\rho_1 = GH\rho$$

where $r$ is the flow resistance per unit length and $\rho_1$ the inertial mass density of the gas in the material. The normalized frequency $\omega/\omega_1$ then can be interpreted as the ratio between the inertial force and the friction force per unit volume in the porous material and thus can be regarded as a type of Reynolds number.

At frequencies below $\omega_1$, the friction force dominates, and as the frequency decreases, the wave motion in the material degenerates into a diffusion process. In this diffusion region the phase velocity can be considerably smaller than the ordinary sound speed, as will be shown in more detail later.

At frequencies much above $\omega_1$, on the other hand, the inertial force dominates, and the wave motion in the material is much like the motion in free space, except for the attenuation, which in this region becomes proportional to the flow resistance.

For porous materiaals, such as bonded glass wool or mineral wool, with a bulk mass density in the range between .05 and .17 $g/cm^3$, corresponding to 3-10 $lbs/ft^3$, the flow resistance lies in the approximate range .5-3 $\rho c$ units per cm, and the correspon-

ding characteristic frequencies ($\omega_1/2\pi$) are apporoximately 1000 to 5000 Hz.

A second characteristic frequency is

$$\omega_2 = r/M = (\rho_1/M)\omega_1 \tag{3.2}$$

For a flexible porous material, the frequency ratio $\omega/\omega_2$ can be thought of as the ratio between the inertial force related to the motion of the porous material and the drag force on it per unit volume. This motion will be significant only at frequencies lower than $\omega_2$.

At frequencies much larger than $\omega_1$, the inertia of the material prevents it from moving significantly, and it can be regarded as rigid. Typically, this second characteristic frequency lies between 65 and 100 for fibrous materials.

Another characteristic frequency is related to the oscillatory heat flow in the material, that results from the compressions and rarefactions of the gas. The heat conductivity of the solid material is much larger than that of the gas, and it follows then from dimensional considerations, that the characteristic frequency, being the inverse of the the characteristic time of diffusion, will be of the form

$$\omega_3 = K/\rho c_p s^2 \tag{3.3.}$$

where K is the heat conduction coefficient of the gas, $\rho$ the gas density, $c_p$ the specific heat per unit mass at constant pressure, and s the average pore size or distance between fibers.

At frequencies much lower than $\omega_3$, the conditions in the porous material can be regarded as isothermal, whereas at frequencies considerably higher than $\omega_3$, the change of state in the gas will be approximately isentropic. In the frequency range of transition, i.e. in the vicinity of $\omega_3$, the thermodynamic changes of

the gas are irreversible, and some of the acoustic energy will be converted into heat as a result of the heat exchange with the porous material. The effect is small, however, compared to the losses produced by the viscous interaction.

For a flexible material, there are additional intrinsic characteristic frequencies. The strain in the material can give rise to internal damping through a number of different mechanisms, with related characteristic relaxation frequencies. In a fibrous material, the friction between fibers in relative motion may also play a role.

In addition to these intrinsic frequencies, there are others, which might be termed geometrical, related to the time of wave travel across a porous layer. Several wave speeds can be involved, not only the sound speed in the gas but in the structure as well, both longitudinal and transverse.

Because of this multiplicity of characteristic frequencies, the acoustic scaling laws for for flexible porous materials are not simple, and it is not possible, in general, to express the frequency dependence of the acoustical properties in terms of a single normalized frequency. For a rigid material, on the other hand, only the intrinsic frequency $\omega_1$ is important.

## 4. Flow impedance and boundary conditions.

The interaction force resulting from the relative motion of the porous material and the gas is the sum of the friction force and the inertia force due to the induced mass, as defined earlier. We express this force as

$$F = z\,(u-u') \qquad (4.1)$$

$$z = r - i\omega g H \rho$$

assuming harmonic time dependence. Here u-u' is the difference between the gas velocity u and the velocity u' of the porous

structure. As expressed in Eq. 4.1, the force F refers to the force on the structure. The force on the gas is equal and opposite, of course. The quantity z will be called the flow impedance It contains the induced mass factor g, which can be epxressed in terms of the structure factor G, g=G-1.

If the restoring force in the structure due to its stiffness is so small, that only the inertia of the material needs to be accounted for in determining the motion resulting from the interaction with the air, the material is "limp". Under these conditions, the velocity u' of the structure becomes

$$u'=uz/(z-i\omega M) \tag{4.2}$$

where, as before, $z=r-i\omega gH\rho$ and u is the average velocity amplitude of the gas in the porous material.

This relation between u and u' plays an important role in establishing the acoustic boundary conditions at the boundary between a porous material and the gas outside.

For an "open" boundary, i.e. one without an impervious skin or layer, the continuity of mass flow normal to the boundary requires, that $\rho(u_1-u')=H\rho(u-u')$, where $u_1$ is the velocity in the gas outside the boundary. In addition, continuity of pressure requires $p_1=p$. Making us Eq. 4.2 these boundary conditions can be expressed as

$$u_1=Cu \tag{4.3}$$
$$p_1=p$$
$$C=H(1+iz/H\omega M)/(1+iz/\omega M)$$
$$z=r-i\omega gH\rho$$

For a "closed" boundary, i.e. with the porous material covered with an impervious skin or layer, the velocity of the skin is the same as that of the structure. Continuity of normal

velocity now requires $u_1 = u'$, and for the pressure we have the condition $p_1 = p - i\omega m_1 u'$, where $m_1$ is the mass per unit area of the impervious layer. Again, making use of Eq. 4.2, these relations can be summarized as

$$u_1 = C'u \tag{4.4}$$
$$p_1 = p - i\omega m_1 C'u$$
$$C' = z/(z - i\omega M), \qquad z = r - i\omega g H\rho$$

## 5. Equations of motion.

In terms of the quantities defined in Section 2, we can express the equations for conservation of mass and momentum for the gas and for the porous structure as

$$\partial(H\rho)/\partial t + \mathrm{div}(H\rho u) = 0 \tag{5.1}$$
$$\partial(H\rho u)/\partial t = -\mathrm{grad}p - r(u - u') - \partial[gH\rho(u - u')]/\partial t \tag{5.2}$$
$$\partial[(1-H)\rho']/\partial t + \mathrm{div}[(1-H)\rho' u'] = 0 \tag{5.3}$$
$$\partial[(1-H)\rho' u']/\partial t = -r(u' - u) - \partial[Hg\rho(u' - u)]/\partial t + v^2 M \nabla^2 \xi' \tag{5.4}$$
$$u' = \partial\xi'/\partial t, \qquad M = (1-H)\rho'$$

In the momentum equation 5.4 for the structure, the last term represents the elastic restoring force, where v is the longitudinal wave speed in the structure and $\xi'$ the longitudinal part of the displacement. In a general analysis of the problem, this term must be included, of course. For many porous materials, however, it is small compared to the viscous interaction term. In order to see this, we consider harmonic time dependence and estimate the ratio between the elastic and the visous force.

With $k = \omega/v_p$, where $v_p$ is the phase velocity of the acoustic wave in the porous material, the elastic force will have a magnitude of the order of $v^2(\omega/v_p)^2 Mu'/\omega$. Estimating the magnitudes of the other terms in similar manner, we can determine $u'/u$ and the

ratio between the elastic force and the friction force. It follows, that this ratio goes to zero as $(v/v_p)^2$. Typically, the longitudinal wave speed in a porous material is quite small, of the order of the order of 10-15 m/sec. The phase velocity in the porous material, as we shall see, typically is about half the sound speed in the gas. This means, that $v/v_p$ will be ot the order of .1, with a corresponding ratio between the elastic force and the friction force of the order of .01. Under these conditions, the omission of the elastic force is justified.

On the basis of this estimate of the relative importance of the forces, we shall assume the material to be limp and omit the last term in Eq. 5.4.

We consider now harmonic time dependence and linearize the equations of motion. In addition to the perturbations in density, pressure, and velocity, there will be a perturbation also in the porosity, which will be denoted by h. Strictly speaking, there will be small changes also in the flow resistance and the structure factor, but these will not be included here. The linearized equations for the complex amplitudes are then

$$-i\omega(\varkappa p+h/H)=-\mathrm{div}u \tag{5.5}$$

$$(-i\omega H\rho+z)u=-\mathrm{grad}p+zu' \tag{5.6}$$

$$-i\omega h/(1-H)=\mathrm{div}u' \tag{5.7}$$

$$-i\omega Mu'=-z(u'-u) \tag{5.8}$$

$$z=r-i\omega gH\rho$$

where we have introduced the compressibility $\varkappa$ of the gas. The effect of heat conduction losses can be accounted for by letting the compressibility be complex.

From the complex amplitude equations 5.5 - 8, we can eliminate the velocity u' and obtain equations for u and p. Then, if we incorporate the variation in the porosity in the compressibility, and introduce a complex density, the equations can be

brought into the "standard" form

$$-i\omega\hat{\varkappa}p=-\mathrm{div}u \tag{5.9}$$

$$-i\omega\hat{\rho}u=-\mathrm{grad}p \tag{5.10}$$

$$\hat{\varkappa}=\varkappa[1-z(1-H)/(z-i\omega HM)]$$

$$\hat{\rho}/\rho=H+z'/\omega\rho$$

$$z'=z/(1+iz/\omega M)$$

$$z=r-i\omega Hg\rho$$

From these equations we obtain the wave equation

$$\nabla^2 p+(\omega/\hat{c})^2 p=0 \tag{5.11}$$

$$1/\hat{c}^2=\hat{\rho}\hat{\varkappa}$$

For a rigid material and at low frequencies, such that $r/\omega\rho<<1$, we have $1/\hat{c}^2\simeq i(r/\omega\rho c^2)$ and the wave equation reduces to

$$\nabla^2 p+i(\omega r/\rho c^2)p=0 \tag{5.12}$$

which corresponds to the diffusion equation

$$\partial p/\partial t=(\rho c^2/r)\nabla^2 p \tag{5.13}$$

## 6. Phase velocity and attenuation.

We shall consider now a harmonic wave travelling in the positive $x$-direction, so that the spatial dependence of the complex amplitude is $\exp(iqx)$, where $q=q_r+iq_i$ is the propagation constant. The phase velocity of the wave is $\omega/q_r$ and the spatial rate of attenuation is determined by $q_i$. It follows from the wave equation that the propagation constant can be expressed as

$$q=\omega/\hat{c}=(\omega/c)[(\hat{\rho}/\rho)(\hat{\varkappa}/\varkappa)]^{\frac{1}{2}} \tag{6.1}$$

The real and imaginary parts of $(\hat{\rho}/\rho)(\hat{\varkappa}/\varkappa)$ readily can be determined from the relations associated with Eqs. 5.9-10. The orresponding real and imaginary parts of the propagation constant are

$$q_r=(1/\sqrt{2})[\sqrt{(C^2+D^2)}+C]^{\frac{1}{2}} \tag{6.2}$$

$$q_i=(1/\sqrt{2})[\sqrt{(C^2+D^2)}-C]^{\frac{1}{2}} \tag{6.3}$$

$$C+iD=(\hat{\rho}/\rho)(\hat{\varkappa}/\varkappa)$$

The phase velocity $v_p$ is determine by the real part $q_r$,

$$v_p=\omega/q_r \tag{6.2}$$

and the attenuation per unit length by the imaginary part $q_i$. The corresponding attenuation in dB of the wave amplitude in a distance x is

$$20\cdot\log[p(0)/p(x)]=20\cdot\log(e)\cdot q_i x\simeq 8.7\ q_i x \tag{6.4}$$

Examples of the computed frequency dependence of the real and imaginary parts of the normalized propagation constant Q=q/k, n in Figs. A1 and A2. For comparison we have considered both rigid and limp materials.

Of particular interest is the reduced attenuation in the flexible material at low frequencies, below the characteristic frequency $r/2\pi M$. As in the present case, this frequency is comparatively low, but it increases with the flow resistance. Due to nonlinear effects, the resistance is known to increase with the wave amplitude, and this may explain, at least in part, the reduced energy absorption and attenuation observed at large amplitudes, as described elsewhere in this report.

It should be noted also, that the real part of the propagation constant is reduced at low frequencies, as a result of the

flexibility, but in the frequency range of interest here, this effect is significant only at relatively large values of the flow resistance.

Examples of the computed frequency dependence of the phase velocity are given in Fig. A3. The flow resistance is in the range of interest for the optimum design of parallel baffle attenuators, as discussed in Section VI, and for these values, we see, that the difference between a rigid and a limp material is rather small as far as the phase velocity is concerned.

The frequency dependence of the attenuation, corresponding to the parameter values of Fig. A3, is shown in Fig. A4. Here the effect flexibility of the material is more apparent, but for frequencies above 100 Hz in this case, it is still small. This transition frequency, of course, increases with increasing flow resistance.

7. Characteristic impedance and reflection coefficient.

The characteristic impedance of the porous material (i.e. the ratio between the complex pressure amplitude and the complex velocity amplitude in a wave travelling in the positive x-direction) is obtained from Eq. 5.10,

$$z_0 = \hat{\rho}\hat{c} = \sqrt{\rho/\varkappa} = \rho c\sqrt{(\tilde{\rho}/\rho)(\varkappa/\tilde{\varkappa})} \qquad (7.1)$$

where we have made use of $q=\omega/c$ and $c^2 = 1/\hat{\rho}\tilde{\varkappa}$. The normalized characteristic impedance $Z_0 = z_0/\rho c$ can be expressed in terms of the normalized propagation constant $Q=q/k$ as

$$Z_0 = (\varkappa/\tilde{\varkappa})Q \qquad (7.2)$$

Accounting for the boundary condition, discussed in Section 4, the velocity amplitude outside an "open" boundary is $u_1 = Cu$, where C is given in Eq. 4.3. The corresponding normalized input impe-

dance of a semi-infinite porous layer is then $Z_1 = Z_0 / C$. Introducing the expression for $\varkappa/\hat{\varkappa}$, given with Eqs. 5.9-10, we find $Z_1 = Q/H$. The corresponding pressure reflection coefficient at the boundary is then

$$R_p = (Z_1 - 1)/(Z_1 + 1) \qquad (7.3)$$

$$Z_1 = Q/H$$

Examples of the computed frequency dependence of the reflection coefficient are given in Fig. A5.

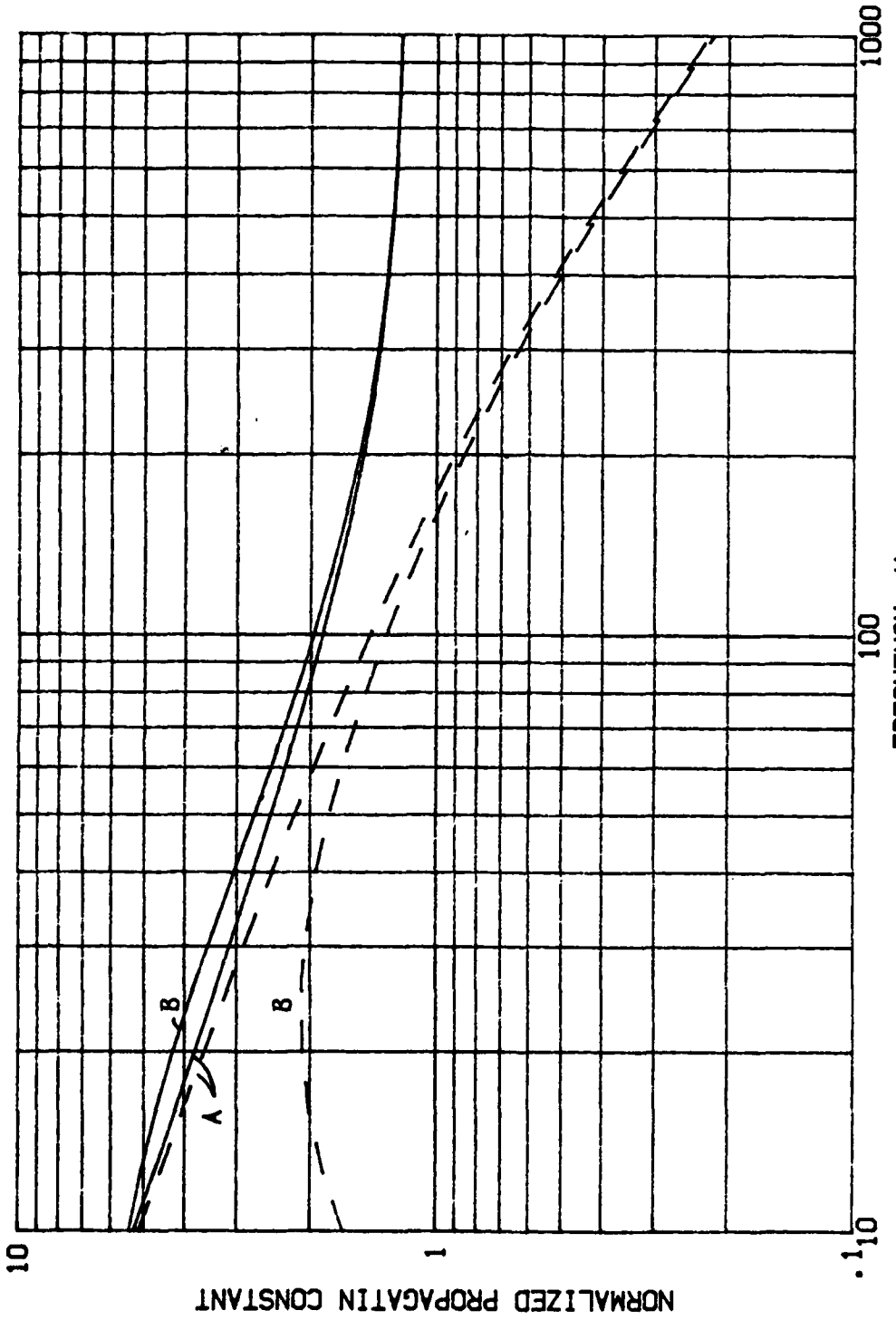


Fig. A1.
NORMALIZED PROPAGATION CONSTANT Q=q/k=Q1+iQ2 FOR POROUS MATERIAL.
REAL PART, Q1, solid lines. IMAGINARY PART, Q2, dashed lines.

DATA. Porous material: Rigid, curves A. Limp, curves B.
Flow resistance, R=.1 rayls/cm. Ratio of mass density and gas density (for limp material), m=38. Porosity, H=.95. Structure factor, G=1.5.

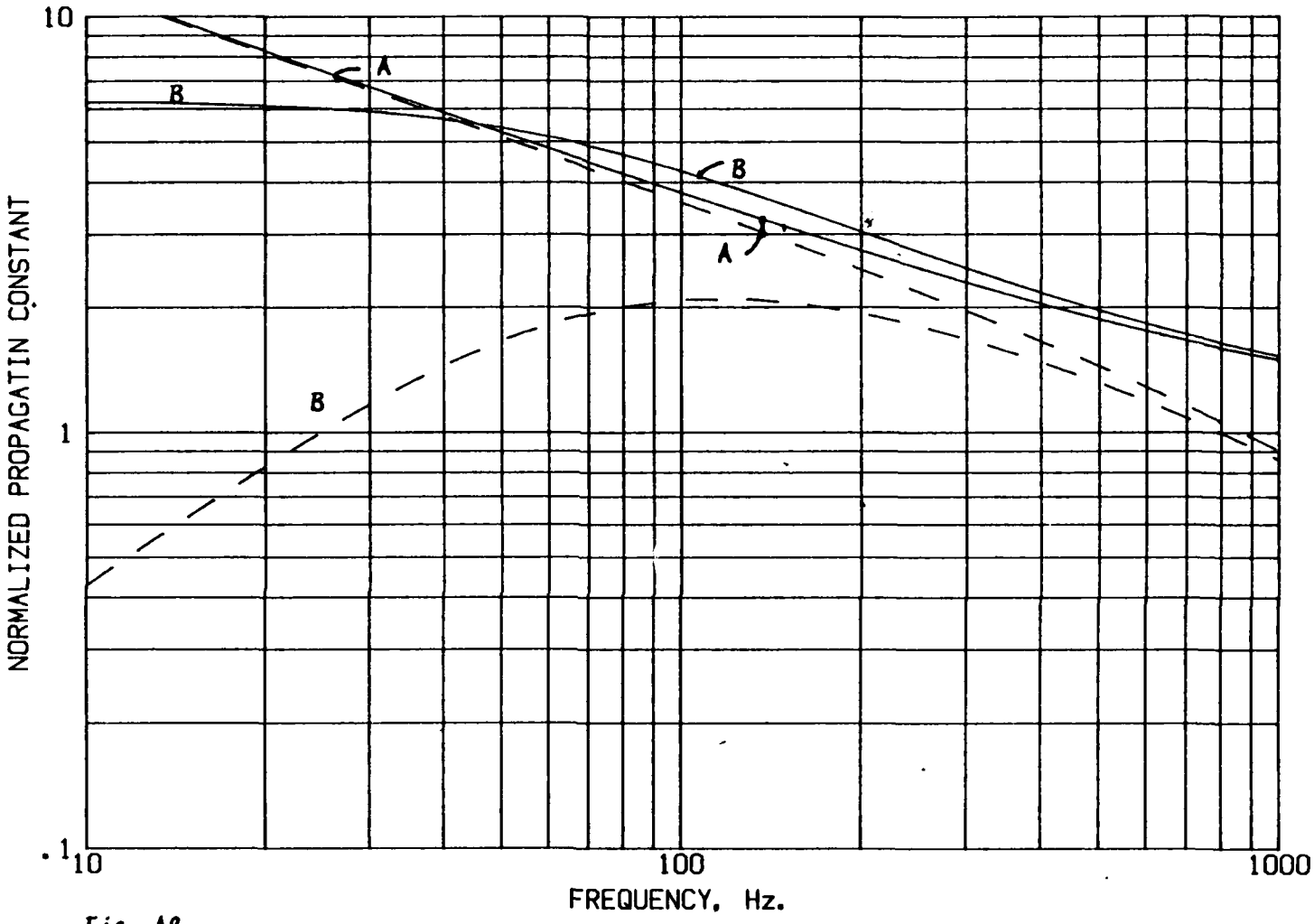


*Fig. A2.*
*NORMALIZED PROPAGATION CONSTANT Q=q/k=Q1+iQ2 FOR POROUS MATERIAL.*
*REAL PART, Q1, solid lines. IMAGINARY PART, Q2, dashed lines.*

*DATA. Porous material: Rigid, curves A. Limp, curves B.*
*Flow resistance, R=.5 ro ce units/cm. Ratio of mass density and gas density (for limp material), m=38. Porosity, H=.95. Structure factor, G=1.5.*

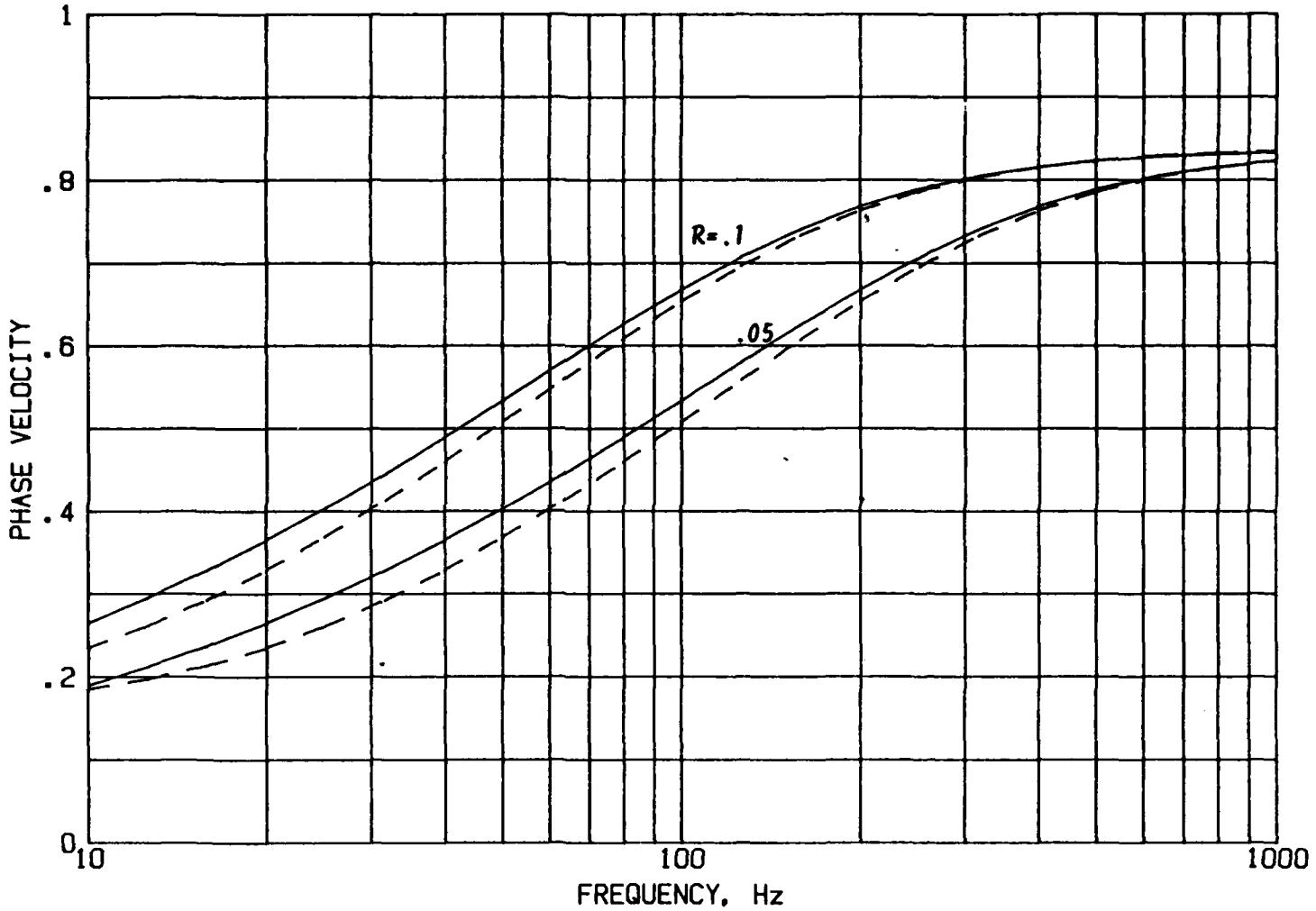


*Fig. A3.*
*PHASE VELOCITY OF SOUND IN A UNIFORM POROUS MATERIAL.*

*DATA. Flow resistance, R=.05, .10 ro-ce units/cm. Porosity, H=.95.*
*Structure factor, G=1.5.*
*Solid lines: Rigid material. Dashed lines: Limp material, M=.05 g/cm$_3$*

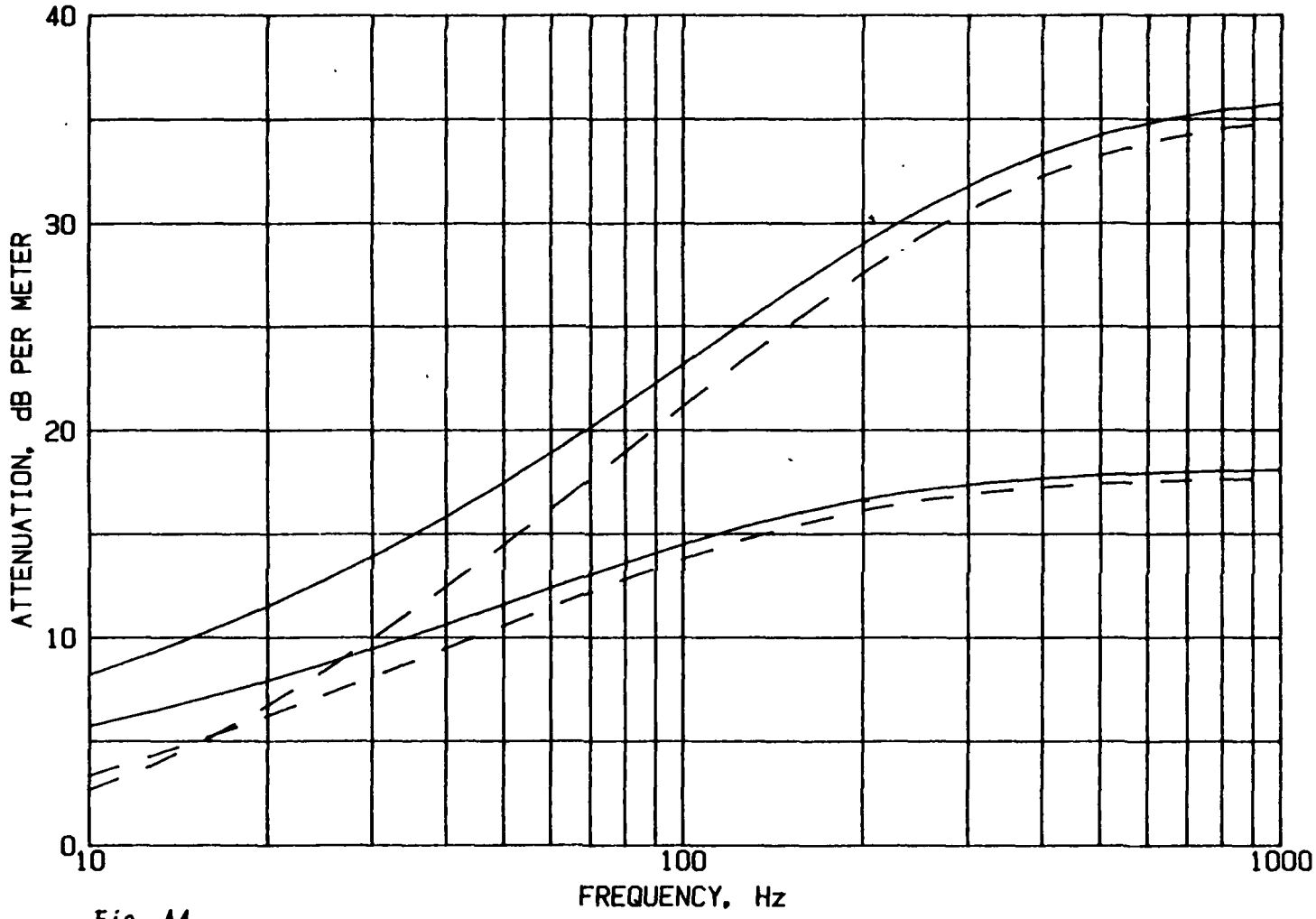


*Fig. A4.*
ATTENUATION OF A PLANE WAVE IN A UNIFORM POROUS MATERIAL.

*DATA. Flow resistance, R=.05, .10 ro-ce units/cm. Porosity, H=.95. Structure factor, G=1.5*
*Solid lines: Rigid material. Dashed lines: Limp material, M=.05 g/cm$^3$*

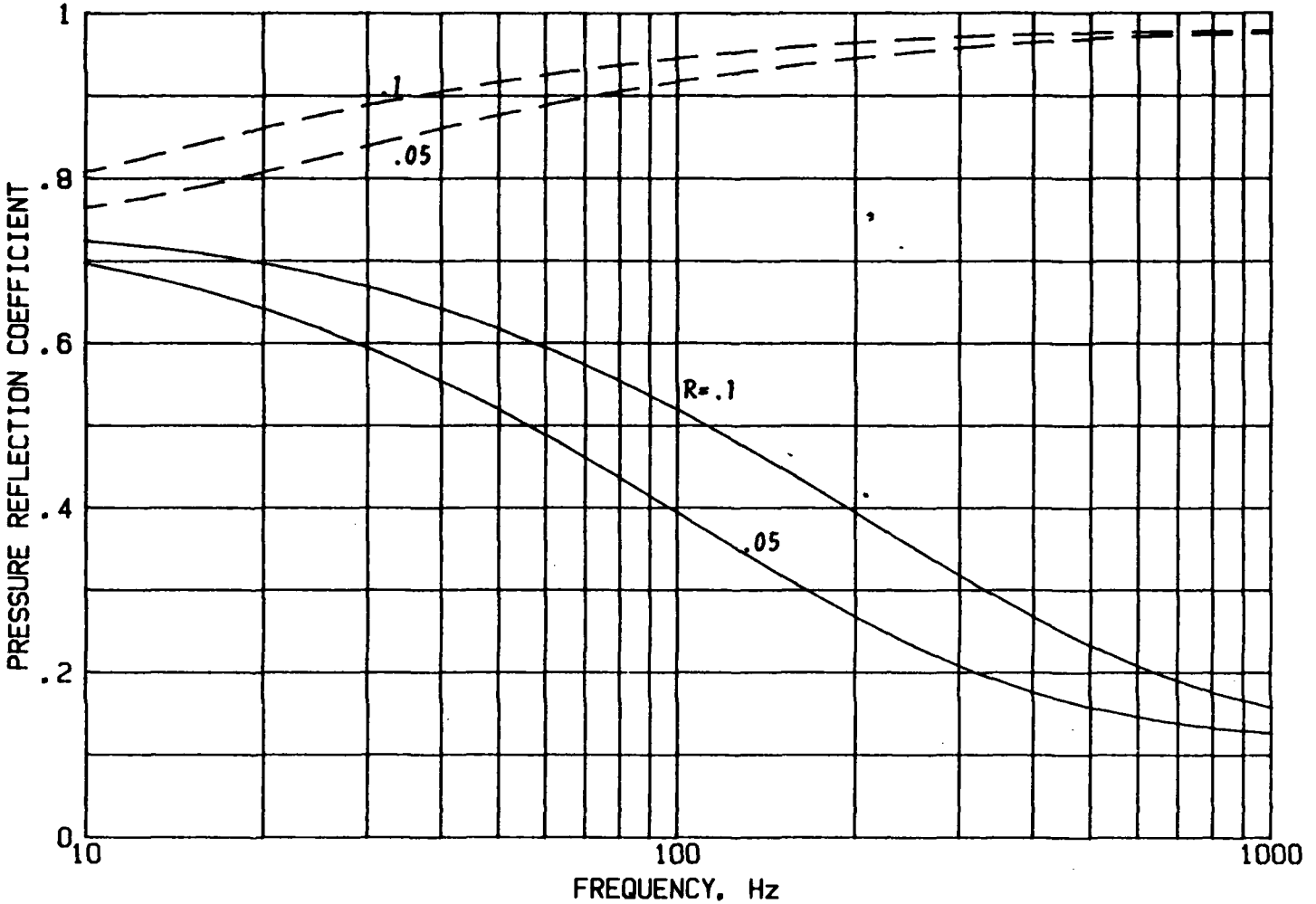


*Fig. A5.*
*PRESSURE REFLECTION COEFFICIENT AT THE BOUNDARY OF A SEMI-INFINITE POROUS LAYER. NORMAL INCIDENCE.*

*DATA. Flow resistance, R=.05, .10 ro-ce units/cm. Porosity, H=.95. Structure factor, G=1.5. Ratio between mass density and gas density m=38. Solid lines: Open boundary. Dashed lines: Closed boundary (impervious skin).*

## References


1. Ingard, K. U., "Locally and Nonlacally Reacting Flexible Porous Layers; A Comparison of Acoustical Properties", ASME 80-WA/NC-14 (1980).

2. Morse, P.M. and Ingard, K.U. Theoretical Acoustics. McGraw-Hill, New York, 1968. pp 383,384.

3. ibid. p 901.

4. Landau, L.D. and Lifshitz, E.M. Fluid Mechanics. Pergamon, 1959. pp 1-14.

5. Rundinger, G. Nonsteady Duct Flow: Wave-Diagram Analysis. Dover, New York, 1969.

6. Lighthill, J., Waves in Fluids. Cambridge University Press, London, 1978. pp 137-143.

7. Van Leer, B. "Towards the Ultimate Conservation Difference Scheme. V. A Second-order Sequel to Godunov's Method", J. Computational Physics 32 (1979), 101-136.

8. Van Leer, B. "On the Relation between the Upwind-Differencing Schemes of Godunov, Engquist-Osher and Roe", ICASE Report 81-11,(1981).

9. Sod, G. A. "A Survey of Several Finite Difference Methods for Systems of Nonlinear Hyperbolic Conservation Laws" J. Computational Physics 27 (1978), 1.

10. Chorin, A.J. "Random Choice Solution of Hyperbolic Systems" J. Computational Physics 22, (1976), 517-533.

11. Morse, P.M. and Ingard, K.U. Theoretical Acoustics McGraw Hill, New York, 1968. p 879.

12. Van Leer, B. "Towards the Ultimate Conservation Difference Scheme. V. A Second-order Sequel to Godunov's Method", J. Computational Physics 32 (1979), 117.

13. Rudinger, G. "On the Reflection of Shock Waves from an Open End of a Duct." J. Applied Physics 26 no. 8, (1955), 981-993.

14. Rudinger, G. "The Reflection of Pressure Waves of Finite Amplitude from an Open End of a Duct." J. Fluid Mech. 3, (1957), 48-66.

15. Rudinger, G. Nonsteady Duct Flow:Wave-Diagram Analysis. Dover, New York, 1969, pp 71-73.

16. Rudinger, G. "The Reflection of Shock Waves from an Orifice at the End of a Duct." J. Appl. Math. Phys. (ZAMP), 9b, (1958), 570-585.

17. Ingard, K.U. and Ising, H., "Acoustic Nonlinearity of an Orifice" J. Acoustical Soc. of Amer. 42 no. 1, (1967), 6-17.

18. Morse, P.M.,"The transmission of sound inside pipes", J. Acoust. Soc. Am. 11, 205, (1939).

19. L. Brillouin, "Acoustical Wave Propagation in Pipes" J. Acoustic. Soc. Am. 11, 10 (1939)

20. R.A. Scott, "The Propagation of Sound between Walls of Porous Materials", Proce. Phys. Soc. (London), 58, 358, (1946)



☆ U.S.Government Printing Office: 1983 — 759-062/605

END

FILMED

2-84

DTIC